

Phenomenological Constraints on Axion Models of Dynamical Dark Matter

Keith R. Dienes^{1,2,3*}, Brooks Thomas^{4†}

¹ *Physics Division, National Science Foundation, Arlington, VA 22230 USA*

² *Department of Physics, University of Maryland, College Park, MD 20742 USA*

³ *Department of Physics, University of Arizona, Tucson, AZ 85721 USA*

⁴ *Department of Physics, University of Hawaii, Honolulu, HI 96822 USA*

In two recent papers [1, 2] we introduced “dynamical dark matter” (DDM), a new framework for dark-matter physics in which the requirement of stability is replaced by a delicate balancing between lifetimes and cosmological abundances across a vast ensemble of individual dark-matter components whose collective behavior transcends that normally associated with traditional dark-matter candidates. We also presented an explicit model involving axions in large extra spacetime dimensions, and demonstrated that this model has all of the features necessary to constitute a viable realization of the general DDM framework. In this paper, we complete our study by performing a general analysis of all phenomenological constraints which are relevant to this bulk-axion DDM model. Although the analysis in this paper is primarily aimed at our specific DDM model, many of our findings have important implications for bulk axion theories in general. Our analysis can also serve as a prototype for phenomenological studies of theories in which there exist large numbers of interacting and decaying particles.

Contents

I. Introduction	2
II. Generalized Axions in Extra Dimensions: A Review	3
III. Axion Production in the Early Universe	5
A. Axion Production from Vacuum Misalignment	6
B. Axion Production from Particle Decays	8
C. Axion Production from Cosmic Strings	13
D. Axion Production from the Thermal Bath	13
IV. Phenomenological Constraints on Dark Axion Ensembles	16
A. Constraints from Background Geometry	17
B. Axion Production with Subsequent Detection: Helioscopes and Light Shining Through Walls	19
C. Microwave-Cavity Experiments and Direct Detection of Dark-Matter Axions	21
D. Axion Production without Subsequent Detection: Stars and Supernovae	21
E. Axion Production at Colliders	24
F. Axion Decays and Distortions of the Cosmic Microwave Background Spectrum	26
G. Axion Decays and Contributions to the Diffuse X-Ray and Gamma-Ray Backgrounds	30
H. Axion Decays and Big-Bang Nucleosynthesis	34
I. Axion Decays and Late Entropy Production	36
J. Vacuum Energy and Overclosure	38
K. Misalignment Production and Isocurvature Perturbations	39
L. Axion Abundances and Quantum Fluctuations During Inflation	41
M. Other Astrophysical Constraints on Light Axions	44
V. Synthesis: Combined Phenomenological Constraints on Axion Models of Dynamical Dark Matter	45
VI. Discussion and Conclusions	46

* E-mail address: dienes@physics.arizona.edu

† E-mail address: thomasbd@phys.hawaii.edu

I. INTRODUCTION

Dynamical dark matter (DDM) [1, 2] is a new framework for dark-matter physics in which the requirement of stability is replaced by a delicate balancing between lifetimes and cosmological abundances across a vast ensemble of individual dark-matter components. Due to the range of lifetimes and abundances of these components, their collective behavior transcends that normally associated with traditional dark-matter candidates. In particular, quantities such as the total dark-matter relic abundance, the proportional composition of the ensemble in terms of its constituents, and the effective equation of state for the ensemble possess a non-trivial time dependence beyond that associated with the expansion of the universe. Indeed, from this perspective, DDM may be viewed as the most general possible framework for dark-matter physics, and traditional dark-matter models are merely a limiting case of the DDM framework in which the states which compose the dark sector are taken to be relatively few in number and therefore stable.

In Ref. [1], we laid out the general theoretical features of the DDM framework. By contrast, in Ref. [2], we presented an explicit realization of the DDM framework: a model in which the particles which constitute the dark-matter ensemble are the KK excitations of an axion-like field propagating in the bulk of large extra spacetime dimensions. We demonstrated that this model has all of the features necessary to constitute a viable realization of the general DDM framework. In this paper, we complete our study by performing a general analysis of all phenomenological constraints which are relevant to this bulk-axion DDM model. Although the analysis in this paper is primarily aimed at our specific DDM model, many of our findings have important implications for theories involving large extra dimensions in general. Furthermore, our analysis can also serve as a prototype for phenomenological studies of theories in which there exist large numbers of interacting and decaying particles.

It is important to emphasize why a general analysis of this sort is necessary, given the existence of numerous prior studies of the phenomenological and cosmological constraints on axions and axion-like fields, unstable relics, and the physical properties of miscellaneous dark-matter candidates. As discussed in Refs. [1, 2], such studies are typically applicable to dark sectors involving one or only a few fields, and are typically quoted in terms of limits on the mass, decay width, or couplings of any individual such field. It is not at all obvious how such bounds apply to a DDM *ensemble* — a dark-matter candidate which is not characterized by a well-defined single mass, decay width, or set of couplings. For example, constraints on a cosmological population of unstable particles derived from big-bang-nucleosynthesis (BBN) considerations or bounds on distortions in the cosmic microwave background (CMB) are generally derived under the assumption that such a population comprises but a single particle species with a well-defined lifetime and branching fractions. Such constraints are not directly applicable to a DDM ensemble (in which lifetimes are balanced against abundances), and must therefore be reexamined in this new context.

In this paper, we shall develop methods for dealing with these issues and for properly characterizing the constraints on models in which the dark-matter candidate is an ensemble of states rather than a single particle. As we shall find, the presence of non-trivial mixings among the KK excitations in our DDM model gives rise to a number of surprising effects which are ultimately critical for its phenomenological viability. One of these is a so-called “decoherence” phenomenon [1–3] which helps to explain how the dark matter in this model remains largely invisible to detection. Another is a suppression, induced by this mixing, of the couplings between the lighter particles in the dark-matter ensemble and the fields of the Standard Model (SM). As we shall see, these effects assert themselves in a variety of phenomenological contexts and play a crucial role in loosening a battery of constraints which would otherwise prove extremely severe.

This paper is organized as follows. In Sect. II, we briefly summarize the physics of axions in extra dimensions and review the notational conventions established in Ref. [2], which we once again adopt in this work. In Sect. III, we examine a number of processes, both thermal and non-thermal in nature, which contribute to the generation of a cosmological population of axions. We calculate the rates associated with these processes and assess the relative importance of the associated production mechanisms within different regions of model-parameter space. In Sect. IV, we then discuss the phenomenological, astrophysical, and cosmological constraints relevant for bulk-axion DDM models and assess how the parameter space of our model is bounded by each of these constraints. In Sect. V, we summarize the collective consequences of these constraints on the parameter space of our bulk-axion DDM model. Finally, in Sect. VI, we discuss the implications of our results for future research.

II. GENERALIZED AXIONS IN EXTRA DIMENSIONS: A REVIEW

In this section, we provide a brief review of the physics of generalized axions in extra dimensions. (More detailed reviews can be found in Refs. [2, 3].) By “generalized axion,” we mean any pseudo-Nambu-Goldstone boson which receives its mass from instanton effects related to a non-Abelian gauge group G which confines at some scale Λ_G . Note that the ordinary QCD axion [4, 5] is a special case of this, in which G is identified with $SU(3)$ color and Λ_G is identified with $\Lambda_{\text{QCD}} \approx 250$ MeV. However, in this paper, we shall leave these scales arbitrary in order to give our analysis a wider range of applicability. We will also assume the existence of a global Abelian symmetry $U(1)_X$ which plays the role played by the Peccei-Quinn symmetry $U(1)_{\text{PQ}}$ in the specific case of a QCD axion.

Our goal in this paper is to study the phenomenological constraints that arise when a generalized axion is allowed to propagate in the bulk [3] of a theory with extra spacetime dimensions [6, 7]. In particular, we consider the case in which the axion propagates in a single, large, flat extra dimension compactified on a S_1/\mathbb{Z}_2 orbifold of radius R . The fields of the SM are assumed to be restricted to a brane located at $x_5 = 0$. We also assume that the additional non-Abelian gauge group G is restricted to the brane at $x_5 = 0$. At temperatures $T \gg \Lambda_G$, the effective action for a bulk axion in five dimensions can be written in the form

$$S_{\text{eff}} = \int d^4x \int_0^{2\pi R} dx_5 \left[\frac{1}{2} \partial_M a \partial^M a + \delta(x_5) (\mathcal{L}_{\text{brane}} + \mathcal{L}_{\text{int}}) \right], \quad (2.1)$$

where ‘ a ’ denotes our five-dimensional axion field, $\mathcal{L}_{\text{brane}}$ contains the terms involving the brane fields alone, and \mathcal{L}_{int} contains the interaction terms coupling the brane-localized fields to the five-dimensional axion. The second of these terms is given by

$$\mathcal{L}_{\text{int}} = \frac{g_G^2 \xi}{32\pi^2 f_X^{3/2}} a \mathcal{G}_{\mu\nu}^a \tilde{\mathcal{G}}^{a\mu\nu} + \sum_i \frac{c_i}{f_X^{3/2}} (\partial_\mu a) \bar{\psi}_i \gamma^\mu \gamma^5 \psi_i + \frac{g_s^2 c_g}{32\pi^2 f_X^{3/2}} a G_{\mu\nu}^a \tilde{G}^{a\mu\nu} + \frac{e^2 c_\gamma}{32\pi^2 f_X^{3/2}} a F_{\mu\nu} \tilde{F}^{\mu\nu} + \dots, \quad (2.2)$$

where $F_{\mu\nu}$, $G_{\mu\nu}^a$, and $\mathcal{G}_{\mu\nu}^a$ are the field strengths respectively associated with the $U(1)_{\text{EM}}$, $SU(3)$ color, and G gauge groups; $\tilde{F}_{\mu\nu}$, $\tilde{G}_{\mu\nu}^a$, and $\tilde{\mathcal{G}}_{\mu\nu}^a$ are their respective duals; e , g_s , and g_G are the respective coupling constants for these groups; f_X is the fundamental five-dimensional scale associated with the breaking of the $U(1)_X$ symmetry; c_γ , c_g , and c_i are coefficients which respectively parametrize the coupling strength of the five-dimensional axion field to the photon, gluon, and fermion fields of the SM; and ξ is an $\mathcal{O}(1)$ coefficient which depends on the specifics of the axion model in question. Note that in Eq. (2.2), we have displayed terms involving only the light fields of the SM (*i.e.*, the photon, gluon, and light fermion fields), as couplings to the heavier SM fields will not play a significant role in our phenomenological analysis.

The five-dimensional axion field can be represented as a tower of four-dimensional KK excitations via the decomposition

$$a(x^\mu, x_5) = \frac{1}{\sqrt{2\pi R}} \sum_{n=0}^{\infty} r_n a_n(x^\mu) \cos\left(\frac{nx_5}{R}\right), \quad (2.3)$$

where the factor

$$r_n \equiv \begin{cases} 1 & \text{for } n = 0 \\ \sqrt{2} & \text{for } n > 0 \end{cases} \quad (2.4)$$

ensures that the kinetic term for each mode is canonically normalized. Substituting this expression into Eq. (2.2) and integrating over x_5 , we obtain

$$S_{\text{eff}} = \int d^4x \left[\sum_{n=0}^{\infty} \left(\frac{1}{2} \partial_\mu a_n \partial^\mu a_n + \frac{g_G^2 \xi}{32\pi^2 \hat{f}_X} r_n a_n \mathcal{G}_{\mu\nu}^a \tilde{\mathcal{G}}^{a\mu\nu} + \sum_i \frac{c_i}{\hat{f}_X} r_n (\partial_\mu a_n) \bar{\psi}_i \gamma^\mu \gamma^5 \psi_i \right. \right. \\ \left. \left. + \frac{g_s^2 c_g}{32\pi^2 \hat{f}_X} r_n a_n G_{\mu\nu}^a \tilde{G}^{a\mu\nu} + \frac{e^2 c_\gamma}{32\pi^2 \hat{f}_X} r_n a_n F_{\mu\nu} \tilde{F}^{\mu\nu} \right) - V(a) \right], \quad (2.5)$$

where the axion potential is given by

$$V(a) = \sum_{n=0}^{\infty} \frac{1}{2} \frac{n^2}{R^2} a_n^2, \quad (2.6)$$

and where the quantity \hat{f}_X , defined by the relation

$$\hat{f}_X^2 \equiv 2\pi R f_X^3, \quad (2.7)$$

represents the effective four-dimensional $U(1)_X$ -breaking scale. Note that each mode in the KK tower couples to the SM fields with a strength inversely proportional to \hat{f}_X . Also note that at these scales, the axion mass-squared matrix

$$\mathcal{M}_{mn}^2 \equiv \left. \frac{\partial^2 V(a)}{\partial a_m \partial a_n} \right|_{\langle a \rangle} \quad (2.8)$$

is purely diagonal.

At scales $T \lesssim \Lambda_G$, an additional contribution to the effective axion potential arises due to instanton effects. In this regime, the potential is modified to

$$V(a) = \sum_{n=0}^{\infty} \frac{1}{2} \frac{n^2}{R^2} a_n^2 + \frac{g_G^2}{32\pi^2} \Lambda_G^4 \left[1 - \cos \left(\frac{\xi}{\hat{f}_X} \sum_{n=0}^{\infty} r_n a_n + \bar{\Theta}_G \right) \right], \quad (2.9)$$

where $\bar{\Theta}_G$ is the analogue of the QCD theta-parameter $\bar{\Theta}$. This results in a modification of the axion mass-squared matrix to

$$\mathcal{M}_{mn}^2 = n^2 M_c^2 \delta_{mn} + \frac{g_G^2 \xi^2}{32\pi^2} \frac{\Lambda_G^4}{\hat{f}_X^2} r_m r_n, \quad (2.10)$$

where $M_c \equiv 1/R$ is the compactification scale. This matrix above takes the form [3]

$$\mathcal{M}^2 = m_X^2 \begin{pmatrix} 1 & \sqrt{2} & \sqrt{2} & \sqrt{2} & \dots \\ \sqrt{2} & 2+y^2 & 2 & 2 & \dots \\ \sqrt{2} & 2 & 2+4y^2 & 2 & \dots \\ \sqrt{2} & 2 & 2 & 2+9y^2 & \dots \\ \vdots & \vdots & \vdots & \vdots & \ddots \end{pmatrix}, \quad (2.11)$$

where

$$y \equiv \frac{M_c}{m_X} \quad \text{and} \quad m_X^2 \equiv \frac{g_G^2 \xi^2}{32\pi^2} \frac{\Lambda_G^4}{\hat{f}_X^2}. \quad (2.12)$$

The eigenvalues λ^2 of this mass-squared matrix are the solutions to the transcendental equation

$$\frac{\pi \lambda m_X}{y} \cot \left(\frac{\pi \lambda}{m_X y} \right) = \lambda^2. \quad (2.13)$$

The corresponding normalized mass eigenstates a_λ are related to the KK-number eigenstates a_n via

$$a_\lambda = \sum_{n=0}^{\infty} U_{\lambda n} a_n \equiv \sum_{n=0}^{\infty} \left(\frac{r_n \tilde{\lambda}^2}{\tilde{\lambda}^2 - n^2 y^2} \right) A_\lambda a_n, \quad (2.14)$$

where $\tilde{\lambda} \equiv \lambda/m_X$. The dimensionless quantity A_λ is given by

$$A_\lambda \equiv \frac{\sqrt{2}}{\tilde{\lambda}} \left[1 + \tilde{\lambda}^2 + \pi^2/y^2 \right]^{-1/2}. \quad (2.15)$$

and obeys the sum rules [3]

$$\sum_{\lambda} A_\lambda^2 = 1, \quad \sum_{\lambda} \tilde{\lambda}^2 A_\lambda^2 = 1. \quad (2.16)$$

For $T \ll \hat{f}_X$, rewriting Eq. (2.5) in terms of the a_λ and expanding the axion potential given in Eq. (2.9) out to $\mathcal{O}(a_\lambda^6/\hat{f}_X^6)$ yields the effective action

$$S_{\text{eff}} = \int d^4x \left[\sum_\lambda \left(\frac{1}{2} \partial_\mu a_\lambda \partial^\mu a_\lambda - \frac{1}{2} \tilde{\lambda}^2 m_X^2 a_\lambda^2 + \frac{e^2 c_\gamma \tilde{\lambda}^2 A_\lambda}{32\pi^2 \hat{f}_X} a_\lambda F_{\mu\nu} \tilde{F}^{\mu\nu} + \frac{g_s^2 c_g \tilde{\lambda}^2 A_\lambda}{32\pi^2 \hat{f}_X} a_\lambda G_{\mu\nu}^a \tilde{G}^{\mu\nu a} \right. \right. \\ \left. \left. + \sum_i \frac{c_i \tilde{\lambda}^2 A_\lambda}{\hat{f}_X} (\partial_\mu a_\lambda) \bar{\psi}_i \gamma^\mu \gamma^5 \psi_i \right) + \frac{g_G^2 \xi^4 \Lambda_G^4}{768\pi^2 \hat{f}_X^4} \sum_{\lambda_i, \lambda_j, \lambda_k, \lambda_\ell} \tilde{\lambda}_i^2 \tilde{\lambda}_j^2 \tilde{\lambda}_k^2 \tilde{\lambda}_\ell^2 A_{\lambda_i} A_{\lambda_j} A_{\lambda_k} A_{\lambda_\ell} a_{\lambda_i} a_{\lambda_j} a_{\lambda_k} a_{\lambda_\ell} \right]. \quad (2.17)$$

Of course, the interaction term between the a_λ and the gluon field is only a useful description of the physics at temperatures above the quark-hadron phase transition at $T \sim \Lambda_{\text{QCD}}$. At temperatures below this threshold, this interaction term gives rise to an effective Lagrangian containing interactions between the a_λ and various hadrons, including the proton p , the neutron n , and the charged and neutral pions π^\pm and π^0 . This Lagrangian takes the form

$$\mathcal{L}_{\text{had}} = \tilde{\lambda}^2 A_\lambda \frac{C_{a\pi}}{f_\pi \hat{f}_X} (\partial_\mu a_\lambda) \left[(\partial^\mu \pi^+) \pi^- \pi^0 + (\partial^\mu \pi^-) \pi^+ \pi^0 - 2(\partial^\mu \pi^0) \pi^+ \pi^- \right] + \tilde{\lambda}^2 A_\lambda \frac{C_{an}}{\hat{f}_X} (\partial_\mu a_\lambda) \bar{n} \gamma^\mu \gamma^5 n \\ + \tilde{\lambda}^2 A_\lambda \frac{C_{ap}}{\hat{f}_X} (\partial_\mu a_\lambda) \bar{p} \gamma^\mu \gamma^5 p + i \tilde{\lambda}^2 A_\lambda \frac{C_{a\pi N}}{f_\pi \hat{f}_X} (\partial_\mu a_\lambda) \left[\pi^+ \bar{p} \gamma^\mu n - \pi^- \bar{n} \gamma^\mu p \right], \quad (2.18)$$

where the coefficients $C_{a\pi}$, C_{an} , *etc.*, depend on the details of the theory. For example, for a “hadronic” QCD axion [8] (*i.e.*, a QCD axion which does not couple directly to the SM quarks), the coefficients C_{ap} and C_{an} , which determine the strength of the axion-nucleon-nucleon interactions, are

$$C_{ap} = 0.24 \left(\frac{z}{1+z} \right) + 0.15 \left(\frac{z-2}{1+z} \right) + 0.02, \quad C_{an} = 0.24 \left(\frac{z}{1+z} \right) + 0.15 \left(\frac{1-2z}{1+z} \right) + 0.02, \quad (2.19)$$

where $z = m_u/m_d \approx 0.56$ is the ratio of the up-quark and down-quark masses. Likewise, the coefficients $C_{a\pi N}$ and $C_{a\pi}$ for such an axion are

$$C_{a\pi N} = \frac{1-z}{2\sqrt{2}(1+z)}, \quad C_{a\pi} = \frac{1-z}{3(1+z)}, \quad (2.20)$$

where $f_\pi \approx 93$ MeV is the pion decay constant and $m_\pi \approx 135.0$ MeV is the neutral pion mass.

Before concluding this review, we note that the effective coupling coefficients c_γ , c_g , and c_i appearing in Eq. (2.2) are highly model-dependent. They need not be $\mathcal{O}(1)$, and in many theories any of them may vanish outright. Indeed it has been argued [9] that the existence of axions and axion-like fields which couple to electromagnetism but not to $SU(3)$ color is a generic feature of certain extensions of the SM, including string theory. In assessing the constraints on our bulk-axion DDM model, we shall therefore focus primarily on a “photonic” axion of this sort — *i.e.*, a general axion with $c_g = 0$ and $c_\gamma \neq 0$. However, we shall also discuss how such phenomenological constraints are modified in the case of a so-called “hadronic” axion with non-vanishing values for both c_g and c_γ . We note that additional subtleties arise in this latter case, due to non-trivial mixings between the a_n and other pseudoscalars present in the theory which also necessarily couple to $G_{\mu\nu}^a \tilde{G}^{a\mu\nu}$. These include hadrons such as π^0 and η , as well as any other axions in the theory which play a role in addressing the strong-CP problem [4, 5]. In discussing constraints on hadronic axions, we shall implicitly assume that the full mass-squared matrix for the theory is such that the relationship between the a_n and the mass eigenstates a_λ defined in Eq. (2.14) is not significantly disturbed. Indeed, given the inherently large number of independent scales and couplings that emerge in scenarios involving multiple axions and other pseudoscalars, this is not an unreasonable assumption; moreover, it is straightforward to show in a general way that these favorable conditions can always be arranged for certain sets of axion and pseudo-scalar mixings. Such an assumption thereby enables us to perform our phenomenological analysis in a model-independent way.

III. AXION PRODUCTION IN THE EARLY UNIVERSE

Axions and axion-like fields can be produced via a number of different mechanisms in the early universe. For example, these particles can be produced thermally, via their interactions with the SM fields in the radiation bath. In addition, a number of non-thermal mechanisms exist through which a sizable population of axions also may be generated. These include production via vacuum misalignment, production from the decays of cosmic strings and other topological defects, and production from the out-of-equilibrium decays of other, heavier fields in the theory.

This last mechanism is particularly relevant in the context of the DDM models, since, by assumption, the dark sector in such models involves large numbers of unstable fields with long lifetimes. Indeed, in the axion DDM model under consideration in this paper, a non-thermal population of any a_λ may be produced via the decays of both heavier KK gravitons and other heavier a_λ .

In Ref. [2], we focused on misalignment production as the primary mechanism responsible for establishing a cosmological population of dark axions. In order for the results for the relic abundances Ω_λ of the a_λ obtained there to be valid, the contributions from all of the alternative production mechanisms mentioned above must be subdominant for each a_λ . Therefore, in this section, we examine each of the relevant axion-production mechanisms in turn, beginning with a brief review of the results for misalignment production itself. Since phenomenological constraints on scenarios involving large, flat extra dimensions prefer that the reheating temperature T_R associated with cosmic inflation be quite low [7], we will hereafter operate within the context of a low-temperature-reheating (LTR) cosmology with $T_R \sim \mathcal{O}(\text{MeV})$. Within such a cosmological context and within the region of model-parameter space in which misalignment production yields a total relic abundance Ω_{tot} comparable to the observed dark-matter relic abundance Ω_{CDM} , we demonstrate that the contributions to each Ω_λ from all other production mechanisms are indeed subdominant.

A. Axion Production from Vacuum Misalignment

We begin our discussion of axion production in the early universe with a brief review of the misalignment mechanism and its implications for axion DDM models. (A more detailed discussion can be found in Ref. [2].) As we shall see, this mechanism turns out to be the dominant production mechanism for dark-matter axions in such models.

At temperatures $T \gg \Lambda_G$, the only contributions to the axion mass-squared matrix are the contributions from the KK masses. Since these contributions to \mathcal{M}^2 are diagonal in the KK eigenbasis, no mixing occurs, and the KK eigenstates are the mass eigenstates of the theory. The potential for each a_n with $n \neq 0$ is therefore non-vanishing, due to the presence of the KK masses, and is minimized at $a_n = 0$. However, the potential for the zero mode a_0 vanishes. In the absence of a potential for a_0 , there is no preferred vacuum expectation value (VEV) $\langle a_0 \rangle$ which minimizes $V(a_0)$. It therefore follows that immediately following the phase transition at $T \sim \hat{f}_X$, the universe comprises a set of domains, each with a different homogeneous background value for the axion field which may be expressed in terms of a “misalignment angle” $\theta \equiv \langle a_0 \rangle / \hat{f}_X$. This angle is generically expected to be $\mathcal{O}(1)$ in any particular domain, but could also be smaller. We assume here that $H_I \lesssim 2\pi\hat{f}_X$, where H_I is the value of the Hubble parameter during inflation, and therefore that the value of θ is uniform over our present Hubble volume. In this case, we find that

$$\langle a_0 \rangle = \theta \hat{f}_X, \quad \langle a_n \rangle = 0 \quad \text{for } n \neq 0. \quad (3.1)$$

Note that the above discussion is strictly valid only in the limit in which the Hubble volume is taken to infinity. In reality, the presence of a finite Hubble volume limits our ability to distinguish fields with wavelengths larger than the Hubble radius from true background values. Because of this ambiguity, all a_n for which $n/R \lesssim H_I$ can also acquire $\mathcal{O}(1)$ background values after $U(1)_X$ breaking. In Sect. IV L, we will analyze the phenomenological consequences of this effect in detail and derive conditions under which it can be safely neglected. As we shall demonstrate, it turns out that within our preferred region of parameter space, these conditions involve only mild restrictions on the cosmological context into which our model is embedded. We will therefore assume from this point forward that the $\langle a_n \rangle$ in our model are given by Eq. (3.1).

At temperatures down to $T \sim \Lambda_G$, the $\langle a_n \rangle$ remain fixed at these initial values. At lower temperatures, however, the situation changes as instanton effects generate a potential for the axion KK modes. Indeed, in the regime in which $T \ll \Lambda_G$ and the brane mass engendered by this potential has attained the constant, low-temperature value m_X given in Eq. (2.12), the time-evolution of each field a_λ is governed by an equation of the form

$$\ddot{a}_\lambda + \frac{\kappa}{t} \dot{a}_\lambda + \Gamma_\lambda \dot{a}_\lambda + \lambda^2 a_\lambda = 0, \quad (3.2)$$

where each dot denotes a time derivative, and where

$$\kappa \equiv \begin{cases} 3/2 & \text{in radiation-dominated (RD) eras} \\ 2 & \text{in matter-dominated (MD) eras} \end{cases}. \quad (3.3)$$

When $\lambda \lesssim 3H/2$, the solution to this equation remains approximately constant. This implies that the energy density stored in a_λ scales approximately like vacuum energy during this epoch. However, at later times, when $\lambda \gtrsim 3H/2$, we

see that a_λ oscillates coherently around the minimum of its potential, with oscillations damped by a “friction” term with coefficient $3H + \Gamma_\lambda$. During this latter epoch, the energy density stored in a_λ scales like massive matter.

At temperatures $T \sim \Lambda_G$, the evolution of a_λ depends more sensitively on the explicit time-dependence of the brane mass $m_X(t)$. In what follows, we adopt a “rapid-turn-on” approximation, in which the instanton potential is assumed to turn on instantaneously at $t = t_G$, where t_G is the time at which the confining transition for the gauge group G occurs. In this approximation, $m_X(t)$ takes the form of a Heaviside step function:

$$m_X(t) = m_X \Theta(t - t_G) . \quad (3.4)$$

In this approximation, the a_n remain fixed at the initial values given in Eq. (3.1) so long as $t < t_G$. At $t = t_G$, the brane mass immediately assumes its constant, late-time value m_X . Since only a_0 is populated immediately prior to the phase transition at t_G , each of the a_λ initially acquires a background value proportional to its overlap with a_0 :

$$\langle a_\lambda(t_G) \rangle = \theta \hat{f}_X A_\lambda , \quad \langle \dot{a}_\lambda(t_G) \rangle = 0 . \quad (3.5)$$

Subsequently, after the a_λ have been populated, each begins oscillating at a characteristic time scale

$$t_\lambda \equiv \max \left\{ \frac{\kappa_\lambda}{2\lambda}, t_G \right\} , \quad (3.6)$$

where κ_λ is the value of κ corresponding to the epoch during which this oscillation begins. At late times $t \gg t_\lambda$, when these oscillations become rapid compared to the rate of change of $\langle a_\lambda \rangle$ and the virial approximation is therefore valid, one finds that the energy density ρ_λ stored in each mode is given by

$$\rho_\lambda(t) = \frac{1}{2} \theta^2 \hat{f}_X^2 \lambda^2 A_\lambda^2 \left(\frac{t_\lambda}{t} \right)^{\kappa_\lambda} e^{-\Gamma_\lambda(t-t_G)} \quad (3.7)$$

during the epoch in which the oscillation began. Computing ρ_λ during subsequent epochs is simply a matter of applying Eq. (3.7) iteratively with the appropriate boundary conditions at each transition point. Consequently, in the LTR cosmology, we have [2]

$$\rho_\lambda^{\text{LTR}}(t) \approx \frac{1}{2} \theta^2 \hat{f}_X^2 \lambda^2 A_\lambda^2 e^{-\Gamma_\lambda(t-t_G)} \times \begin{cases} \left(\frac{t_\lambda}{t} \right)^2 & t_\lambda \lesssim t \lesssim t_{\text{RH}} \\ \left(\frac{t_\lambda^2}{t_{\text{RH}}^{1/2} t^{3/2}} \right) & t_{\text{RH}} \lesssim t \lesssim t_{\text{MRE}} \\ \left(\frac{t_\lambda^2 t_{\text{MRE}}^{1/2}}{t^2 t_{\text{RH}}^{1/2}} \right) & t \gtrsim t_{\text{MRE}} , \end{cases} \quad (3.8)$$

where t_{RH} denotes the reheating time — *i.e.*, the time at which $T = T_{\text{RH}}$, and the universe transitions from an initial epoch of matter domination by the coherent oscillations of the inflaton field to the usual radiation-dominated era.

Given the energy-density expression in (3.8), it is straightforward to obtain the relic abundance $\Omega_\lambda \equiv \rho_\lambda / \rho_{\text{crit}}$ for each a_λ , where $\rho_{\text{crit}} \equiv 3M_P^2 H^2$. For the heavier modes in the tower, for which $t_\lambda = t_G$, one finds

$$\Omega_\lambda^{\text{LTR}} \approx 3 \left(\frac{\theta \hat{f}_X m_X}{M_P} \right)^2 t_G^2 \left[1 + \frac{\lambda^2}{m_X^2} + \frac{\pi^2 m_X^2}{M_c^2} \right]^{-1} e^{-\Gamma_\lambda(t-t_G)} \times \begin{cases} \frac{1}{4} & 1/\lambda \lesssim t \lesssim t_{\text{RH}} \\ \frac{4}{9} \left(\frac{t}{t_{\text{RH}}} \right)^{1/2} & t_{\text{RH}} \lesssim t \lesssim t_{\text{MRE}} \\ \frac{1}{4} \left(\frac{t_{\text{MRE}}}{t_{\text{RH}}} \right)^{1/2} & t \gtrsim t_{\text{MRE}} . \end{cases} \quad (3.9)$$

For the modes in the tower for which $t_\lambda > t_G$, the corresponding result is

$$\Omega_\lambda^{\text{LTR}} \approx 3 \left(\frac{\theta \hat{f}_X m_X}{M_P} \right)^2 \lambda^{-2} \left[1 + \frac{\lambda^2}{m_X^2} + \frac{\pi^2 m_X^2}{M_c^2} \right]^{-1} e^{-\Gamma_\lambda(t-t_G)} \times \begin{cases} \frac{1}{4} & 1/\lambda \lesssim t \lesssim t_{\text{RH}} \\ \frac{4}{9} \left(\frac{t}{t_{\text{RH}}} \right)^{1/2} & t_{\text{RH}} \lesssim t \lesssim t_{\text{MRE}} \\ \frac{1}{4} \left(\frac{t_{\text{MRE}}}{t_{\text{RH}}} \right)^{1/2} & t \gtrsim t_{\text{MRE}} . \end{cases} \quad (3.10)$$

The total contribution Ω_{tot} to the dark-matter relic abundance from the axion tower is simply the sum over these individual contributions. While the generic behavior of Ω_{tot} as a function of \hat{f}_X , M_c , and Λ_G is somewhat complicated, simple analytical results can be obtained in certain limiting cases of physical importance. For example, let us consider the limit in which $t_\lambda = t_G$ for all modes in the tower and H_I is sufficiently large that none of the a_λ which would otherwise contribute significantly to Ω_{tot} begin oscillating before the end of inflation. In this limit, all of the Ω_λ take the form given in Eq. (3.9), and one finds that the present-day value of Ω_{tot} , here denoted Ω_{tot}^* , is given by the simple closed-form expression [2]

$$\Omega_{\text{tot}}^* \approx \frac{3}{256\pi^2} (g_G \xi)^2 \left(\frac{\theta \Lambda_G^2}{M_P} \right)^2 t_G^{3/2} t_{\text{MRE}}^{1/2} \left(\frac{t_G}{t_{\text{RH}}} \right)^{1/2}. \quad (3.11)$$

In the opposite limit, when all of modes which contribute significantly toward Ω_{tot}^* begin oscillating at $t_\lambda > t_G$ and have oscillation-onset times which depend on λ and are therefore staggered in time, Ω_λ is given by Eq. (3.10) for all a_λ . In this limit, the expression for Ω_{tot}^* reduces to [2]

$$\Omega_{\text{tot}}^* \approx \frac{3}{8} \left(\frac{\theta \hat{f}_X}{M_P} \right)^2 \left(\frac{t_{\text{MRE}}}{t_{\text{RH}}} \right)^{1/2}. \quad (3.12)$$

The preferred region of parameter space from the perspective of dark-matter phenomenology is that within which Ω_{tot}^* represents an $\mathcal{O}(1)$ fraction of the dark-matter relic abundance inferred from WMAP data [10]:

$$\Omega_{\text{CDM}} h^2 = 0.1131 \pm 0.0034, \quad (3.13)$$

where $h \approx 0.72$ is the Hubble constant. From a dynamical dark-matter perspective, it is also preferable that the full axion tower contribute meaningfully to Ω_{tot}^* . For an $\mathcal{O}(1)$ value of the misalignment angle θ and a reheating temperature within the preferred range $T_R \sim 4 - 30$ MeV for theories with large extra dimensions, one finds [2] that these two conditions are realized for $\hat{f}_X \sim 10^{14} - 10^{15}$ GeV and $\Lambda_G \sim 10^2 - 10^5$ GeV, provided that M_c is small enough that $y \lesssim 1$. Within this region of parameter space, the t_λ of all a_λ which contribute meaningfully toward Ω_{tot}^* are staggered in time, and therefore the lighter modes yield a proportionally greater contribution to that total abundance. We will often focus our attention on this particular region of parameter space when discussing constraints on axion DDM models.

B. Axion Production from Particle Decays

Another mechanism by which a non-thermal population of relic particles may be generated in the early universe is through the decays of heavier, unstable relics. In scenarios involving extra dimensions, these relics include the higher KK modes of any fields which propagate within at least some subspace of the extra-dimensional bulk. For example, since the graviton field necessarily propagates throughout the entirety of the bulk, a population of unstable KK gravitons is a generic feature of all such scenarios. In the minimal bulk-axion DDM model under consideration here, the unstable relics whose decays can serve as a source for any given a_λ include these KK gravitons as well as other, heavier a_λ . Moreover, since these fields span a broad range of masses from the sub-eV to multi-TeV scale and beyond, one would expect the population of axions produced by their collective decays to possess by a highly non-trivial phase-space distribution. However, as we shall demonstrate below, the total contribution $\Gamma^{(\text{IE})}$ to the decay rate of any a_λ from *intra-ensemble* decays (*i.e.*, decays to final states which include one or more dark-sector fields in addition to any visible-sector fields that might also be present) is far smaller than that from decays to final states involving visible-sector fields alone. That the total branching fraction for intra-ensemble decays is negligible suggests that the population of axions produced by such decays will, in general, be quite small. Thus, provided the initial abundances of the a_λ are set by some mechanism such as vacuum misalignment for which the Ω_λ of the heavier a_λ are initially similar to or smaller than those of the light fields, it is reasonable to assume that the contributions from intra-ensemble decays are subleading and may therefore be safely neglected.

One class of processes which contribute to $\Gamma^{(\text{IE})}$ are those which arise due to the axion self-interactions implied by the final term in Eq. (2.17). The leading such contribution comes from three-body decay processes of the form $a_\lambda \rightarrow a_{\lambda_1} a_{\lambda_2} a_{\lambda_3}$. An upper bound on the total contribution $\Gamma(a_\lambda \rightarrow 3a)$ to the decay width of a given a_λ from all kinematically allowed decays of this form was derived in Ref. [2]:

$$\Gamma(a_\lambda \rightarrow 3a) \leq \frac{g_G^4 \xi^8}{45(4\pi)^7} \frac{\lambda^4}{M_c^3} \left(\frac{\Lambda_G}{\hat{f}_X} \right)^8. \quad (3.14)$$

It was also shown in Ref. [2] that the partial width of the a_λ to a pair of photons is given by

$$\Gamma(a_\lambda \rightarrow \gamma\gamma) = G_\gamma (\tilde{\chi}^2 A_\lambda)^2 \frac{\lambda^3}{f_X^2}, \quad (3.15)$$

with $G_\gamma \equiv c_\gamma^2 \alpha^2 / 256 \pi^3$, where $\alpha \equiv e^2 / 4\pi$ is the fine-structure constant. Within the preferred region of parameter space discussed above, in which $\hat{f}_X \sim 10^{14} - 10^{15}$ GeV and $\Lambda_G \gtrsim 10^2 - 10^5$ GeV, we see that $\Gamma_\lambda(a \rightarrow 3a)$ is negligible compared to $\Gamma(a_\lambda \rightarrow \gamma\gamma)$. It then follows that $\Gamma_\lambda(a \rightarrow 3a)$ represents a vanishingly small contribution to the total decay width Γ_λ of any a_λ in any theory with an $\mathcal{O}(1)$ value of c_γ . We therefore conclude that decays of the form $a_\lambda \rightarrow a_{\lambda_1} a_{\lambda_2} a_{\lambda_3}$ do not play a significant role in the phenomenology of realistic bulk-axion models of dynamical dark matter.

In addition to these decays, however, an additional set of decay channels — those involving lighter graviton or radion fields in the final state — are also open to the a_λ . In order to assess whether such decay channels are capable of yielding a significant contribution to the relic abundance of any of the a_λ , we begin by identifying the relevant interactions among the modes in the KK graviton and axion towers. Since we are considering the case of a flat extra dimension and assuming fluctuations of the metric to be small, it is justified to work in the regime of linearized gravity. The relevant term in the five-dimensional action is therefore

$$S = - \int d^4x \int_0^{2\pi R} dy \frac{1}{M_5^{3/2}} T_{MN} h^{MN}, \quad (3.16)$$

where T_{MN} is the stress-energy tensor, and h_{MN} is the metric perturbation defined according to the relation

$$g_{MN} = \eta_{MN} + \frac{2}{M_5^{3/2}} h_{MN}. \quad (3.17)$$

The piece of the stress-energy tensor which involves the five-dimensional axion field a includes both a bulk contribution and a contribution arising from terms in the interaction Lagrangian which involve interactions of the axion with the brane-localized fields of the SM. The bulk contribution is given by

$$T_{MN}^{\text{bulk}} = \partial_M a \partial_N a - \frac{1}{2} \eta_{MN} (\partial_P a \partial^P a). \quad (3.18)$$

Upon KK decomposition, this contribution, when coupled to h_{MN} as in Eq. (3.16), gives rise to three-point interactions between a KK graviton or radion field and a pair of a_λ . These interactions lead to decays of the form $a_\lambda \rightarrow G_{\mu\nu}^{(m)} a_{\lambda'}$, where $G_{\mu\nu}^{(m)}$ denotes a KK graviton with KK mode number m . In the absence of an instanton-induced brane mass term m_X for the axion field (*i.e.*, in the $m_X \rightarrow 0$ limit, in which all mixing between the axion KK modes vanishes and $a_\lambda \rightarrow a_n$), KK-momentum conservation would imply that only a single, marginal decay channel would exist for each a_λ . Hence the contribution to Γ_λ from such decays can be neglected. However, the instanton contribution to the axion mass-squared matrix violates KK-momentum conservation, and therefore, despite the fact that these axion-axion-graviton interactions are Planck-suppressed, they can still potentially contribute significantly to Γ_λ , due to the large number of modes into which each a_λ can decay.

By contrast, the brane-localized contribution, which is given by

$$\begin{aligned} T_{MN}^{\text{brane}} = & \delta(y) \delta_M^\mu \delta_N^\nu \left[\frac{1}{2} \sum_i \frac{c_i}{f_X^{3/2}} \left[(\partial_\mu a) \bar{\psi}_i \gamma_\nu \gamma^5 \psi_i + (\partial_\nu a) \bar{\psi}_i \gamma_\mu \gamma^5 \psi_i - 2 \eta_{\mu\nu} (\partial_\rho a) \bar{\psi}_i \gamma^\rho \gamma^5 \psi_i \right] \right. \\ & \left. + \frac{c_\gamma e^2}{32\pi^2 f_X^{3/2}} a \left(4 \tilde{F}_{\mu\rho} F_\nu{}^\rho - \eta_{\mu\nu} \tilde{F}^{\rho\sigma} F_{\rho\sigma} \right) + \frac{\xi g_s^2}{32\pi^2 f_X^{3/2}} a \left(4 \tilde{G}_{\mu\rho}^a G_\nu{}^{\rho a} - \eta_{\mu\nu} \tilde{G}^{\rho\sigma a} G_{\rho\sigma}^a \right) \right], \end{aligned} \quad (3.19)$$

leads to four-, five-, and six-point interactions between the graviton field, the a_λ , and the various SM fields. These interactions take the same form as those discussed in Section III B, save that each vertex involves the coupling of an additional KK graviton and is suppressed, relative to the corresponding interaction involving the axion and SM fields alone, by an additional factor of M_P . The rates for such interactions will therefore always be much smaller than those calculated in Section III B. Indeed, even the total contribution to the decay rate of a given a_λ from such processes, summed over graviton KK modes, will still be suppressed by a factor of roughly M_5 , where M_5 denotes the five-dimensional Planck scale, relative to the contribution from decays to SM fields alone. It is therefore sufficient, at least for our present purposes, to neglect T_{MN}^{brane} and to focus solely on the interactions arising from the bulk contribution T_{MN}^{bulk} .

We begin our analysis of axion-axion-graviton interactions by expanding the five-dimensional axion field, as well as the various components $h_{\mu\nu}$, $h_{\mu 5}$, and h_{55} of the metric perturbation h_{MN} , in terms of KK modes. The mode expansion of the axion field for the orbifold compactification considered here was given in Eq. (2.3); the mode expansions of $h_{\mu\nu}$, $h_{\mu 5}$, and h_{55} are analogously given by

$$\begin{aligned} h_{\mu\nu} &= \frac{1}{\sqrt{2\pi R}} \sum_{m=0}^{\infty} r_m h_{\mu\nu}^{(m)} \cos\left(\frac{my}{R}\right) \\ h_{\mu 5} &= \frac{1}{\sqrt{2\pi R}} \sum_{m=1}^{\infty} r_m h_{\mu 5}^{(m)} \sin\left(\frac{my}{R}\right) \\ h_{55} &= \frac{1}{\sqrt{2\pi R}} \sum_{m=0}^{\infty} r_m h_{55}^{(m)} \cos\left(\frac{my}{R}\right). \end{aligned} \quad (3.20)$$

Note in particular that $h_{\mu 5}$ must be odd with respect to the parity transformation $x_5 \rightarrow -x_5$. Upon substituting these KK-mode decompositions into the linearized-gravity action given in Eq. (3.16) and integrating over y , we find that the terms in the effective, four-dimensional interaction Lagrangian which govern the interactions between the graviton and axion KK modes consist of the following three contributions:

$$\begin{aligned} \int_0^{2\pi R} \frac{h_{\mu\nu} T_{\text{bulk}}^{\mu\nu}}{M_5^{3/2}} dy &= \sum_{m,n,p=0}^{\infty} \frac{r_m r_n r_p}{4M_P} h_{\mu\nu}^{(m)} \left[\left(2\partial^\mu a^{(n)} \partial^\nu a^{(p)} - \eta^{\mu\nu} \partial^\rho a^{(n)} \partial_\rho a^{(p)} \right) \Delta_{mnp}^+ \right. \\ &\quad \left. + \eta^{\mu\nu} \left(\frac{np}{R^2} \right) a^{(n)} a^{(p)} \Delta_{mnp}^- \right] \\ \int_0^{2\pi R} \frac{h_{55} T_{\text{bulk}}^{55}}{M_5^{3/2}} dy &= \sum_{m,n,p=0}^{\infty} \frac{r_m r_n r_p}{4M_P} h_{55}^{(m)} \left[\partial^\rho a^{(n)} \partial_\rho a^{(p)} \Delta_{mnp}^+ + \left(\frac{np}{R^2} \right) a^{(n)} a^{(p)} \Delta_{mnp}^- \right] \\ \int_0^{2\pi R} \frac{h_{\mu 5} T_{\text{bulk}}^{\mu 5}}{M_5^{3/2}} dy &= \sum_{m=1}^{\infty} \sum_{n,p=0}^{\infty} \frac{r_m r_n r_p}{2M_P} \left(\frac{p}{R} \right) h_{\mu 5}^{(m)} (\partial^\mu a^{(n)}) a^{(p)} \Delta_{nmp}^-, \end{aligned} \quad (3.21)$$

where

$$\Delta_{mnp}^\pm \equiv \left[\delta_{m,n-p} + \delta_{m,p-n} \right] \pm \left[\delta_{m,n+p} + \delta_{m,-n-p} \right]. \quad (3.22)$$

For the purposes of computing Feynman diagrams, it is convenient to work in the unitary gauge, in which the $h_{\mu 5}^{(m)}$ and $h_{55}^{(m)}$ fields with $m > 0$ are set to zero by the five-dimensional gauge transformations $g_{MN} \rightarrow g_{MN} + \partial_M \epsilon_N + \partial_N \epsilon_M$, where ϵ_M is the gauge parameter. In this gauge, the contributions in the second and third line of Eq. (3.21) vanish (save for the interactions between the axion KK modes and the radion field $h_{55}^{(0)}$, which will be discussed in due time), and the physical, gauge-invariant graviton fields

$$G_{\mu\nu}^{(m)} \equiv h_{\mu\nu}^{(m)} + \left(\frac{R}{m} \right) \left[\partial_\mu h_{\nu 5}^{(m)} + \partial_\nu h_{\mu 5}^{(m)} \right] - \left(\frac{R^2}{m^2} \right) \partial_\mu \partial_\nu h_{55}^{(m)} \quad (3.23)$$

reduce to $h_{\mu\nu}^{(m)}$ for all $m > 0$. The relevant part of the effective Lagrangian consequently reduces to

$$\mathcal{L}_{\text{int}}^{(m>0)} = - \sum_{m=1}^{\infty} \sum_{n,p=0}^{\infty} \frac{r_n r_p}{2\sqrt{2}M_P} h_{\mu\nu}^{(m)} \left[\left(2\partial^\mu a^{(n)} \partial^\nu a^{(p)} - \eta^{\mu\nu} \partial^\rho a^{(n)} \partial_\rho a^{(p)} \right) \Delta_{mnp}^+ + \eta^{\mu\nu} \left(\frac{np}{R^2} \right) a^{(n)} a^{(p)} \Delta_{mnp}^- \right]. \quad (3.24)$$

The expression in Eq. (3.24) can be rewritten in terms of the mass eigenstates a_λ via the mixing matrix $U_{\lambda n}$ in

Eq. (2.14). The result is

$$\begin{aligned}
\mathcal{L}_{\text{int}}^{(m>0)} &= - \sum_{m=1}^{\infty} \sum_{n,p=0}^{\infty} \sum_{\lambda,\lambda'} \frac{r_n r_p}{2\sqrt{2}M_P} h_{\mu\nu}^{(m)} U_{n\lambda}^\dagger U_{p\lambda'}^\dagger \left[\left(2\partial^\mu a_\lambda \partial^\nu a_{\lambda'} - \eta^{\mu\nu} \partial^\rho a_\lambda \partial_\rho a_{\lambda'} \right) \Delta_{mnp}^+ + \eta^{\mu\nu} \left(\frac{np}{R^2} \right) a_\lambda a_{\lambda'} \Delta_{mnp}^- \right] \\
&= - \sum_{m=1}^{\infty} \sum_{n=0}^{\infty} \sum_{\lambda,\lambda'} \frac{r_n}{2\sqrt{2}M_P} h_{\mu\nu}^{(m)} U_{n\lambda}^\dagger \left\{ \left(2\partial^\mu a_\lambda \partial^\nu a_{\lambda'} - \eta^{\mu\nu} \partial^\rho a_\lambda \partial_\rho a_{\lambda'} \right) \right. \\
&\quad \times \left(r_{n-m} U_{n-m,\lambda'}^\dagger + r_{n+m} U_{n+m,\lambda'}^\dagger + r_{m-n} U_{m-n,\lambda'}^\dagger + r_{-n-m} U_{-n-m,\lambda'}^\dagger \right) + \eta^{\mu\nu} \frac{n}{R^2} a_\lambda a_{\lambda'} \\
&\quad \times \left[(n-m)(r_{n-m} U_{n-m,\lambda'}^\dagger + r_{m-n} U_{m-n,\lambda'}^\dagger) + (n+m)(r_{n+m} U_{n+m,\lambda'}^\dagger + r_{-n-m} U_{-n-m,\lambda'}^\dagger) \right] \Big\}, \quad (3.25)
\end{aligned}$$

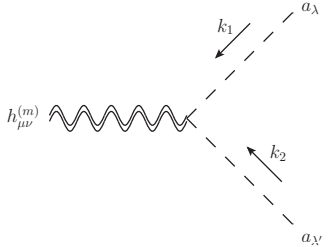
where in going from the first equality to the second we have exploited the Kronecker deltas in Δ_{mnp}^\pm to evaluate the sum over p . It should be noted that in the notation employed in the above expression, $U_{n\lambda}^\dagger = 0$ by definition for $n < 0$. The sum over n in Eq. (3.25) can also be performed analytically, and the resulting, final expression for the Lagrangian in terms of the a_λ is found to be

$$\mathcal{L}_{\text{int}}^{(m>0)} = - \sum_{m=1}^{\infty} \sum_{\lambda,\lambda'} \frac{1}{2\sqrt{2}M_P} h_{\mu\nu}^{(m)} \left[\left(2\partial^\mu a_\lambda \partial^\nu a_{\lambda'} - \eta^{\mu\nu} \partial^\rho a_\lambda \partial_\rho a_{\lambda'} \right) C_{m\lambda\lambda'}^{(1)} + \eta^{\mu\nu} M_c^2 a_\lambda a_{\lambda'} C_{m\lambda\lambda'}^{(2)} \right], \quad (3.26)$$

where the coefficients $C_{m\lambda\lambda'}^{(1)}$ and $C_{m\lambda\lambda'}^{(2)}$ are given by

$$\begin{aligned}
C_{m\lambda\lambda'}^{(1)} &= \frac{-8m^2 y^2 \tilde{\lambda}^2 \tilde{\lambda}'^2 A_\lambda A_{\lambda'}}{m^4 y^4 - 2m^2 y^2 (\tilde{\lambda}^2 + \tilde{\lambda}'^2) + (\tilde{\lambda}^2 - \tilde{\lambda}'^2)^2} \\
C_{m\lambda\lambda'}^{(2)} &= \frac{4\tilde{\lambda}^2 \tilde{\lambda}'^2 [m^2 y^2 (\tilde{\lambda}^2 + \tilde{\lambda}'^2) - (\tilde{\lambda}^2 - \tilde{\lambda}'^2)^2] A_\lambda A_{\lambda'}}{y^2 [m^4 y^4 - 2m^2 y^2 (\tilde{\lambda}^2 + \tilde{\lambda}'^2) + (\tilde{\lambda}^2 - \tilde{\lambda}'^2)^2]}. \quad (3.27)
\end{aligned}$$

From the interaction Lagrangian in Eq. (3.26), it is straightforward to obtain the Feynman rule for the graviton-axion-axion interaction vertex in the unitary gauge:



$$= - \frac{i}{\sqrt{2}M_P} \left[(k_{1\mu} k_{2\nu} + k_{1\nu} k_{2\mu} - \eta_{\mu\nu} k_1 \cdot k_2) C_{m\lambda\lambda'}^{(1)} - \eta_{\mu\nu} M_c^2 C_{m\lambda\lambda'}^{(2)} \right].$$

Using this vertex rule along with the graviton-polarization sum rule given in Refs. [11, 12], we find

$$\begin{aligned}
|\mathcal{M}(a_\lambda \rightarrow h_{\mu\nu}^{(m)} a_{\lambda'})|^2 &= \frac{(C_{m\lambda\lambda'}^{(1)})^2}{12M_P^2 (mM_c)^4} \left[\lambda^4 + (mM_c)^4 + \lambda'^4 - 2(mM_c)^2 \lambda^2 - 2(mM_c)^2 \lambda'^2 - 2\lambda^2 \lambda'^2 \right]^2 \\
&= \frac{16}{3} \left(\frac{m_X^4}{M_P^2} \right) (\tilde{\lambda}^2 A_\lambda)^2 (\tilde{\lambda}'^2 A_{\lambda'})^2 \quad (3.28)
\end{aligned}$$

for $\lambda' < \lambda$. Consequently, the partial width of a_λ from such a decay is

$$\Gamma(a_\lambda \rightarrow h_{\mu\nu}^{(m)} a_{\lambda'}) = \frac{m_X^4}{3\pi\lambda^3 M_P^2} (\tilde{\lambda}^2 A_\lambda)^2 (\tilde{\lambda}'^2 A_{\lambda'})^2 \left[\lambda^4 + (mM_c)^4 + \lambda'^4 - 2(mM_c)^2 (\lambda^2 + \lambda'^2) - 2\lambda^2 \lambda'^2 \right]^{1/2}. \quad (3.29)$$

Once again, in order to obtain the full contribution $\Gamma(a_\lambda \rightarrow h_{\mu\nu} a)$ to Γ_λ from decays of the form $a_\lambda \rightarrow h_{\mu\nu}^{(m)} a_{\lambda'}$, it is necessary to sum over all combinations of final-state graviton and axion modes which are kinematically accessible.

As before, we will approximate the mode sums over both m and λ' as integrals. This yields the result

$$\begin{aligned} \Gamma(a_\lambda \rightarrow h_{\mu\nu}a) &\lesssim \frac{4m_X^4(\tilde{\lambda}^2 A_\lambda)^2}{3\pi\lambda^3 M_c M_P^2} \int_{\lambda_0}^{\lambda} d\lambda' \int_0^{(\lambda-\lambda')/M_c} dm (\tilde{\lambda}'^2 A_{\lambda'})^2 \\ &\quad \times \left[\lambda^4 + (mM_c)^4 + \lambda'^4 - 2(mM_c)^2(\lambda^2 + \lambda'^2) - 2\lambda^2\lambda'^2 \right]^{1/2} \\ &= \frac{8m_X^4(\tilde{\lambda}^2 A_\lambda)^2}{9\pi\lambda^3 M_c^2 M_P^2} \int_{\lambda_0}^{\lambda} d\lambda' (\tilde{\lambda}'^2 A_{\lambda'})^2 (\lambda + \lambda') \left[(\lambda^2 + \lambda'^2) E\left(\frac{(\lambda - \lambda')^2}{(\lambda + \lambda')^2}\right) - 2\lambda\lambda' K\left(\frac{(\lambda - \lambda')^2}{(\lambda + \lambda')^2}\right) \right], \end{aligned} \quad (3.30)$$

where $K(x)$ and $E(x)$ denote the complete elliptic integrals of the first and second kind, respectively:

$$K(x) = \int_0^{\pi/2} \frac{d\theta}{\sqrt{1 - x^2 \sin^2 \theta}}, \quad E(x) = \int_0^{\pi/2} d\theta \sqrt{1 - x^2 \sin^2 \theta}. \quad (3.31)$$

In order to compare $\Gamma(a_\lambda \rightarrow h_{\mu\nu}a)$ to the rate for a_λ decays to SM fields, we numerically integrate Eq. (3.30) over λ' and compare the resulting expression to the decay rate $\Gamma(a_\lambda \rightarrow \gamma\gamma)$ to photon pairs. In Fig. 1, we plot the ratio $\Gamma(a_\lambda \rightarrow h_{\mu\nu}a)/\Gamma(a_\lambda \rightarrow \gamma\gamma)$ as a function of λ for a variety of different choices of \hat{f}_X . In each case, we have set $\Lambda_G = 1$ TeV, $M_c = 10^{-11}$ GeV, and $\xi = g_G = 1$. It is evident from this plot that only for values of \hat{f}_X above the preferred range $\hat{f}_X \sim 10^{14} - 10^{15}$ GeV does the decay rate for $a_\lambda \rightarrow h_{\mu\nu}a_{\lambda'}$ become similar in magnitude to the rate for axion decays into brane fields. Indeed, for values \hat{f}_X within this preferred range, $\Gamma(a_\lambda \rightarrow h_{\mu\nu}a)/\Gamma(a_\lambda \rightarrow \gamma\gamma)$ never exceeds 0.06, even for the lightest modes in the tower. Furthermore, for values of \hat{f}_X of this magnitude, the lifetimes for all a_λ light enough to have $\Gamma(a_\lambda \rightarrow h_{\mu\nu}a)/\Gamma(a_\lambda \rightarrow \gamma\gamma)$ near this maximal value are parametrically larger than the present age of the universe, even once the additional contribution to Γ_λ from $a_\lambda \rightarrow h_{\mu\nu}a_{\lambda'}$ decays is taken into account. Consequently, the decays of such fields are not cosmologically relevant, and since the branching fraction for all other, heavier a_λ into final states involving KK gravitons is utterly negligible. We therefore conclude that intra-ensemble decays are not phenomenologically relevant for bulk-axion models of dynamical dark matter.

Up to this point, we have focused chiefly on the effect of the tensor KK modes of the higher-dimensional graviton field on axion production in the early universe. However, we have yet to address the effect of graviscalars such as the radion on axion production. Since our minimal DDM model involves only a single extra dimension, only a single physical graviscalar mode (proportional to $h_{55}^{(0)}$) appears in the theory. Furthermore, while the masses of the $h_{\mu\nu}^{(m)}$ are dictated by the compactification geometry alone, the mass of this radion field depends on the details of the mechanism through which the radius of the extra dimension is stabilized, and is consequently highly model-dependent.

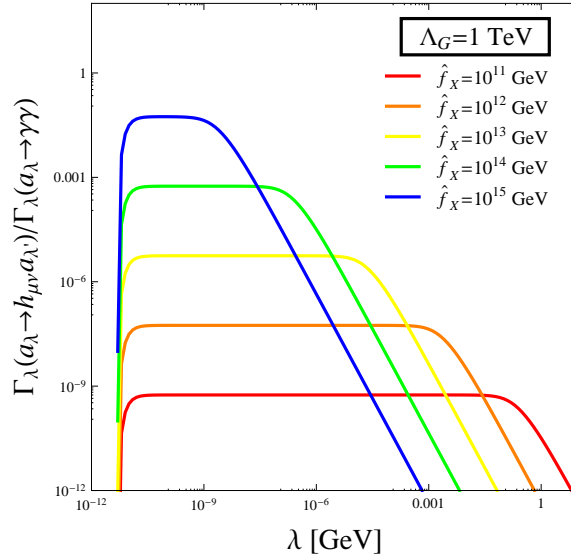


FIG. 1: The ratio $\Gamma(a_\lambda \rightarrow h_{\mu\nu}a)/\Gamma(a_\lambda \rightarrow \gamma\gamma)$, shown as a function of λ for several different values of \hat{f}_X . Here we have set $\Lambda_G = 1$ TeV and $\xi = g_G = 1$, and we have taken the compactification scale to be $M_c = 10^{-11}$ GeV. It is clear from this plot that this ratio is safely below unity for \hat{f}_X within our preferred region $10^{14} - 10^{15}$ GeV.

In this paper, we assume that the physical radion field is sufficiently heavy so as not to play a significant role in the decay phenomenology of the light a_λ fields which contribute significantly to Ω_{tot}^* . Nevertheless, we note that in scenarios which involve multiple extra dimensions of comparable size, or scenarios in which a specific model for radion stabilization is invoked, graviscalars may play a more significant role in the phenomenology of the dark sector.

C. Axion Production from Cosmic Strings

A population of cold axions can also be generated by the decays of topological defects. In our axion DDM model, this includes decays of the cosmic strings associated with the breaking of the global $U(1)_X$ symmetry. Such decays are relevant in situations in which this symmetry remains unbroken until after inflation, *i.e.*, $H_I \gtrsim 2\pi\hat{f}_X$. By contrast, in situations in which $H_I \lesssim 2\pi\hat{f}_X$ and the $U(1)_X$ is spontaneously broken prior to the inflationary epoch, cosmic strings and other topological defects are washed out by the rapid expansion of the universe during cosmic inflation. Consequently, in this latter case, axion production from the decays of cosmic strings can safely be ignored.

In this paper, we are primarily interested in high values of $\hat{f}_X \sim 10^{14} - 10^{15}$ GeV, as these values characterize our preferred region of parameter space. Likewise, we will primarily be interested in relatively low values of H_I , which may be realized naturally in the LTR cosmology. For this reason we shall assume that $H_I \lesssim 2\pi\hat{f}_X$ in what follows. We see, then, that no significant population of axions is produced by cosmic-string decay.

D. Axion Production from the Thermal Bath

Another mechanism through which a relic population of axions may be produced in the early universe is a thermal one: via their interactions with the SM fields in the radiation bath. Unlike the axion population generated by vacuum misalignment, which is characterized by a highly non-thermal velocity distribution (essentially that of a Bose-Einstein condensate) and is therefore by nature cold, this population is characterized by a thermal velocity distribution. Indeed, the properties of a thermal population of axions can differ substantially from that of a population of axions generated via misalignment production.

A number of processes contribute to thermal axion production in the early universe, and the processes which are the most relevant for the production of standard axions dominate for each a_λ in this scenario as well. Among hadronic processes, which play an important role in axion production when c_g is non-vanishing, $q\gamma \rightarrow qa_\lambda$ and $qg \rightarrow qa_\lambda$ dominate for $T \gtrsim \Lambda_{\text{QCD}}$, while pion-axion conversion off nuclei (including all processes of the form $N\pi \rightarrow N'a_\lambda$, where $N, N' = \{n, p\}$ and π denotes either a charged or neutral pion) and the purely pionic process $\pi\pi \rightarrow \pi a_\lambda$ dominate at lower temperatures. The rate for the high-temperature process is [13]

$$\Gamma(q\gamma \rightarrow qa_\lambda) = \frac{g_s^2 T^3 \tilde{\chi}^4 A_\lambda^2}{64\pi^5 \hat{f}_X^2} \ln \left[\left(\frac{T}{m_g} \right)^2 + 0.406 \right], \quad (3.32)$$

where m_g is the plasma mass for the gluon, given in terms of the effective number of quark flavors N_f at temperature T by

$$m_g(T) = \frac{g_s T}{3} \sqrt{3 + N_f/2}. \quad (3.33)$$

Likewise, the rates for pion-conversion off nuclei and pionic production are well estimated by the expressions [14–16]

$$\begin{aligned} \Gamma(N\pi \rightarrow N'a_\lambda) &= \frac{T^{7/2} m_N^{3/2} \tilde{\chi}^4 A_\lambda^2 e^{-m_N/T}}{6\zeta(3)(2\pi)^{5/2} \hat{f}_X^2 f_\pi^2} \left[1.64(5C_{an}^2 + 5C_{ap}^2 + 2C_{an}C_{ap}) + 6C_{a\pi N}^2 \right] \int_0^\infty dx_1 \frac{x_1 y_1^3}{e^{y_1} - 1} \\ \Gamma(\pi\pi \rightarrow \pi a_\lambda) &= \frac{3\zeta(3) T^5 C_{a\pi}^2 \tilde{\chi}^4 A_\lambda^2}{1024\pi^7 \hat{f}_X^2 f_\pi^2} \int_0^\infty \int_0^\infty \frac{dx_1 dx_2 x_1^2 x_2^2}{y_1 y_2 (e^{y_1} - 1)(e^{y_2} - 1)} \int_{-1}^1 d\mu \frac{(s - m_\pi^2)^3 (5s - 2m_\pi^2)}{s^2 T^4}, \end{aligned} \quad (3.34)$$

where, once again, $\zeta(x)$ denotes the Riemann zeta function, and the effective coupling coefficients C_{ap} , C_{an} , $C_{a\pi}$, and $C_{a\pi N}$ are given in Eqs. (2.19) and (2.20). Since these processes are mediated by strong interactions, they tend to dominate the production rate for a hadronic axion at temperatures $T \gtrsim 100$ MeV, at which the number densities of pions and other hadronic species are unsuppressed.

In addition to these hadronic processes, there are several process involving the interactions between the a_λ and the e^\pm and photon fields which contribute to the axion production rate, and indeed dominate that rate at temperatures

$T \ll \Lambda_{\text{QCD}}$. The first of these is the inverse-decay process $\gamma\gamma \rightarrow a_\lambda$, the rate for which is given by

$$\Gamma(\gamma\gamma \rightarrow a_\lambda) = 2 \frac{\lambda^5 G_\gamma (\tilde{\lambda}^2 A_\lambda)^2}{\zeta(3) \hat{f}_X^2 T^2} K_1\left(\frac{\lambda}{T}\right) \quad (3.35)$$

where $K_1(x)$ and $K_2(x)$ respectively denote the Bessel function of the first and second kind, and $G_\gamma = \alpha^2 c_\gamma^2 / 256 \pi^2$. Another is the Primakoff process $e^\pm \gamma \rightarrow e^\pm a$. For $T, m_e \gg \lambda$, the rate for this process is well approximated by [17]

$$\Gamma_{\text{Prim}}(e^\pm \gamma \rightarrow e^\pm a_\lambda) = \frac{\alpha^3 c_\gamma^2 n_e}{192 \zeta(3) \hat{f}_X^2} \tilde{\lambda}^4 A_\lambda^2 \left[\ln\left(\frac{T^2}{m_\gamma^2}\right) + 0.8194 \right], \quad (3.36)$$

where the plasma mass m_γ of the photon is given by $m_\gamma = eT/3$. In the approximation of vanishing chemical potential, the number density of electrons (plus positrons) n_e takes the well-known form

$$n_e = \begin{cases} \frac{3\zeta(3)}{\pi^2} T^3, & T \gtrsim m_e \\ 4 \left(\frac{T m_e}{2\pi}\right)^{3/2} e^{-m_e/T} & T \lesssim m_e. \end{cases} \quad (3.37)$$

Finally, if $c_e \neq 0$ in Eq. (2.5) and the axion couples directly to the electron field, there can be an additional contribution to the $e^\pm \gamma \rightarrow e^\pm a$ rate from a process akin to Compton scattering, but with an axion replacing the photon in the final state. The rate for this process can be estimated as [18]:

$$\Gamma_{\text{Comp}}(e^\pm \gamma \rightarrow e^\pm a_\lambda) \sim \frac{4\alpha c_e^2 n_e}{\hat{f}_X^2} (\tilde{\lambda}^2 A_\lambda)^2 \times \begin{cases} \frac{m_e^2}{T^2} & T \gtrsim m_e \\ 1 & T \lesssim m_e. \end{cases} \quad (3.38)$$

In Fig. 2, we provide a pictorial comparison of the rates for the axion-production processes enumerated above as functions of temperature. The left panel shows the rates for the production of a single axion species a_λ with $\lambda = 1$ MeV in a scenario with $\hat{f}_X = 10^{15}$ GeV, $M_c = 10^{-11}$ GeV, and $\Lambda_G = 1$ TeV. As before, we have taken $\xi = 1$ and set $c_g = c_\gamma = c_e = 1$. The red curve corresponds to the rate $\Gamma(\pi\pi \rightarrow \pi a_\lambda)$ for the pionic process; the orange curve to the rate $\Gamma_{\text{Prim}}(e^\pm \gamma \rightarrow e^\pm a_\lambda)$ for the Primakoff process; the green curve to the rate $\Gamma(\gamma\gamma \rightarrow a)$ for the inverse-decay process; the blue curve to the rate $\Gamma(N\pi \rightarrow N' a_\lambda)$ for the pion-conversion process off nuclei; and the purple curve to the rate $\Gamma(q\gamma \rightarrow q a_\lambda)$ for the quark-gluon process. As the hadron description of the theory is valid only for $T \lesssim \Lambda_{\text{QCD}}$, and likewise, the quark/gluon description is only valid for $T \gtrsim \Lambda_{\text{QCD}}$, the rates $\Gamma(\pi\pi \rightarrow \pi a_\lambda)$, $\Gamma(N\pi \rightarrow N' a_\lambda)$, and $\Gamma(q\gamma \rightarrow q a_\lambda)$ are only defined on one side or the other of this scale. The yellow curve corresponds to the rate $\Gamma_{\text{Comp}}(\pi\pi \rightarrow \pi a_\lambda)$ for the Compton-like process for $c_e = 1$. For purposes of comparison, we also show the Hubble parameter as a function of T for two different cosmologies: the standard cosmology (black dashed curve), and an LTR cosmology with a reheating temperature $T_{\text{RH}} = 5$ MeV (black dot-dashed curve). The value of λ we have chosen here is well within the asymptotic regime for this choice of M_c and \hat{f}_X ; hence the rates displayed here represent take essentially the maximal values possible for any a_λ in the scenario. In the right panel of Fig. 2, we show, for the same choice of M_c and \hat{f}_X , the total contribution to the axion-production rate obtained by summing the rates for all a_λ for which $\lambda \leq T$ — *i.e.*, those which will be kinematically accessible at a given temperature.

The most salient lesson to draw from Fig. 2 is that even after the contributions from all kinetically accessible a_λ states are included in the thermal axion-production rate, none of the relevant processes by which a thermal population of axions might be produced comes close to satisfying the $\Gamma \sim H$ criterion. This implies that the a_λ , even when taken together, never attain thermal equilibrium with the plasma after inflation ends. Furthermore, these results also justify the claims made above, that the electron Primakoff process and inverse decays of the form $\gamma\gamma \rightarrow a$ are the most relevant axion-production processes for $T \lesssim \Lambda_{\text{QCD}}$, while hadronic processes dominate the axion-production rate for $T \gtrsim \Lambda_{\text{QCD}}$.

Let us now estimate the contribution to Ω_{tot} from thermal axion production in the context of an LTR cosmology with a reheating temperature of $T_{\text{RH}} = 5$ MeV. For concreteness, we focus on the case of a photonic axion with $c_\gamma = 1$ and $c_g = c_i = 0$ for all i ; however, the results for other coupling assignments should not differ drastically from those obtained here. We begin by noting that any contribution to Ω_λ generated at temperatures $T \gtrsim T_{\text{RH}}$, *i.e.*, during the reheating phase, will be substantially diluted due to entropy production from inflaton decays. It is therefore legitimate to restrict our attention to axion production within the subsequent RD era. For a photonic axion, the processes which contribute to thermal axion production are inverse decays and $e^\pm \gamma \rightarrow e^\pm a$, the latter of which, since we are assuming

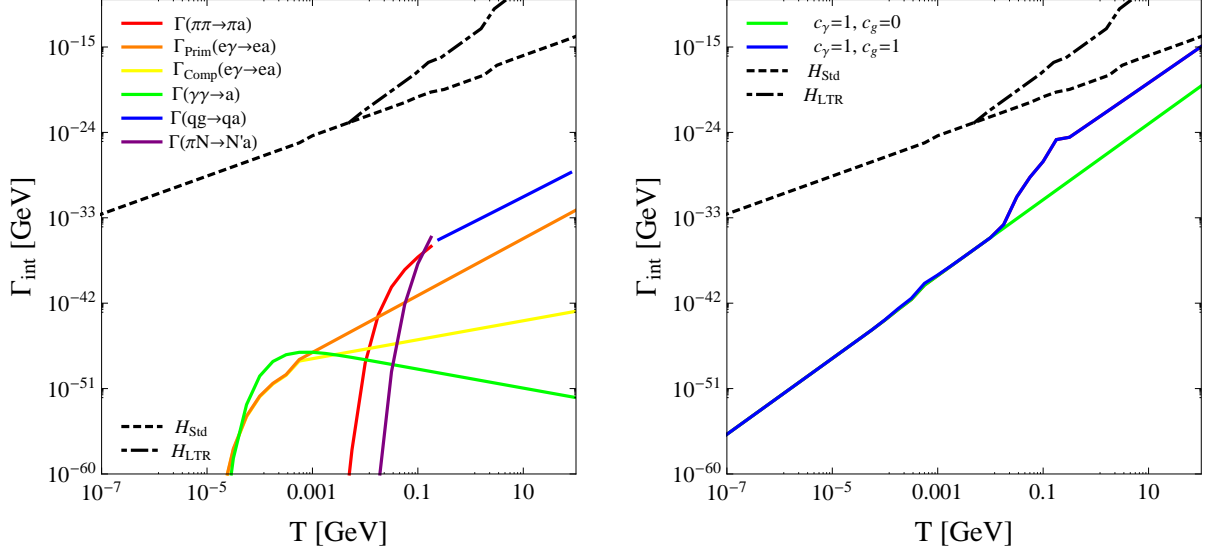


FIG. 2: A comparison of the rates associated with different axion-production processes in the early universe. Here we have taken $M_c = 10^{-11}$ GeV, $\hat{f}_X = 10^{15}$ GeV, $\Lambda_G = 1$ TeV, $T_{RH} = 5$ MeV, and $\xi = 1$. The left panel shows the production rate for each process for an individual axion species a_λ with $\lambda = 1$ MeV (*i.e.*, a value well within the asymptotic, large- λ regime, where the rates are the least suppressed). The right panel shows the integrated production rate for each process, including contributions from all modes with $\lambda < T$. The most relevant processes for thermal axion production in this scenario are $\pi\pi \rightarrow \pi a_\lambda$ production (red curve), $e^\pm\gamma \rightarrow e^\pm a_\lambda$ via the Compton process (yellow curve), $e^\pm\gamma \rightarrow e^\pm a_\lambda$ production via the Primakoff process (orange curve), inverse decays of the form $\gamma\gamma \rightarrow a_\lambda$ (green curve), production via the quark-gluon process $qg \rightarrow qa$ (blue curve), and pion-production off nuclei (purple curve). It should be noted that the Compton process requires a non-zero electron-electron-axion coupling c_e , and that the curve shown here corresponds to the case in which $c_e = 1$. The value of the Hubble parameter as a function of T in both the Standard (black dashed curve) and LTR (black dash-dotted curve) cosmologies are also shown.

$c_e = 0$, is dominated by the Primakoff process. The Boltzmann equation for the number density n_λ of each a_λ is therefore effectively given by

$$\dot{n}_\lambda + (3H + \Gamma_\lambda)n_\lambda = C_\lambda^{\text{ID}}(T) + C_\lambda^{\text{Prim}}(T) \quad (3.39)$$

for $T \lesssim T_{RH}$, where $C_\lambda^{\text{Prim}}(T)$ and $C_\lambda^{\text{ID}}(T)$ are the contact terms associated with the electron-Primakoff and inverse-decay rates given in Eqs. (3.36) and (3.35), respectively. For $T \gg \lambda, m_e$, these contact terms are well-approximated by the expressions

$$\begin{aligned} C_\lambda^{\text{Prim}}(T) &\approx \frac{2\alpha}{3\pi^2} G_\gamma (\tilde{\lambda}^2 A_\lambda)^2 \frac{T^6}{\hat{f}_X^2} \left[\ln \left(\frac{9}{4\pi\alpha} \right) + 0.8194 \right] \\ C_\lambda^{\text{ID}}(T) &\approx 2G_\gamma (\tilde{\lambda}^2 A_\lambda)^2 \frac{\lambda^5 T}{\pi^2 \hat{f}_X^2} K_1 \left(\frac{\lambda}{T} \right), \end{aligned} \quad (3.40)$$

where $K_1(x)$ denotes the Bessel function of the first kind. To obtain a rough estimate of the relic abundance in situations in which either m_e or λ is comparable to or greater than T , we modify the expression for $C_\lambda^{\text{Prim}}(T)$ given in Eq. (3.40) by including an additional exponential factor $e^{-(\lambda+m_e)/T}$ to model the effect of Boltzmann suppression.

From Eq. (3.39) we estimate the relic abundance of axions produced by interactions with the SM particles in the thermal bath. To do so, we neglect the decay term and rewrite the resulting equation in terms of the quantity $Y_\lambda \equiv n_\lambda/s$, where s is the entropy density, in order to remove the Hubble term:

$$s\dot{Y}_\lambda \approx C_\lambda^{\text{ID}}(T) + C_\lambda^{\text{Prim}}(T)e^{-(\lambda+m_e)/T}. \quad (3.41)$$

By numerically integrating this equation, we obtain an estimate of the thermal contribution $\Omega_\lambda^{(\text{therm})}$ to the abundance Ω_λ of each a_λ at present time:

$$\Omega_\lambda^{(\text{therm})} \approx \frac{\lambda T_{\text{now}}^3 t_{\text{MRE}}}{\rho_{\text{crit}}} \int_{T_{\text{now}}}^{T_{RH}} \frac{3}{\kappa(T)} \left(\frac{T_{\text{MRE}}}{T} \right)^{3/\kappa(T)} \frac{g_{*s}(T_{\text{now}})}{g_{*s}(T)} \left[C_\lambda^{\text{ID}}(T) + C_\lambda^{\text{Prim}}(T)e^{-(\lambda+m_e)/T} \right] dT, \quad (3.42)$$

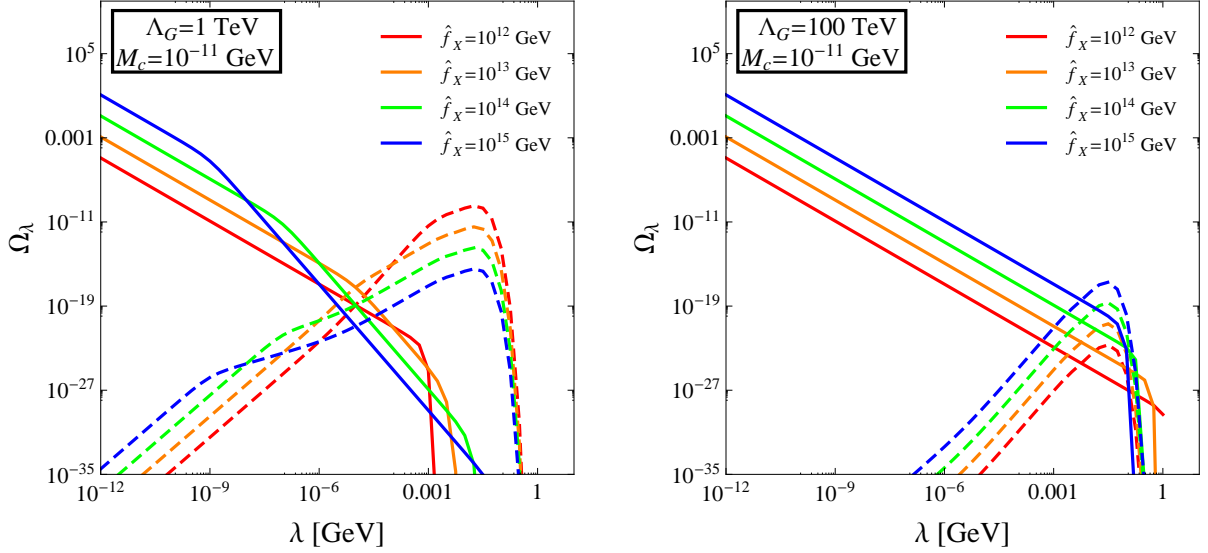


FIG. 3: Contributions to the individual mode abundances Ω_λ for a photonic axion from thermal production (dashed curves) and misalignment production (solid curves), plotted as functions of λ for $\hat{f}_X = 10^{12}$ GeV (red curves), $\hat{f}_X = 10^{13}$ GeV (orange curves), $\hat{f}_X = 10^{14}$ GeV (green curves), $\hat{f}_X = 10^{15}$ GeV (blue curves). The left panel displays the results for $\Lambda_G = 1$ TeV, while the right panel displays the results for $\Lambda_G = 100$ TeV. The other model parameters have been set to $M_c = 10^{-11}$ GeV, $T_{\text{RH}} = 5$ MeV, $\xi = g_G = c_\gamma = 1$.

where $g_{*s}(T)$ is the number of interacting degrees of freedom present in the thermal bath at temperature T , and where $\kappa(T)$ is defined in Eq. (3.3). The results of this integration are displayed in Fig. 3. In this figure, we compare the contributions to the relic abundance Ω_λ of a given a_λ from misalignment production and thermal production for a variety of different choices of the model parameters.

It is clear from Fig. 3 that for these parameter assignments, $\Omega_\lambda^{(\text{therm})}$ only becomes comparable with the relic-density contribution $\Omega_\lambda^{(\text{mis})}$ from vacuum misalignment for reasonably heavy a_λ . Neither $\Omega_\lambda^{(\text{mis})}$ nor $\Omega_\lambda^{(\text{therm})}$ for such a_λ is non-negligible compared with the $\Omega_\lambda^{(\text{mis})}$ contribution from the lighter modes. Indeed, summing over λ to obtain the total thermal contribution $\Omega_{\text{tot}}^{(\text{therm})}$ to the axion relic abundance at present time yields $3.8 \times 10^{-6} \lesssim \Omega_{\text{tot}}^{(\text{therm})} \lesssim 3.8 \times 10^{-4}$. We may therefore safely conclude that $\Omega_{\text{tot}}^{(\text{therm})} \ll \Omega_{\text{tot}}^{(\text{mis})}$ within the preferred region of parameter space for bulk-axion models of dynamical dark matter, and that the population of a_λ generated by the misalignment mechanism dominates the relic density of the DDM ensemble.

To summarize the results of this section, we have examined the primary mechanisms through which a cosmological population of DDM axions may be generated, including misalignment production, thermal production, and production by decaying relics. We have shown that within the preferred region of parameter space specified in Ref. [2], the contribution to the total present-day dark-matter relic abundance from misalignment production $\Omega_{\text{tot}}^{(\text{mis})}$ indeed dominates over the contributions from all other production mechanisms. This justifies the emphasis placed on misalignment production in Ref. [2]. Still, we note that although populations of axions produced via those other channels collectively represent a negligible fraction of Ω_{tot} , those populations can nevertheless play an important role in constraining bulk-axion DDM models. For example, the thermal population of axions discussed above can still leave a significant imprint on the diffuse X-ray spectrum despite the small size of $\Omega_{\text{tot}}^{(\text{therm})}$, because $\Omega_\lambda^{(\text{therm})} \ll \Omega_\lambda^{(\text{mis})}$ when λ is large. We shall return to this point in Sect. IV G, where we will show that this imprint is nevertheless consistent with current observational limits.

IV. PHENOMENOLOGICAL CONSTRAINTS ON DARK AXION ENSEMBLES

In the previous section we characterized the various mechanisms which contribute to the generation of a cosmological population of relic axions in axion DDM models and compared the sizes of their contributions to Ω_{tot}^* . Given that this population constitutes the dark-matter ensemble in our axion DDM model, we now turn to examine the relevant

phenomenological, astrophysical, and cosmological constraints on that population of axions. As we shall see, some of these constraints pertain generically to any theory of dark matter, or to any theory containing late-decaying relics. Others are particular to models involving light, weakly-coupled fields. Still others pertain to theories with large extra dimensions in general, regardless of the presence or absence of a bulk axion field.

As we have seen in Refs. [1, 2], the properties of the dark-matter ensemble and its constituent fields in our bulk-axion DDM model are determined primarily by three parameters: the compactification scale M_c , the $U(1)_X$ -breaking scale \hat{f}_X , and the confinement scale Λ_G for the gauge group G . Because these parameters play such a central role in characterizing the dark sector in our model, we shall seek to phrase our phenomenological constraints in terms of restrictions on M_c , \hat{f}_X , and Λ_G whenever possible. Of course, in addition to these primary parameters, a number of other ancillary quantities also have an impact on the phenomenology of our model, and thus are also constrained by data. These include the scales H_I and T_{RH} associated with cosmic inflation, the coupling coefficients c_g , c_γ , and c_i , and so forth. Generally speaking, these additional parameters play a subordinate role in determining the mass spectrum and relic abundances of the a_λ , and the values they take are typically far more model-dependent than M_c , \hat{f}_X , and Λ_G . Thus, while certain experimental and observational limits serve to constrain the values these additional parameters may take, it ultimately turns out to be possible to phrase the majority of constraints on our model as bounds on M_c , \hat{f}_X , and Λ_G . Indeed, as we shall see in Sect. V, most of the critical bounds can be expressed conveniently in this manner. We will also be interested in how these bounds constrain certain derived quantities of physical importance, such as the quantity y defined in Eq. (2.12), which quantifies the amount of mixing that occurs across our DDM ensemble.

A. Constraints from Background Geometry

The first set of constraints we consider are those which apply generically to theories with extra dimensions, independently of the presence or properties of the bulk axion field whose KK excitations constitute the DDM ensemble in our model. These constraints arise primarily from experimental limits on the physical effects to which the tower of KK gravitons necessarily present in such theories gives rise. We will primarily focus here on scenarios involving n flat extra dimensions in which the fields of the SM are localized on a 3-brane, while gravity, as always, necessarily propagates throughout the entirety of the $D = (4 + n)$ -dimensional bulk.

Perhaps the most significant and direct bound on M_c in theories with extra dimensions arises due to modifications of Newton's law at short distances as a consequence of KK-graviton exchange. The lack of evidence for any such effect at modified-gravity experiments to date implies constraints on the sizes and shapes of those extra dimensions. For the case of a single large, flat extra dimension, the current limit on the compactification scale from such experiments is [19]

$$M_c \gtrsim 3.9 \times 10^{-12} \text{ GeV} . \quad (4.1)$$

This lower limit on the compactification scale is robust in the sense that even if there exist additional compact dimensions with radii $r_i \ll 1/M_c$, this bound is essentially unaffected. For this reason, Eq. (4.1) turns out to represent the most significant constraint on the parameter space of bulk-axion DDM models from considerations which derive solely from the presence of extra dimensions.

There also exist additional constraints on the compactification geometry which arise due the relationship between this scale, the effective four-dimensional Planck scale M_P , and the fundamental scale of quantum gravity M_D . These constraints are generally more sensitive to the details of the compactification scenario. In general, the fundamental scale M_D is related to M_P by [6]

$$M_P^2 = V_n M_D^{2+n} , \quad (4.2)$$

where V_n is the volume of the n -dimensional manifold on which the extra dimensions are compactified. For the simple case in which this manifold is a flat, rectangular n -torus, the volume V_n is simply the product of $(2\pi r_i)$ for each cycle of the torus. Assuming all radii are equal to a common radius r , we then have

$$r^{-1} \geq 2\pi M_D^{\text{min}} \left(\frac{M_D^{\text{min}}}{M_P} \right)^{2/n} . \quad (4.3)$$

Bounds on the scale M_D appearing in the literature are frequently predicated on these assumptions. However, we emphasize that in situations in which the r_i are not all equal, or in which the compactification geometry differs from that of a flat, rectangular n -torus, those bounds can be considerably modified.

Under the assumption that the compactification geometry resembles that on which Eq. (4.3) is predicated, one may derive constraints on M_D , r , or combinations of the two. For example, one class of constraints which arise in theories with extra dimensions are those implied by the non-observation of effects related to thermal KK graviton production in astrophysical sources such as stars [20] and supernovae [21, 22]. A brief synopsis of the most relevant bounds in this class is given in Ref. [20], all of which depend crucially on the fundamental quantum-gravity scale M_D . The most stringent of these constraints currently derives from limits on photoproduction and stellar heating by gravitationally trapped KK gravitons in the halos of neutron stars. Indeed, for a theory involving n extra dimensions with equal radii, one finds that for $n = 2$, the bound is $r^{-1} \geq 5.8 \times 10^{-7}$ GeV, while for $n = 3$, one finds $r^{-1} \geq 3.8 \times 10^{-10}$ GeV [20].

Collider data also place limits on r and M_D in theories with extra dimensions. Searches for evidence of KK-graviton production in the monojet (*i.e.*, $j + \cancel{E}_T$) channel have been performed by the ATLAS [29, 30] and CMS [31] collaborations. The most recent ATLAS analysis [30], conducted with 1 fb^{-1} of integrated luminosity, constrains $M_D \gtrsim \{3.16, 2.50, 2.15\}$ TeV at 95% C.L. for $n = \{2, 3, 4\}$ flat extra dimensions with equal radii. The most recent CMS analysis [31], conducted at a comparable integrated luminosity, yields the slightly more stringent constraint $M_D \gtrsim \{4.03, 3.21, 2.80\}$ TeV at 95% C.L. for the corresponding values of n . Limits from searches for KK-graviton effects in the diphoton [32] and dimuon [33] channels at 36 pb^{-1} and 39 pb^{-1} of integrated luminosity, respectively, have also been derived by the CMS collaboration, but these are currently less stringent than the constraints from the $j + \cancel{E}_T$ channel.

It is important to realize that the aforementioned bounds on M_D as a function of the compactification geometry do *not* necessarily translate directly into analogous bounds on f_X for a given \hat{f}_X . Unlike the graviton field, the bulk axion field in our DDM model need not necessarily propagate throughout the entirety of the extra-dimensional volume, but may in principle also be confined to a $(4 + n_a)$ -dimensional subspace of that volume, where $n_a < n$. When this is the case, \hat{f}_X is related to f_X by the generalization of Eq. (2.7):

$$\hat{f}_X^2 = V_{n_a} f_X^{2+n_a}. \quad (4.4)$$

Note that this relationship differs from that which exists between M_P and M_D because $n_a < n$. In this paper, as in Ref. [2], we focus on the case in which the axion field propagates in a single extra dimension of radius R , irrespective of the size, shape, or number of extra dimensions which compose the totality of the bulk. Accordingly, we define $M_c = 1/R$ to be the compactification scale associated with this particular extra dimension, and we shall use this notation throughout. In this paper, we are not aiming to set M_D at or even near the TeV scale, since we are not attempting to solve the hierarchy problem, but rather to address the dark-matter problem. We will therefore assume that the structure of any additional bulk dimensions is such that phenomenological constraints on M_D and the associated compactification geometry are satisfied. Note, however, that the Newton's-law bound in Eq. (4.1) does apply to M_c , as it applies to the compactification scale associated with any individual extra dimension.

Another class of constraints on scenarios involving large extra dimensions applies to ancillary variables which characterize the cosmological context in which our model is situated. For example, the prediction of the observed abundances of the light elements via big-bang nucleosynthesis (BBN) is one of the greatest successes of the standard cosmology. Consistency with these predictions requires that effects stemming from the presence of these extra dimensions not disrupt BBN. Successful nucleosynthesis requires that the expansion rate of the universe during the BBN epoch, as quantified by the Hubble parameter $H(T)$, must not deviate from its usual, four-dimensional value by more than around 10% [7]. In other words, there exists some temperature $T_* \geq T_{\text{BBN}} \sim 1 \text{ MeV}$ (usually dubbed the “normalcy temperature” in the literature) below which the radii of all extra dimensions are effectively fixed and the bulk is effectively empty of energy density. A variety of different considerations constrain T_* , most of which are related to the potentially observable effects of KK-graviton dynamics in the early universe:

- Interactions between the SM fields on the brane and the bulk graviton field result in a transfer of energy from the brane to the bulk, and a consequent cooling of the radiation bath on the brane. Substantial energy loss via this “evaporative cooling” mechanism would result in a modification of the expansion rate of the universe. At temperatures $T \lesssim T_{\text{BBN}}$, such a modification would distort the light-element abundances away from those predicted by standard BBN. Thus, the strength of the interactions between SM particles and excitations of the graviton field is constrained.
- If the collective energy density associated with the graviton KK modes is substantial, that energy density could cause the universe to become matter-dominated too early. In extreme cases, it could even overclose the universe.
- Late decays of KK gravitons could result in distortions of the abundances of light elements away from the values predicted by BBN [7], which accord well with the observed values for these abundances. Such decays could also result in significant entropy production.

- The relationship between the Hubble parameter H and the total energy density ρ of the universe is modified at early times in higher-dimensional scenarios, even when that energy density is overwhelmingly dominated by brane-localized states [23–25]. Such a modification could have a substantial effect on BBN as well.

The constraints on T_* implied by these considerations have been reckoned by a number of authors [7, 26], and while the precise values of the bounds so derived again depend on the number, size, and shape of the extra dimensions, the value of M_D , *etc.*, the most stringent (which tend to come from limits on the late decays of the excited KK modes) generally tend to restrict T_* to within the rough range $4 \text{ MeV} \lesssim T_* \lesssim 20 \text{ MeV}$ [7].

One possibility for achieving such conditions is to posit that T_* be identified with the reheating temperature T_{RH} associated with a period of cosmic inflation initiated by an inflaton field which is localized on the same 3-brane as the SM fields. During such an inflationary epoch, any contributions to the energy density of the universe from bulk states which existed prior to the inflationary epoch (save for those which, like the contributions to ρ_λ from vacuum misalignment, scale like vacuum energy) are inflated away. Furthermore, if the inflaton field decays primarily to other brane-localized states, no substantial population of bulk states is regenerated during the subsequent reheating phase. Thus, by adopting a LTR cosmology with a reheating temperature $4 \text{ MeV} \lesssim T_{\text{RH}} \lesssim 20 \text{ MeV}$, we thereby ensure that the relevant constraints related to KK-graviton production in the early universe are satisfied. We also note that a reheating temperature of $T_{\text{RH}} \gtrsim 4 \text{ MeV}$ is sufficient to ensure that the thermal populations of the SM fields (and, in particular, the three neutrino species) required in standard BBN are generated by the thermal bath after reheating [27, 28].

In summary, while stringent constraints exist on theories with large extra dimensions, these constraints can be satisfied by adopting an LTR cosmology with $4 \text{ MeV} \lesssim T_{\text{RH}} \lesssim 20 \text{ MeV}$ and a compactification manifold for which the astrophysical bounds listed above may consistently be satisfied for a given choice of M_D and f_X . Since Ω_{tot}^* is generated via non-thermal means in our bulk-axion model, as discussed in Sect. III, such a low value of T_{RH} is not an impediment to obtaining a dark-matter relic abundance $\Omega_{\text{tot}}^* \approx \Omega_{\text{CDM}}$. In fact, as shown in Ref. [2], adopting an LTR cosmology is actually an *asset* in terms of generating a dark-matter relic abundance of the correct magnitude. Likewise, since the relationship between \hat{f}_X and f_X need not be identical to the relationship between M_P and M_D , constraints which concern the effects of KK gravitons can be satisfied without imposing equally severe restrictions on the parameters \hat{f}_X , M_C , and Λ_G which govern the properties of the dark-matter ensemble. Indeed, the only significant model-independent constraint on these parameters turns out to be the constraint quoted in Eq. (4.1) from tests of Newton’s law at short distances.

B. Axion Production with Subsequent Detection: Helioscopes and Light Shining Through Walls

We now address the constraints which relate directly to the phenomenological, astrophysical, and cosmological implications associated with the KK tower of axion fields which constitute the DDM ensemble in our model. We begin by discussing the limits derived from a wide variety of experiments designed to detect axions and axion-like particles via their interactions with the photon field. (For extensive reviews of these experiments, see Refs. [34, 35].) To date, none of these experiments have seen any conclusive evidence for such particles, and the null results of these experiments therefore imply constraints on the effective couplings between such axion-like particles and the photon field.

In order to determine how the results of the experiments listed above serve to constrain the parameter space of our bulk-axion DDM model, it is useful to divide those experiments into several broad classes, based on the sort of physical process each probes. One important class of experiments comprises those in which axions are produced via their interactions with the fields of the SM and then subsequently detected via those same interactions. These include helioscope experiments such as CAST [36] and “light-shining-through-walls” (LSW) experiments such as BEV, GammaeV, and ALPS. Searches for coherent conversion of solar axions to X-ray photons in germanium and sodium-iodide crystals via Bragg diffraction which have been performed at experiments such as DAMA [37], TEXONO [38], SOLAX [39], and COSME [40] also fall into this category. The characteristic which distinguishes experiments in this class from others is that these experiments are affected by decoherence phenomena. Indeed, it has been observed [3] that in theories with bulk axions, such phenomena result in a substantial suppression of the rate for any process involving the production and subsequent decay of axion modes relative to naïve expectations.

Let us briefly review the origin of this suppression by focusing on the interaction between the photon field and the axion KK modes given in Eq. (2.5). (The results for the coupling between these modes and the other SM fields are completely analogous.) We begin by defining a state

$$a' \equiv \frac{1}{\sqrt{N}} \sum_n^N r_n a_n, \quad (4.5)$$

which represents the particular linear combination of KK eigenstates a_n that couples to any physics on the brane, such as $F_{\mu\nu}\tilde{F}^{\mu\nu}$ or any pair of SM fields. Here $N \sim f_X/M_c$ denotes the number of modes in the sum. Written in terms of a' , the relevant term in the interaction Lagrangian becomes

$$L_{\text{int}} \ni \frac{\alpha c_\gamma \sqrt{N}}{8\pi^2 \hat{f}_X} a' F_{\mu\nu} \tilde{F}^{\mu\nu} . \quad (4.6)$$

In other words, a' couples to the SM fields with a strength proportional to $\sqrt{N}/\hat{f}_X \sim 1/f_X$. Consequently, the cross-section for any physical process which involves axions production via interactions with the SM fields followed by subsequent detection via the same sorts of interactions will take the form

$$\sigma(t) \propto \frac{N^2}{\hat{f}_X^4} \times P(t) , \quad (4.7)$$

where $P(t) = |\langle a'(t) | a'(t_0) \rangle|^2$ is the probability for a state a' created at time t_0 to be in the same state a' at time t . It can be shown that when N is large, $P(t)$ is given by

$$P(t) = \frac{1}{N^2} \left[\sum_{\lambda} \tilde{\lambda}^8 A_{\lambda}^4 + 2 \sum_{\lambda} \sum_{\lambda' < \lambda} \tilde{\lambda}^4 \tilde{\lambda}'^4 A_{\lambda}^2 A_{\lambda'}^2 \cos \left(\frac{(\lambda^2 - \lambda'^2)(t - t_0)}{2p} \right) \right] , \quad (4.8)$$

where p is the initial momentum of the axion.

At very early times, when $t \approx t_0$, the cosine factor in $P(t)$ is approximately unity for all values of λ and λ' . At such times, all of the terms in the sum appearing in the second term on the right side of Eq. (4.8) add coherently. As a result, this term, combined together with the first term, yields a factor on the order of N^2 . However, as the system evolves, the cosine terms will no longer sum coherently, and a random-walk behavior ensues, according to which the two terms combine to yield a factor of $\mathcal{O}(N)$ rather than of $\mathcal{O}(N^2)$. The time scale τ_D associated with this decoherence — or, more precisely, the scale at which $P(t) = 0.1P(t_0)$ — is found to be [3]

$$\tau_D \approx 10^{-5} \left(\frac{2p}{m_{\text{PQ}}^2} \right) \frac{y^2}{N^2} \approx 1.32 \times 10^{-29} \left(\frac{p}{\text{GeV}} \right) \left(\frac{\hat{f}_X}{\text{GeV}} \right)^{-2} \text{ s} , \quad (4.9)$$

where y is defined in Eq. (2.12). Since τ_D is clearly quite small for any combination of p and f_X values of experimental relevance, any method of detecting axions which relies on their production and subsequent detection will feel the effect of this decoherence. By contrast, detection methods which rely on axion production without subsequent detection (such as missing-energy signals at colliders, energy dissipation from supernovae, *etc.*) or which probe for evidence of a cosmic population of relic axions (such as microwave-cavity experiments) will be unaffected by this phenomenon.

The consequences of axion decoherence for physical processes in the decoherence regime are readily apparent. In this regime, as discussed above, the term in brackets in $P(t)$ scales like N rather than N^2 ; hence any cross-section which takes the form given in Eq. (4.7) will scale with $N \sim f_X/M_c$ according to

$$\sigma(t > \tau_D) \propto \frac{N}{\hat{f}_X^4} \sim \frac{1}{N} \frac{1}{f_X^4} . \quad (4.10)$$

In other words, such cross-sections are suppressed by an additional factor of N relative to the naïve expectation obtained by setting $\hat{f}_X \rightarrow f_X$ in Eq. (4.7). Thus, due to the decoherence effect, any experimental bound on the effective coupling $G_{a\gamma\gamma}$ of a single four-dimensional axion to the photon field which takes the form $G_{a\gamma\gamma}^2 < (G_{a\gamma\gamma}^{\text{max}})^2$ translates to a bound $G_{a\gamma\gamma}^2 < (G_{a\gamma\gamma}^{\text{max}})^2 / \sqrt{N}$ for five-dimensional axion, rather than to $G_{a\gamma\gamma}^2 < (G_{a\gamma\gamma}^{\text{max}})^2 / N$. Given the parametrization for $G_{a\gamma\gamma}$ given in Eq. (2.5), we can phrase any such constraint as a bound on \hat{f}_X :

$$\hat{f}_X \gtrsim \frac{c_\gamma \alpha}{2\pi G_{a\gamma\gamma}^{\text{max}}} \left(\frac{M_c}{f_X} \right)^{1/4} . \quad (4.11)$$

Using Eq. (2.7), we may rewrite this constraint in the form

$$\hat{f}_X \gtrsim \frac{1}{(2\pi)^{13/10}} \left(\frac{c_\gamma \alpha}{G_{a\gamma\gamma}^{\text{max}}} \right)^{6/5} \frac{1}{M_c^{1/5}} = (2.50 \times 10^{-4}) c_\gamma (G_{a\gamma\gamma}^{\text{max}})^{-6/5} M_c^{-1/5} . \quad (4.12)$$

The most stringent limit from the class of experiments categorized above (*i.e.*, those for which the phenomenon of decoherence is relevant) is currently the $G_{a\gamma\gamma} \lesssim 8.8 \times 10^{-11} \text{ GeV}^{-1}$ bound obtained by CAST [36]. The most stringent limit from crystalline detectors is the $G_{a\gamma\gamma} \lesssim 1.7 \times 10^{-9} \text{ GeV}^{-1}$ bound from DAMA [37], and limits on $G_{a\gamma\gamma}$ from LSW experiments are typically roughly three orders of magnitude higher than the CAST limit. The corresponding bound on \hat{f}_X from Eq. (4.12) is

$$\hat{f}_X \gtrsim (2.92 \times 10^8) c_\gamma^{6/5} \left(\frac{M_c}{\text{GeV}} \right)^{-1/5} \text{ GeV} . \quad (4.13)$$

Note that even for M_c at the experimental lower limit given in Eq. (4.1), the constraint in Eq. (4.13) is satisfied as long as $\hat{f}_X \gtrsim 5.58 \times 10^{10} \text{ GeV}$.

C. Microwave-Cavity Experiments and Direct Detection of Dark-Matter Axions

Another class of experiments which place constraints on the couplings of axions and axion-like fields to SM particles consists of those which involve the direct detection of a cosmological population of axions. The most sensitive experiments in this class are those associated with dedicated microwave-cavity detectors such as ADMX [41] and CARRACK [42]. Detectors of this sort are used to search for the resonant conversion of dark-matter axions with mass m_a to photons with energies $E_\gamma \approx m_a$ in the presence of a strong magnetic field. As a result, the observation of a signal at such a detector depends crucially on whether the mass of the axion in question lies within the range of photon energies probed. The axion mass range currently covered by ADMX spans only from $1.9 \times 10^{-15} \text{ GeV}$ to $3.5 \times 10^{-15} \text{ GeV}$ [41], and the projected future mass sensitivity extends only as high as 10^{-13} GeV . Likewise, the projected sensitivity for CARRACK extends only as high as $3.5 \times 10^{-14} \text{ GeV}$.

As discussed in Ref. [2], the region of parameter space which is the most interesting from a DDM perspective is that within which $y \lesssim 1$ and mixing among the light axion KK modes is substantial, for it is this region within which the full tower contributes meaningfully to Ω_{tot}^* . Within this region of parameter space, the lightest mode in the tower has a mass $\lambda_0 \approx M_c/2$. Taken in conjunction with the bound on M_c from modified-gravity experiments given in Eq. (4.1), this result implies that $\lambda_0 \gtrsim 1.5 \times 10^{-12} \text{ GeV}$ in highly-mixed bulk-axion scenarios. The projected ranges for both ADMX and CARRACK lie well below this threshold for λ_0 . We therefore conclude that no meaningful constraints on bulk-axion DDM models can be derived from the results of these experiments.

D. Axion Production without Subsequent Detection: Stars and Supernovae

We now turn to examine an additional class of constraints on bulk-axion DDM models: those related to astrophysical processes in which the a_λ are produced through their interactions with the SM field, but never directly detected. Among the constraints in this class are limits on axions, moduli, and other light scalars derived from the non-observation of their would-be effects on the lifetimes, energy-loss rates, *etc.*, of various astrophysical sources such as stars and supernovae. These effects include the following:

- Axions and other light fields whose interactions with the particles of the SM are extremely weak and whose mean free paths are consequently extremely long can dissipate energy from stars extremely efficiently. Such dissipation can accelerate stellar cooling and result in observable alterations in stellar life cycles, including the life cycle of our own sun.
- Similarly, such light fields can carry away a substantial fraction of the energy liberated by supernovae. Limits may therefore be placed on the strengths of these interactions from the non-observation of such effects for supernova SN1987A.
- A diffuse population of long-lived axions or KK gravitons initially produced by stars and supernovae could decay at late times, distorting light-element abundances and producing an observable X-ray or γ -ray signal in the keV – MeV range or higher. No evidence for such a signal has been seen by EGRET, FERMI, HEAO, Chandra, COMPTEL, *etc.*

As is well known, these considerations lead to some of the most stringent constraints on standard, four-dimensional QCD axions. We now turn to examine how these limits constrain the parameter space of generalized bulk-axion models.

The primary distinction between processes in which the presence of the a_λ is ascertained by direct detection and those in which it is only inferred from an energy deficit is that in the latter class of processes, the a_λ appear as particles in the asymptotic final state. Thus, the contributions from the individual a_λ to the overall event rate for any such a process add not at the amplitude level, but at the cross-section level. The decoherence phenomena discussed in Sect. IV B are therefore irrelevant for such processes, and the total cross-section $\sigma_{\text{tot}}^{\text{prod}}$ for the production of “missing energy” in the form of a_λ fields by any given physical process is simply the sum of the individual production cross-sections $\sigma_\lambda^{\text{prod}}$ for each axion species. Since the effective coupling between each a_λ and any pair of SM fields includes a factor $\tilde{\lambda}^2 A_\lambda / \hat{f}_X$ from mass mixing, as indicated in Eq. (2.17), each of these individual production cross-sections scales as

$$\sigma_\lambda^{\text{prod}} \propto \frac{1}{\hat{f}_X^2} (\tilde{\lambda}^2 A_\lambda)^2. \quad (4.14)$$

When it occurs, axion production will have a characteristic energy scale E_{ch} determined by the surrounding environment. This energy scale may be associated, for example, with the temperature of a star or supernova core, or with the center-of-mass energy \sqrt{s} of a collider. Provided that $E_{\text{ch}} \gg M_c$ (an assumption valid for all physical contexts of relevance in bounding the large-extra-dimension scenarios considered here), it follows that $\lambda \ll E_{\text{ch}}$ for a large number of a_λ . Such a_λ can be considered to be effectively massless as far as production kinematics is concerned, implying that to a very good approximation, $\sigma_\lambda^{\text{prod}}$ depends on λ exclusively through the coupling-modification factor appearing in Eq. (4.14). (For those modes for which threshold effects are important, such an approximation will overestimate $\sigma_\lambda^{\text{prod}}$ and result in an overly conservative bound.) By contrast, $\sigma_\lambda^{\text{prod}}$ will be effectively zero for those a_λ with masses $\lambda \gg E_{\text{ch}}$ in any thermal environment due to Boltzmann suppression, and will vanish outright in a non-thermal one. Therefore, it is reasonable to evaluate $\sigma_{\text{tot}}^{\text{prod}}$ by taking any additional factors in Eq. (4.14) to be essentially independent of λ and by truncating the sum over modes at $\lambda \sim E_{\text{ch}}$. Thus, we find that

$$\sigma_{\text{tot}}^{\text{prod}} \propto \aleph^2(E_{\text{ch}}) / \hat{f}_X^2 \quad (4.15)$$

where the “effective” coupling $\aleph(E_{\text{ch}})$ is given by

$$\aleph(E_{\text{ch}}) \equiv \left[\sum_{\lambda=\lambda_0}^{E_{\text{ch}}} (\tilde{\lambda}^2 A_\lambda)^2 \right]^{1/2}. \quad (4.16)$$

Since the number of modes contributing to $\sigma_{\text{tot}}^{\text{prod}}$ is large by assumption, and since their masses are closely spaced, it is generally legitimate to approximate $\aleph(E_{\text{ch}})$ by an integral

$$\aleph(E_{\text{ch}}) \approx \left[\frac{1}{M_c} \int_{\lambda_0}^{E_{\text{ch}}} (\tilde{\lambda}^2 A_\lambda)^2 d\lambda \right]^{1/2}. \quad (4.17)$$

The quantity $\aleph(E_{\text{ch}})$ clearly plays a crucial role in the phenomenology of bulk-axion scenarios. It is therefore worth pausing a moment to examine in detail how $\aleph(E_{\text{ch}})$ depends on the physical scales \hat{f}_X , M_c , and Λ_G . A straightforward calculation shows that $\aleph(E_{\text{ch}})$ has the parametric scaling behaviors

$$\aleph(E_{\text{ch}}) \sim \begin{cases} \frac{E_{\text{ch}}^{3/2} M_c^{1/2} \hat{f}_X^2}{\Lambda_G^4} & \hat{f}_X \ll \frac{\Lambda_G^2}{M_c} \\ \left(\frac{E_{\text{ch}}}{M_c} \right)^{1/2} & \hat{f}_X \gg \frac{\Lambda_G^2}{M_c} \end{cases}. \quad (4.18)$$

The first case in Eq. (4.18) corresponds to $y \ll 1$, signaling a highly-mixed axion KK tower for which $\tilde{\lambda}^2 A_\lambda \sim \tilde{\lambda}$. By contrast, the second case corresponds to $y \gg 1$, signaling a relatively unmixed axion KK tower for which $\tilde{\lambda}^2 A_\lambda \sim \text{constant}$. These results for $\aleph(E_{\text{ch}})$ are illustrated in the left panel of Fig. 4 for $E_{\text{ch}} = 30$ MeV, a value which is physically meaningful in that it corresponds roughly to the core temperature of supernova SN1987A. Remarkably, we observe that $\aleph(E_{\text{ch}})$ experiences a *suppression* for $y \ll 1$. In other words, mixing within the axion KK tower acts to suppress the magnitude of the total production cross-section for processes in which the a_λ appear as missing energy. This is an important result, for it indicates that constraints on the parameter space of our bulk-axion DDM model derived from limits on axion production in stars, supernovae, colliders, *etc.*, will be considerably weaker than one

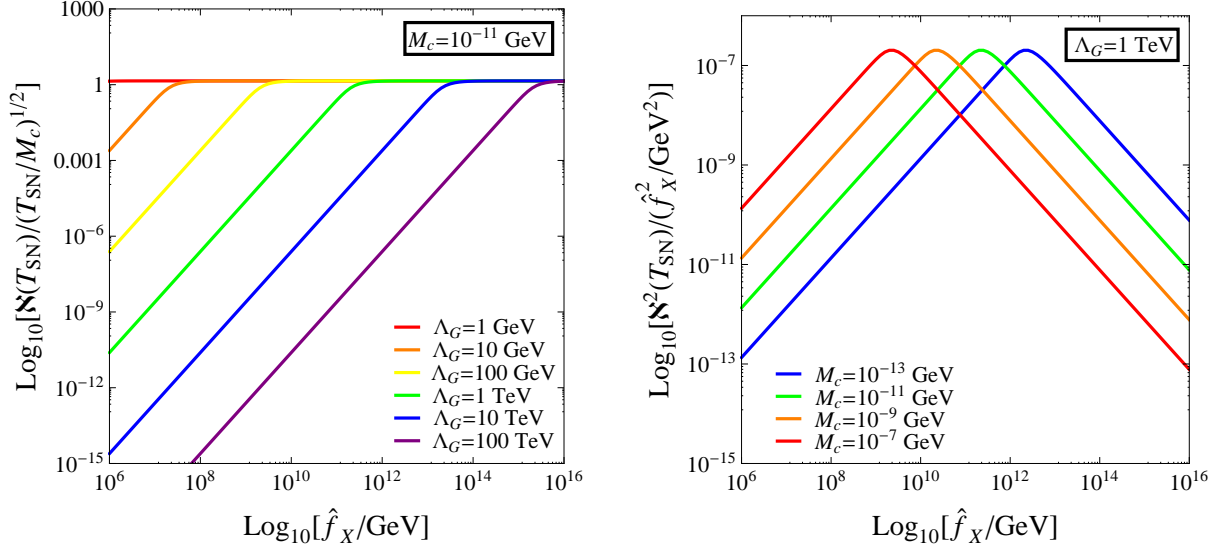


FIG. 4: The dimensionless “effective coupling” factor $\mathcal{N}(E_{\text{ch}})$ defined in Eq. (4.16), shown as a function of the relevant scales M_c , \hat{f}_X , and Λ_G . In the left panel, we display curves of $\mathcal{N}(E_{\text{ch}})$, each corresponding to a particular value of Λ_G and normalized to the value $(E_{\text{ch}}/M_c)^{1/2}$ taken by $\mathcal{N}(E_{\text{ch}})$ in the absence of mixing, as a function of \hat{f}_X with fixed $M_c = 10^{-11}$ GeV. It is readily apparent that the net effect of mixing within the KK axion tower is to significantly suppress this effective coupling, thereby loosening the corresponding production-cross-section constraints. In the right panel, we display curves showing the overall cross-section-suppression factor $\mathcal{N}^2(E_{\text{ch}})/\hat{f}_X^2$ as a function of \hat{f}_X for fixed $\Lambda = 1$ TeV, each corresponding to a particular value of M_c . For each set of curves, we have taken $\xi = g_G = 1$, and have chosen $E_{\text{ch}} = 30$ MeV, which corresponds roughly to the core temperature T_{SN} of SN1987A.

might expect from naïve dimensional analysis. Moreover, this result applies more generally to any theory involving KK towers of scalar fields whose squared-mass matrix contains both brane-mass and KK-mass terms.

In order to illustrate more explicitly the physical consequences of $\mathcal{N}(E_{\text{ch}})$ in our bulk-axion DDM model, we likewise display the behavior of the overall scaling factor $\mathcal{N}^2(E_{\text{ch}})/\hat{f}_X^2$ for $\sigma_{\text{tot}}^{\text{prod}}$ in the right panel of Fig. 4. The results shown in this panel further illustrate a significant general property of this scaling factor: namely, that the cross-section is actually suppressed not only for large \hat{f}_X , but also for small \hat{f}_X , due to the parametric behavior of $\mathcal{N}(E_{\text{ch}})$ described in Eq. (4.18). Thus, for any given choice of Λ_G and M_c , there exists a maximum possible value for $\sigma_{\text{tot}}^{\text{prod}}$, which is only attained at some particular value of \hat{f}_X . These results again illustrate the dramatic effect that $\mathcal{N}(E_{\text{ch}})$ can have in suppressing $\sigma_{\text{tot}}^{\text{prod}}$ in our bulk-axion DDM model.

Within the class of constraints from processes in which axions are produced but not subsequently detected, use of $\mathcal{N}(E_{\text{ch}})$ allows us to translate experimental bounds on four-dimensional axion models into bounds on theories including towers of bulk scalars. The leading such bound is obtained from energy-loss limits from SN1987A. For a standard four-dimensional QCD axion, this bound is roughly [43]

$$f_a \gtrsim 4 \times 10^8 \text{ GeV} . \quad (4.19)$$

By contrast, in the bulk-axion scenario under consideration here, each a_λ light enough to be produced within the thermal environment of SN1987A can contribute to the overall energy-dissipation rate. Since the temperature T_{SN} associated with the supernova core is roughly 30 MeV, the appropriate modification of Eq. (4.19) for a general axion which couples to hadrons with a coupling coefficient comparable in magnitude to that of a QCD axion is

$$\hat{f}_X \gtrsim (4 \times 10^8 \text{ GeV}) \mathcal{N}(T_{\text{SN}}) . \quad (4.20)$$

It then follows that in highly-mixed scenarios, this constraint can be significantly weaker than the corresponding constraint on KK-graviton production derived in Ref. [7], due to suppression by $\mathcal{N}(T_{\text{SN}})$. Indeed, the corresponding constraint on KK-graviton production is directly obtained by replacing $\hat{f}_X \rightarrow M_P$ and $\mathcal{N}(T_{\text{SN}}) \rightarrow T_{\text{SN}}/M_c$ in Eq. (4.20).

While the SN1987A bound is indeed one of the most stringent constraints on the QCD axion, it is not necessarily applicable for all general axions. This is because the bound quoted in Eq. (4.19) is predicated on the assumption that

nucleon bremsstrahlung ($N + N \rightarrow N + N + a$) and other hadronic processes dominate the rate for the production of the light scalar in question in the supernova core. This presupposes that the light scalar couples to nuclei with a strength comparable to that of a QCD axion. If this is not the case, however, the constraints obtained from SN1987A energy-loss limits can differ considerably from the standard QCD-axion bound. For example, if from among the SM particles, the general axion couples only to the photon field, the dominant production processes will be $e^- \gamma \rightarrow e a_\lambda$, $p^+ \gamma \rightarrow p^+ a_\lambda$, and $p^+ n \rightarrow p^+ n \gamma a_\lambda$. In this case, the considerably weaker bound [44]

$$\hat{f}_X \gtrsim (2.32 \times 10^6 \text{ GeV}) c_\gamma \quad (4.21)$$

is obtained for a four-dimensional field. Translating this result to the case of a KK tower of axions, as above, we find that

$$\hat{f}_X \gtrsim (2.32 \times 10^6 \text{ GeV}) c_\gamma \aleph(T_{\text{SN}}) . \quad (4.22)$$

Furthermore, in general axion models, c_γ may not necessarily be of $\mathcal{O}(1)$. In other words, the SN1987A constraint is sensitive to the $U(1)_X$ and $SU(2) \times U(1)_Y$ charges of the fields in the model, and is thus highly model-dependent.

An analogous limit on \hat{f}_X can be derived from observations of the lifetimes of globular-cluster (GC) stars. The ambient temperatures T_{GC} of such objects are only $\mathcal{O}(10 \text{ keV})$, so axion production primarily proceeds through the Primakoff processes $\gamma + e^- \rightarrow a + e^-$ and $\gamma + n_Z \rightarrow a + n_Z$, where n_Z denotes a nucleus with atomic number Z . (Note that the dominant processes in this environment differ from the axion-nucleon bremsstrahlung processes which dominate the axion-production rate in supernovae.) Such a bound will therefore arise for any general axion for which $c_\gamma \neq 1$, regardless of whether or not it couples to the gluon field. The observation limit on axion production in GC stars is commonly phrased as an upper bound on the effective coupling $G_{a\gamma\gamma}$ between a standard, four-dimensional axion (or any other similar particle) and a pair of photons, and the current bound is $G_{a\gamma\gamma} \lesssim 1 \times 10^{-10} \text{ GeV}^{-1}$ [45]. Since $T_{\text{GC}} \approx 10 \text{ keV}$, the corresponding bound on \hat{f}_X is

$$\hat{f}_X \gtrsim (1.16 \times 10^7 \text{ GeV}) c_\gamma \aleph(T_{\text{GC}}) . \quad (4.23)$$

Note that this constraint is independent of the SN1987A bounds, as it differs from the latter in two significant ways. First, because the relevant production process involves the coupling of the axion modes to photons rather than to nuclei, it depends on c_γ alone and not on c_g . Second, since $T_{\text{GC}} \ll T_{\text{SN}}$, far fewer of the a_λ will be produced with any significant frequency in GC stars. Consequently, the enhancement factor from the sum over kinetically-accessible axion modes for GC stars is far smaller.

Finally, bounds similar to those from SN1987A and GC stars can also be derived from the non-observation of effects related to axion production in other astrophysical sources, such as our own sun [46]. However, these bounds are found to be subleading in comparison with the SN1987A and GC-star constraints, essentially because they take place in far cooler environments, where the number of kinematically accessible modes is even further suppressed by the cutoff at E_{ch} inherent in $\aleph(E_{\text{ch}})$.

E. Axion Production at Colliders

We now consider the collider constraints applicable to our bulk-axion DDM model. Due to the highly suppressed couplings between the axion and the SM fields in standard four-dimensional axion models, collider data have virtually no relevance in constraining the parameter space of such models. Nevertheless, because of the huge multiplicity of light modes that arises in theories with light bulk fields in large extra dimensions, the net contribution to the event rates for certain processes from all of these modes taken together can potentially yield observable signals. For example, modes which are stable on collider time scales all appear as missing energy, and can lead to signals in channels such as $pp \rightarrow j + \cancel{E}_T$ and $pp \rightarrow \gamma + \cancel{E}_T$. In addition, the heavier, more unstable modes which decay before exiting the detector can potentially give rise to additional signature patterns which may include displaced vertices. Indeed, we have already discussed in Sect. IV A how current limits from LHC data constrain the parameter space of one such bulk field — the higher-dimensional graviton — for which the monojet and monophoton channels mentioned above are of particular importance. Since the a_λ in our bulk-axion model couple to the fields of the SM in much the same manner as KK gravitons, it is no surprise that the collider phenomenology of the a_λ turns out to be quite similar to that of KK gravitons.

We begin by discussing those signals which arise due to the combined effect of the a_λ which are sufficiently long-lived so as to manifest themselves in a collider detector as missing energy. Collider processes in which the a_λ appear as \cancel{E}_T are yet further examples of the class of processes discussed in the previous section in which axions are produced

but not subsequently detected. The net cross-section for any such process is therefore likewise suppressed by axion mixing in the manner described in Eq. (4.15), with E_{ch} given by the center-of-mass energy \sqrt{s} of the collider.

Which specific channels are relevant for the discovery of a bulk axion at hadron colliders depends crucially on how the five-dimensional axion couples to the SM fields, and in particular on whether or not it couples appreciably to either light quarks or gluons. For a field with an $\mathcal{O}(1)$ value of either c_g or c_q (where $q = \{u, d, s, c\}$), the principal discovery channel at both the Tevatron and the LHC is $pp \rightarrow j + \cancel{E}_T$, a channel which is also one of the principal discovery channels for KK gravitons. Thus, in order to obtain a rough estimate of the constraints on the parameter space of our bulk-axion model from the null results of monojet searches, we translate the bound on the fundamental scale M_D established by such searches into a bound on \hat{f}_X . The cross-section for KK-graviton production in association with a single jet at a hadron collider in a theory with n large, flat extra dimensions of equal length compactified on an n -torus, including contributions from all kinematically accessible modes, is roughly proportional to [7]

$$\sigma_{\text{prod}}(pp \rightarrow j + G) \propto \left(\frac{\sqrt{s}}{2\pi} \right)^n \frac{1}{M_D^{n+2}}. \quad (4.24)$$

This implies that a bound of the form $M_D > M_D^{\text{min}}$ can be translated into a rough bound on the parameter space of our bulk-axion model of the form

$$\frac{\aleph^2(\sqrt{s})}{\hat{f}_X^2} \lesssim \left(\frac{\sqrt{s}}{2\pi} \right)^n \frac{1}{(M_D^{\text{min}})^{n+2}}, \quad (4.25)$$

where $\aleph(E_{\text{ch}})$ is defined in Eq. (4.16). While this approximate bound does not take into account the differences in coupling structure between KK graviton and axion fields or the sum over polarizations for a massive graviton, it is sufficient to obtain parametric estimates of the resulting constraints on our three fundamental parameters \hat{f}_X , M_c , and Λ_G .

In Fig. 5, we indicate the rough bounds on the parameter space of our bulk-axion DDM model which can be derived in this manner, given a chosen value of M_D^{min} . The contours shown in this figure correspond to constraints of the form $M_D > M_D^{\text{min}}$ for the illustrative values $M_D^{\text{min}} = \{1, 10, 100\}$ TeV.

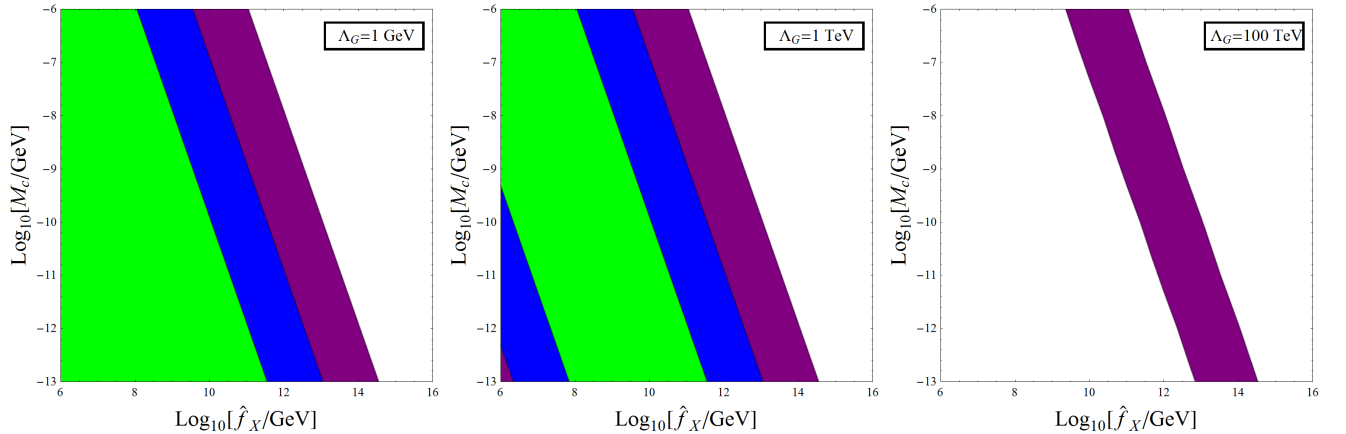


FIG. 5: Excluded regions of the (\hat{f}_X, M_c) parameter space of our DDM model in which the collider constraint in Eq. (4.25) is violated for $M_D^{\text{min}} = 1$ TeV (green); $M_D^{\text{min}} = 10$ TeV (green and blue); and $M_D^{\text{min}} = 100$ TeV (green, blue, and purple). As Λ_G increases, we see that satisfying the collider constraints becomes increasingly easy, particularly for small \hat{f}_X . In each case, we have taken $\xi = g_c = 1$ and assumed that the axion couples to at least one light, strongly-interacting SM particle with an $\mathcal{O}(1)$ coupling coefficient c_g or c_q .

We now compare these results to actual constraints on M_D from current experimental data and examine the projected LHC reach for our bulk-axion DDM model. The most stringent constraints from LHC data (which indeed come from the $pp \rightarrow j + \cancel{E}_T$ channel) were given in Sect. IV A. Estimates of the future LHC reach for a theory with a single extra dimension are $M_D^{\text{min}} \approx \{14, 17\}$ TeV at integrated luminosities $\mathcal{L}_{\text{int}} = \{10, 100\} \text{ fb}^{-1}$, respectively [47]. Likewise, Tevatron data imply a limit $M_D^{\text{min}} \approx 2.4$ TeV for a theory with a single extra dimension [47]. Comparing these results to those in Fig. 5, we see that current collider constraints, while quite stringent, do not significantly impact the preferred region of parameter space for our bulk-axion DDM model, even in cases in which the axion couples to one or more strongly-interacting SM fields with an $\mathcal{O}(1)$ coupling coefficient. In such cases, since the most

stringent current LHC limits imply a bound of roughly $M_D^{\min} \approx 1$ TeV, the region of the parameter space of our model excluded by these limits roughly corresponds to the green shaded regions shown in Fig. 5. Since the green exclusion regions in this figure embody the most stringent such limits applicable to our DDM model, we shall take these to represent our collider constraints throughout the rest of this paper. However, we note that for photonic axions and other axion species which do not couple directly to quarks or gluons, the corresponding collider constraints (which arise from channels such as $pp \rightarrow \gamma + \cancel{E}_T$) are somewhat weaker.

Before concluding this section, there is one important point which deserves emphasis. The collider processes we have been discussing thus far are those whose event rates receive their contributions from the low-lying modes in the tower — *i.e.*, those a_λ with lifetimes $\tau_\lambda \gtrsim 10^{-12}$ s. By contrast, those heavy a_λ with lifetimes $\tau_\lambda \lesssim 10^{-12}$ s tend to decay to pairs of SM fields *within* the detector volume. The decays of such states can in principle give rise to an entirely different set of signature patterns. For example, a promptly decaying a_λ which couples to light quarks or gluons as well as photons would in principle contribute to event rates in the $pp \rightarrow jjj$ and $pp \rightarrow \gamma\gamma + j$ channels. However, since the total event rate in these channels receives contributions from a broad spectrum of a_λ with different λ , many event-selection techniques which are particularly useful in standard searches for new physics in these channels cannot be applied to a tower of decaying bulk axions. For example, since the set of decaying axions cannot be characterized by a single, well-defined mass or cross-section, no identifiable peak can be expected to appear in the invariant-mass distribution for the decay products of the heavy axions. Such considerations render the results of standard searches for new physics in these channels inapplicable to our bulk-axion model — and indeed to DDM models in general. Moreover, they also likely render the identification of a conclusive signal of non-standard dark-matter physics in these channels particularly challenging. Nevertheless, the information that could potentially be revealed about the nature of the dark sector via such an identification is of sufficient magnitude and importance that an analysis of the discovery potential in these channels is an interesting topic for future study.

F. Axion Decays and Distortions of the Cosmic Microwave Background Spectrum

Up to this point, we have considered those phenomenological constraints on our DDM model which are related to the production of particles which compose our bulk-axion ensemble, both with and without their subsequent detection. By contrast, we now turn to discuss an entirely different set of phenomenological constraints, namely those which arise due to the potential decays of a *pre-existing* cosmological population of such particles. Indeed, such constraints emerge generically in all dark-matter scenarios in which the dark sector contains unstable, long-lived particles, and can be derived from observational limits on the physical consequences of the late decays of those particles.

There are many considerations which can be used to place such limits on scenarios involving decaying dark-matter particles. For example, photons produced via the decays of such particles can yield observable distortions in the CMB spectrum; contribute to the diffuse extragalactic X-ray and gamma-ray backgrounds; upset BBN predictions for the primordial abundances of light elements; and result in unacceptably large entropy production during critical epochs in the history of the universe. Constraints on dark-matter candidates from considerations of this sort depend not only on the decay rate of the particle species in question, but also on the relic abundance of that species. For this reason, the constraints applicable to single-particle models of dark-matter are generally not directly applicable to models within the DDM framework. It is therefore necessary to revisit the observational limits on dark-matter decays within the context of our bulk-axion model of dynamical dark matter and assess how these limits constrain the parameter space of this model.

In this section, we begin our analysis of the constraints on the late decays of the a_λ in our bulk-axion DDM model by examining observational limits on the distortions of the CMB which such decays can induce. The type of CMB distortion to which a late-decaying particle contributes depends on the time at which that particle decays. In the very early universe, photons produced by particle decays are brought into thermal and kinetic equilibrium with CMB photons via a number of processes. The dominant processes by which newly-produced photons can equilibrate *thermally* with CMB photons are double-Compton scattering ($e^- \gamma \rightarrow e^- \gamma \gamma$) and bremsstrahlung ($e^- X^\pm \rightarrow e^- X^\pm \gamma$, where X^\pm is an ion). However, once these processes freeze out, photons produced from a_λ decays are unable to thermally equilibrate with the radiation bath, resulting in the generation of a non-zero value for the pseudo-degeneracy parameter μ . The interaction rates for these processes are given by [48]

$$\begin{aligned} \Gamma_{\text{DC}} &\approx 5.73 \times 10^{-39} \left(1 - \frac{Y_p}{2}\right) (\Omega_B h^2) \left(\frac{T_{\text{now}}}{2.7 \text{ K}}\right)^{3/2} \left(\frac{t_{\text{MRE}}}{t}\right)^{9/4} \text{ GeV} \\ \Gamma_{\text{BR}} &\approx 1.57 \times 10^{-36} \left(1 - \frac{Y_p}{2}\right) (\Omega_B h^2)^{3/2} \left(\frac{T_{\text{now}}}{2.7 \text{ K}}\right)^{-5/4} \left(\frac{t_{\text{MRE}}}{t}\right)^{13/8} \text{ GeV}, \end{aligned} \quad (4.26)$$

where $T_{\text{now}} \approx 2.725$ K is the present-day CMB temperature, $Y_p \approx 0.23$ is the helium mass fraction, $\Omega_B \approx 0.044$ is

the baryon density of the universe, and $h \approx 0.72$ is the Hubble constant. (Note that since z is quite large during the entirety of the relevant time frame, we have here approximated $1 + z \approx z$.) Once these processes freeze out, in the sense that the rates given in Eq. (4.26) drop below the expansion rate H of the universe, photons produced by a_λ decay will no longer be able to attain thermal equilibrium with the CMB photons. Even after double-Compton scattering and bremsstrahlung effectively shut off, a number of photon-number-conserving interactions still serve to bring photons produced at even later times into *kinetic* equilibrium with the radiation bath. Dominant among these processes is elastic Compton scattering ($e^- \gamma \rightarrow e^- \gamma$), which efficiently serves to bring photons produced by a_λ decays into kinetic equilibrium until a much later time $t_{\text{EC}} \sim 9 \times 10^9$ s, at which point this process too effectively freezes out. However, since elastic Compton scattering conserves photon number, it cannot similarly suffice to bring those photons into *thermal* equilibrium. As a result, CMB distortions in the form of a non-zero value for the pseudo-degeneracy parameter μ can be generated by a_λ decays during this epoch. In addition, after elastic Compton scattering freezes out, photons produced by a_λ decay achieve neither kinetic nor thermal equilibrium with the radiation bath. As a result, these photons no longer contribute the generation of μ , but instead contribute to the generation of a Compton y parameter (here denoted y_C , so as to distinguish it from the ratio $y = M_c/m_X$). Finally, at $t \sim 10^{13}$ s, matter and radiation decouple, and any a_λ decays occurring after this point not affect the CMB, but instead simply persist as a contribution to the diffuse photon background. This last sort of contribution will be dealt with separately, in Sect. IV G.

We thus see that axion decays have the potential to generate both a non-zero μ and a non-zero y_C . We can therefore establish constraints on our bulk-axion DDM model by calculating the theoretical predictions for these quantities in our model and comparing these predictions to observational data.

We begin our analysis of CMB distortions from a_λ decays by addressing those decays which result in the generation of the pseudo-degeneracy parameter μ . In general, provided that the additional contribution $\delta\rho_\gamma$ to the photon energy density ρ_γ from the decay of the a_λ fields is small compared to the total ρ_γ , the time-evolution of μ can be described by the equation [48, 49]

$$\frac{d\mu}{dt} = \frac{d\mu_a}{dt} - \mu (\Gamma_{\text{DC}} + \Gamma_{\text{BR}}) . \quad (4.27)$$

Here Γ_{DC} and Γ_{BR} are the interaction rates for double-Compton scattering and bremsstrahlung, respectively, and $d\mu_a/dt$ denotes the differential contribution to μ from axion decay. For an arbitrary $d\mu_a/dt$, the solution to this differential equation takes the form

$$\mu(t) = \exp \left[\frac{4}{5} (2C_{\text{BR}} t^{-5/8} + C_{\text{DC}} t^{-5/4}) \right] \int_{t_e}^t \left[\frac{d\mu_a}{dt}(t') \right] \exp \left[-\frac{4}{5} (2C_{\text{BR}} t'^{-5/8} + C_{\text{DC}} t'^{-5/4}) \right] dt' , \quad (4.28)$$

where $t_e \approx 1.69 \times 10^3$ s is the time scale associated with electron-positron annihilation in the early universe, and where the quantities C_{DC} and C_{BR} are constants related to the double-Compton-scattering and bremsstrahlung rates Γ_{DC} and Γ_{BR} in Eq. (4.26) by $\Gamma_{\text{DC}} \equiv C_{\text{DC}} t^{-9/4}$ and $\Gamma_{\text{BR}} \equiv C_{\text{BR}} t^{-13/8}$. Moreover, the differential contribution $d\mu_a/dt$ to μ from axion decays is given by the standard expression for contributions due to the late injection of photons from a generic source:

$$\frac{d\mu_a}{dt} = \frac{1}{2.143} \left(\frac{3}{\rho_\gamma} \frac{d\rho_\gamma}{dt} - \frac{4}{n_\gamma} \frac{dn_\gamma}{dt} \right) . \quad (4.29)$$

In general, the rate of change in the photon energy density is given by the Boltzmann equation for the evolution of ρ_γ . In our bulk-axion DDM model, this equation includes a source term from each decaying state in the dark-matter ensemble. Thus, at late times, after all of the a_λ have already begun oscillating coherently and the contribution to ρ_γ from inflaton decays can safely be neglected, we find that

$$\frac{d\rho_\gamma}{dt} = -4H\rho_\gamma + \sum_\lambda \text{BR}_\lambda^{(2\gamma)} \Gamma_\lambda \rho_\lambda , \quad (4.30)$$

where $\text{BR}_\lambda^{(2\gamma)}$ is the branching fraction of a_λ into a pair of photons. Note that the source term in the Boltzmann equation for ρ_γ is simply a sum of the contributions from the various a_λ fields. Using Eq. (4.30), along with the relations

$$\frac{1}{(R^4 \rho_\gamma)} \frac{d(R^4 \rho_\gamma)}{dt} = \frac{1}{\rho_\gamma} \left(\frac{d\rho_\gamma}{dt} + 4H\rho_\gamma \right) , \quad \frac{1}{(R^3 n_\gamma)} \frac{d(R^3 n_\gamma)}{dt} = \frac{1}{n_\gamma} \left(\frac{dn_\gamma}{dt} + 3Hn_\gamma \right) , \quad (4.31)$$

we can rewrite Eq. (4.27) in the form

$$\frac{d\mu_a}{dt} = \frac{1}{2.143} \left[\frac{3}{\rho_\gamma} \sum_\lambda \text{BR}_\lambda^{(2\gamma)} \Gamma_\lambda \rho_\lambda - \frac{8}{n_\gamma} \sum_\lambda \text{BR}_\lambda^{(2\gamma)} \Gamma_\lambda \frac{\rho_\lambda}{\lambda} \right]. \quad (4.32)$$

For the purpose of establishing a conservative bound, we focus here on the case of a purely photonic axion. As we saw in Sect. IIIB, the contribution to Γ_λ from intra-ensemble decays is negligible for any a_λ which decays on time scales relevant for the generation of CMB distortions. It is therefore justifiable to approximate Γ_λ by the expression for $\Gamma(a \rightarrow \gamma\gamma)$ given in Eq. (3.15) and thus to take $\text{BR}_\lambda^{(2\gamma)} \approx 1$. Since the energy density ρ_λ associated with each a_λ is given in Eq. (3.7), we find that in this approximation, the first source term on the right side of Eq. (4.32) takes the form

$$\sum_\lambda \text{BR}_\lambda^{(2\gamma)} \Gamma_\lambda \rho_\lambda \approx \frac{1}{2} \theta^2 G_\gamma m_X^4 \sum_\lambda \lambda \left(\frac{t_\lambda^2}{t_{\text{RH}}^{1/2}} \right) (\tilde{\lambda}^2 A_\lambda)^4 e^{-\frac{G_\gamma \lambda^3}{f_X^2} (\tilde{\lambda}^2 A_\lambda)^2 (t-t_G)} \times \begin{cases} t_{\text{RH}}^{1/2} t^{-2} & t \lesssim t_{\text{RH}} \\ t^{-3/2} & t_{\text{RH}} \lesssim t \lesssim t_{\text{MRE}} \\ t_{\text{MRE}}^{1/2} t^{-2} & t \gtrsim t_{\text{MRE}} \end{cases} \quad (4.33)$$

where we have defined G_γ is defined below Eq. (3.15). The second term takes the same form, but with one factor of λ fewer in the summand.

In principle, one could evaluate this sum numerically at each moment in time, and then use these results to numerically solve Eq. (4.32). However, we find that by making a few additional well-motivated approximations, we can obtain a closed-form, analytical result for $d\mu_a/dt$. We begin by dividing the tower into sections, based on the two criteria which determine the dependence of Γ_λ and ρ_λ on λ . The first of these is whether the oscillation-onset time for a given a_λ is within the staggered regime (*i.e.*, $t_\lambda > t_G$), or the simultaneous turn-on regime (*i.e.*, $t_\lambda = t_G$). In the former case, t_λ depends on λ according to Eq. (3.6); in the latter case, t_λ is independent of λ . The second pertinent criterion concerns the relationship between λ and the quantity

$$\lambda_{\text{trans}} \equiv \pi m_X^2 / M_c, \quad (4.34)$$

introduced in Ref. [2]. This quantity corresponds roughly to the transition point between the small- λ regime, in which the a_λ are highly mixed, the large- λ regime, in which mixing is negligible. Indeed, for $\lambda \ll \lambda_{\text{trans}}$, we find that $\tilde{\lambda}^2 A_\lambda \approx \sqrt{2} \tilde{\lambda} / (1 + \pi^2/y^2)^{1/2}$, while for $\lambda \gg \lambda_{\text{trans}}$, we find that $\tilde{\lambda}^2 A_\lambda \approx \sqrt{2}$. Given these criteria, our first approximation will be to replace $\tilde{\lambda}^2 A_\lambda$ with its asymptotic large- λ form for all $\lambda > \lambda_{\text{trans}}$, and with its asymptotic small- λ form for all $\lambda < \lambda_{\text{trans}}$. Our second will be to approximate the sum over λ by a set of source-term integrals $I_i(m, n, \alpha, \beta, \lambda_{\text{min}}, \lambda_{\text{max}})$, each corresponding to a different regime in the tower of modes characterized by a particular dependence of the integrand on λ . These source-term integrals may be evaluated analytically by making use of the identity

$$\begin{aligned} I_i(m, n, \alpha, \beta, \lambda_{\text{min}}, \lambda_{\text{max}}) &\equiv \alpha \int_{\lambda_{\text{min}}}^{\lambda_{\text{max}}} \lambda^m e^{-\beta \lambda^n} d\lambda \\ &= \alpha \frac{1}{n} \beta^{-(m+1)/n} \left[\Gamma\left(\frac{m+1}{n}, \beta \lambda_{\text{min}}^n\right) - \Gamma\left(\frac{m+1}{n}, \beta \lambda_{\text{max}}^n\right) \right], \end{aligned} \quad (4.35)$$

which is valid for $n > 0$ and any real values of m , α , and β . Here $\Gamma(s, x)$ denotes the incomplete gamma function:

$$\Gamma(s, x) \equiv \int_x^\infty t^{s-1} e^{-t} dt. \quad (4.36)$$

Employing the approximations discussed above, we find that the first source term on the right side of Eq. (4.32) reduces to

$$\sum_\lambda \text{BR}_\lambda^{(2\gamma)} \Gamma_\lambda \rho_\lambda = \frac{2G_\gamma \theta^2}{M_c} \sum_{i=1}^4 I_i(m_i, n_i, \alpha_i, \beta_i, \lambda_{i-1}^{\text{CMB}}, \lambda_i^{\text{CMB}}) \times \begin{cases} t_{\text{RH}}^{1/2} t^{-2} & t \lesssim t_{\text{RH}} \\ t^{-3/2} & t_{\text{RH}} \lesssim t \lesssim t_{\text{MRE}} \\ t_{\text{MRE}}^{1/2} t^{-2} & t \gtrsim t_{\text{MRE}} \end{cases} \quad (4.37)$$

i	Oscillation regime	Mixing regime	m_i	n_i	α_i	β_i
1	$t_\lambda > t_G$	$\lambda < \lambda_{\text{trans}}$	3	5	$4t_{\text{RH}}^{-1/2}[1 + \pi^2/y^2]^{-2}$	$2G_\gamma t(\hat{f}_X m_X)^{-2}[1 + \pi^2/y^2]^{-1}$
2		$\lambda \geq \lambda_{\text{trans}}$	-1	3	$4m_X^4 t_{\text{RH}}^{-1/2}$	$2G_\gamma t \hat{f}_X^{-2}$
3	$t_\lambda = t_G$	$\lambda < \lambda_{\text{trans}}$	5	5	$t_G^{\kappa_G} t_{\text{RH}}^{3/2-\kappa_G}[1 + \pi^2/y^2]^{-2}$	$2G_\gamma t(\hat{f}_X m_X)^{-2}[1 + \pi^2/y^2]^{-1}$
4		$\lambda \geq \lambda_{\text{trans}}$	1	3	$m_X^4 t_G^{\kappa_G} t_{\text{RH}}^{3/2-\kappa_G}$	$2G_\gamma t \hat{f}_X^{-2}$

TABLE I: Values of m_i , n_i , α_i , and β_i which correspond to different regimes, labeled by the index i , in a generic axion tower, for use in Eqs. (4.38) and (4.49). The symbol κ_G denotes the specific value of κ , as defined in Eq. (3.3), which corresponds to t_G .

Inserting this result (and the analogous result for the second source term) into Eq. (4.29) and using the fact that μ -type distortions are generated by decays occurring within the RD era, we obtain the result

$$\frac{d\mu_a}{dt} \approx 0.935 \times \frac{G_\gamma \theta^2}{M_c t^{3/2}} \left[\frac{3}{\rho_\gamma^{\text{eq}}} \sum_{i=1}^4 I_i(m_i, n_i, \alpha_i, \beta_i, \lambda_{i-1}^{\text{CMB}}, \lambda_i^{\text{CMB}}) - \frac{8}{n_\gamma^{\text{eq}}} \sum_{i=1}^4 I_i(m_i - 1, n_i, \alpha_i, \beta_i, \lambda_{i-1}^{\text{CMB}}, \lambda_i^{\text{CMB}}) \right], \quad (4.38)$$

where the expressions for α_i , β_i , m_i , and n_i valid in each a_λ regime are listed in Table I. Note that in obtaining this expression, we have assumed that the additional contributions to n_γ and ρ_γ due to the injection of photons from a_λ are sufficiently small that these quantities can be approximated by the equilibrium expressions $n_\gamma^{\text{eq}} = 2\zeta(3)T^3/\pi^2$ and $\rho_\gamma^{\text{eq}} = \pi^2 T^4/15$. Furthermore, we have used the fact that the time frame during which CMB distortions to μ can arise lies entirely within the RD era. Obtaining a final result for the magnitude of μ -type distortions to the CMB engendered by the presence of a tower of decaying DDM axions is then simply a matter of substituting the result for $d\mu_a/dt$ in Eq. (4.38) into Eq. (4.28) and numerically evaluating the integral for a given choice of input parameters.

The contribution to y_C from the late decays of the a_λ may be evaluated in much the same way as the corresponding contribution to μ . The decays which contribute to y_C are those which occur during the window $9 \times 10^9 \lesssim t \lesssim 1.2 \times 10^{13}$ s, during which the rate $\Gamma_{\text{EC}} \sim H$ associated with elastic Compton scattering can no longer bring the photons from a_λ decay into kinetic equilibrium even though radiation has yet to decouple from matter. The evolution of y_C is governed by the relation [50]

$$\frac{dy_C}{dt} = \frac{1}{4\rho_\gamma} \frac{d\rho_\gamma}{dt}. \quad (4.39)$$

Proceeding with the mode sum as above and adopting the same approximations as above, we find that

$$\frac{dy_C}{dt} \approx \frac{2G_\gamma \theta^2}{M_c \rho_\gamma^{\text{eq}}} \sum_{i=1}^4 I_i(m_i, n_i, \alpha_i, \beta_i, \lambda_{i-1}^{\text{CMB}}, \lambda_i^{\text{CMB}}) \times \begin{cases} t^{-3/2} & t \lesssim t_{\text{MRE}} \\ t_{\text{MRE}}^{1/2} t^{-2} & t_{\text{MRE}} \lesssim t \lesssim t_{\text{LS}} \\ 0 & t \gtrsim t_{\text{LS}} \end{cases}, \quad (4.40)$$

where $t_{\text{LS}} \sim 1.19 \times 10^{13}$ s is the time of last scattering and $I_i(m, n, \alpha, \beta, \lambda_{\text{min}}, \lambda_{\text{max}})$ is once again given by Eq. (4.35). Note that since matter-radiation equality occurs prior to last scattering, at around $t_{\text{MRE}} \sim 10^{11}$ s, the epoch during which a_λ decays can affect y_C straddles both the RD and MD eras. Numerically evaluating the expression in Eq. (4.40) from t_{EC} to t_{LS} , we obtain our final results for y_C distortions due to late a_λ decay.

In order to assess the CMB constraints on the parameter space of our bulk-axion DDM model, we now compare the results obtained by numerically integrating Eqs. (4.28) and (4.40) with observational limits on μ and y_C . The current limits on these quantities are [45]

$$|\mu| < 9 \times 10^{-5}, \quad y_C < 1.2 \times 10^{-5}. \quad (4.41)$$

The bound on y_C for a photonic axion with $c_\gamma = 1$ yields the constraints on \hat{f}_X , M_c , and Λ_G shown in Fig. 6. In this figure, we display contours of the values of y_C in (\hat{f}_X, M_c) space which arise in a bulk-axion model with $\Lambda_G = 1$ GeV (left panel) and with $\Lambda_G = 1$ TeV (right panel). In each case, we have taken $\xi = g_G = \theta = 1$, $H_I = 1$ GeV, and $T_{\text{RH}} = 5$ MeV. Contours indicating $y \equiv M_c/m_X = 1$ (solid red line) and $y = \{0.01, 0.1, 10, 100\}$ (dashed red lines)

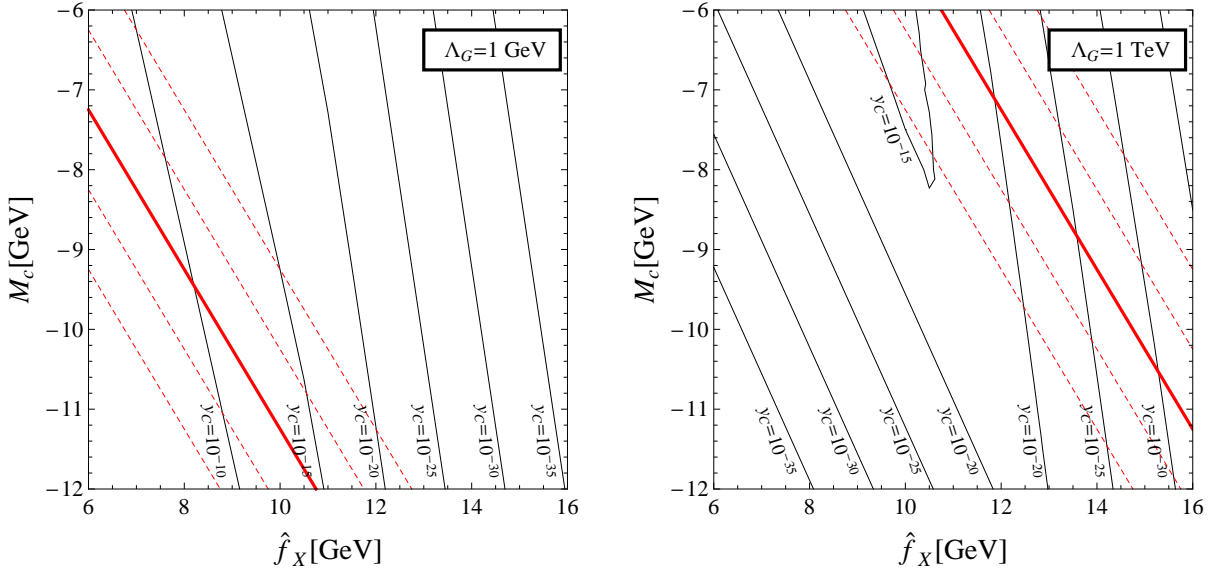


FIG. 6: Contours of the CMB Compton- y -parameter distortion y_C (black lines) produced as a result of axion decays in a bulk-axion DDM model with $\Lambda_G = 1$ GeV (left panel) and $\Lambda_G = 1$ TeV (right panel). In each case, we have assumed a photonic axion with $c_\gamma = 1$ and have taken $\xi = g_G = \theta = 1$, with $H_I = 1$ GeV and $T_{RH} = 5$ MeV. Contours corresponding to $y \equiv M_c/m_X = 1$ (solid red line) and to $y = \{0.01, 0.1, 10, 100\}$ (dashed red lines) are also shown. For each panel, it is evident that our bulk-axion DDM model amply satisfies the CMB constraints in Eq. (4.41) for all relevant values of \hat{f}_X and M_c , regardless of the value of y .

have also been superimposed. For each panel, it is evident that our bulk-axion DDM model amply satisfies the CMB constraints for all relevant values of \hat{f}_X and M_c , regardless of the value of y .

It turns out that the constraints from the corresponding bound on μ in Eq. (4.41) are even less stringent than those from the bound on y_C . Thus, we conclude that both the y_C -type and μ -type distortions which result from a_λ decays in our bulk-axion DDM model are well below present experimental sensitivities. Indeed, no meaningful constraint arises for our bulk-axion DDM model from present limits on distortions in the CMB.

As we have discussed, neither μ nor y_C can be affected by any photons which are produced by a_λ decays at times $t \gtrsim t_{LS}$, after radiation and matter decouple. Such photons do, however, contribute to the diffuse photon background. In the next section, we will discuss the physical effects of this diffuse photon background in detail.

G. Axion Decays and Contributions to the Diffuse X-Ray and Gamma-Ray Backgrounds

As mentioned above, the potentially observable effects of late photoproduction from axion decays include not only distortions of the CMB, but also imprints on the diffuse X-ray and gamma-ray backgrounds. Observational limits on such imprints from instruments such as HEAO [51], COMPTEL [52], XMM, and Chandra [53] therefore impose additional constraints on the parameter space of our bulk-axion DDM model. As discussed in Sect. III, there are two cosmological populations of decaying a_λ whose decays to photons can potentially leave observable imprints on the diffuse X-ray and gamma-ray backgrounds. The first is the population of cold axions produced by vacuum misalignment, which collectively compose the DDM ensemble. The second is the far smaller population of axions produced by interactions among the SM fields in the thermal bath after inflation. While the former population provides a far greater contribution to Ω_{tot} , the latter population contains a far larger proportion of heavier, more unstable a_λ , as indicated in Fig. 3. It is not clear *a priori* which population yields the more stringent constraint. Thus, it is necessary to examine the contribution to the diffuse photon background from each of these populations in turn.

A photon produced at time t with initial energy $E_\gamma(t)$ will only contribute to the diffuse photon background if the universe remains transparent to electromagnetic radiation over the entire range of energies through which that photon redshifts as the universe evolves from t to t_{now} . A detailed analysis of the time scales and photon-energy ranges for which this transparency condition is attained is presented in Ref. [54]. Roughly speaking, the transparency window spans an energy range $1 \text{ keV} \lesssim E_\gamma \lesssim 10 \text{ TeV}$ and a time range $10^{12} - 10^{14} \text{ s} \lesssim t \lesssim t_{now}$, with the lower limit

depending on the particular value of E_γ . Motivated by these results, we approximate the universe to be transparent to all photons with energies which fall within this range at all times $t > t_{\text{LS}}$ and opaque to all photons otherwise. This approximation yields a conservative bound. Moreover, we emphasize that since the dominant contribution to the diffuse X-ray and gamma-ray flux in our model is due to modes which decay at much later times $t \gg t_{\text{LS}}$, our results are essentially insensitive to the precise contours chosen for the transparency window.

The calculation of the photon flux due to late a_λ decays proceeds in a manner similar to the calculation of the flux from KK-graviton decays outlined in Ref. [26]. The Boltzmann equation for the *number* density n_γ of photons in the presence of a tower of decaying a_λ takes the form

$$\dot{n}_\gamma + 3Hn_\gamma = 2 \sum_\lambda \text{BR}_\lambda^{(2\gamma)} \Gamma_\lambda \frac{\rho_\lambda}{\lambda}, \quad (4.42)$$

where once again ρ_λ is given by Eq. (3.8). Solving this equation for n_γ as a function of time, we obtain

$$n_\gamma(t) = 2 \frac{s(t)}{s_{\text{LS}}} \sum_\lambda \text{BR}_\lambda^{(2\gamma)} \frac{\rho_\lambda(t_{\text{LS}})}{\lambda} \left[1 - e^{-\Gamma_\lambda(t-t_{\text{LS}})} \right], \quad (4.43)$$

where $s(t)$ is the entropy density of the universe at time t , and s_{LS} is the entropy density of the universe at the time of last scattering. The present-day differential energy spectrum dn_γ/dE_γ of these photons may readily be computed from the relation

$$\frac{dn_\gamma}{dE_\gamma} = \frac{dn_\gamma}{dt} \frac{dt}{dz} \frac{dz}{dE_\gamma}, \quad (4.44)$$

where z is the cosmological redshift and E_γ is the photon energy at redshift z . The first of these factors may be obtained by explicitly differentiating Eq. (4.43) with fixed $s = s_{\text{now}}$, which yields a series of terms of the form

$$\left[\frac{dn_\gamma}{dt} \right]_\lambda = 2 \left(\frac{s_{\text{now}}}{s_{\text{LS}}} \right) \text{BR}_\lambda^{(2\gamma)} \Gamma_\lambda \frac{\rho_\lambda(t_{\text{LS}})}{\lambda} e^{-\Gamma_\lambda(t_{\text{now}}-t_{\text{LS}})}, \quad (4.45)$$

one for each different value of λ . The second factor in Eq. (4.44) may be obtained by noting that the relationship between time and redshift during the present, matter-dominated era is well-approximated by $t = t_{\text{now}}(1+z)^{-3/2}$. Consequently, for each value of λ we have

$$\left[\frac{dt}{dz} \right]_\lambda = -\frac{3}{2} t_{\text{now}} \left(\frac{2E_\gamma}{\lambda} \right)^{5/2} \quad (4.46)$$

during the epoch of interest. The third factor in Eq. (4.44) may be obtained by noting that each of the photons produced by an axion tower state a_λ which decays at redshift z will be monochromatic, with energy $\lambda/2$, at the moment of decay. This implies that the present-day energies of such photons are given by $E_\gamma(1+z) = \lambda/2$, and hence that for each value of λ , we have

$$\left[\frac{dz}{dE_\gamma} \right]_\lambda = -\frac{\lambda}{2E_\gamma^2}. \quad (4.47)$$

Combining these expressions and summing over λ , we arrive at a general formula for the contribution to the diffuse photon flux produced by the tower of decaying a_λ :

$$\left. \frac{dn_\gamma}{dE_\gamma} \right|_{\text{now}} = 6t_{\text{now}} \sqrt{2E_\gamma} \left(\frac{s_{\text{now}}}{s_{\text{LS}}} \right) \sum_\lambda \text{BR}_\lambda^{(2\gamma)} \Gamma_\lambda \frac{\rho_\lambda(t_{\text{LS}})}{\lambda^{5/2}} e^{-\Gamma_\lambda(t_{\text{now}}-t_{\text{LS}})}. \quad (4.48)$$

Calculating the contribution to the diffuse X-ray and gamma-ray backgrounds in our bulk-axion DDM model is then simply a matter of applying Eq. (4.48) to the contribution from the two relevant populations of decaying axions discussed above.

We begin by addressing the contribution from the population of axions produced by vacuum misalignment — *i.e.*, the DDM ensemble itself. Once again, we focus our attention on the case of a photonic axion, for which $\Gamma_\lambda \approx \Gamma(a \rightarrow \gamma\gamma)$ and $\text{BR}_\lambda^{(2\gamma)} \approx 1$. In this case, we find that the contribution to the present-day diffuse photon background from the collective decays of the a_λ fields is given by

$$\left. \frac{dn_\gamma}{dE_\gamma} \right|_{\text{now}} = 3\sqrt{2E_\gamma} G_\gamma \theta^2 m_X^4 \left(\frac{s_{\text{now}}}{s_{\text{LS}}} \right) \sum_\lambda \left(\frac{t_\lambda^{1/2} t_{\text{MRE}}^2}{t_{\text{LS}}^2 t_{\text{RH}}^{1/2}} \right) \lambda^{-3/2} (\tilde{\lambda}^2 A_\lambda)^4 e^{\frac{G_\gamma \lambda^3}{f_G^2} (\tilde{\lambda}^2 A_\lambda)^2 (t_{\text{now}}-t_G)}. \quad (4.49)$$

Just as for the contributions to μ and y_C in Sect. IV F, we approximate the sum over axion modes appearing in Eq. (4.49) as an integral over λ . The lower limit of integration is determined by the requirement that in order for a photon with redshifted energy E_γ to have been produced by the decay of the axion species a_λ before present day, we must have $\lambda \geq 2E_\gamma$. Likewise, photons which decay before the processes which equilibrate them with the radiation bath freeze out will not contribute to features in the diffuse photon background. Thus, the upper limit of integration is set by the condition $\lambda \lesssim 2E_\gamma(t_{\text{now}}/t_{\text{LS}})^{2/3}$. Furthermore, we must also require that λ not exceed the cutoff scale f_G , or be smaller than the lightest mode in the tower. Once again, we find that the resulting integral expressions can be written in terms of the functions $I_i(m, n, \alpha, \beta, \lambda_{\text{min}}, \lambda_{\text{max}})$ defined in Eq. (4.35):

$$\left. \frac{dn_\gamma}{dE_\gamma} \right|_{\text{now}} \approx 12G_\gamma \theta^2 \frac{\sqrt{2E_\gamma} t_{\text{now}}}{M_c} \left(\frac{s_{\text{now}}}{s_{\text{LS}}} \right) \left(\frac{t_{\text{MRE}}^{1/2}}{t_{\text{LS}}^2} \right) \sum_{i=1}^4 I_i(m_i - 5/2, n_i, \alpha_i, \beta_i, \lambda_{i-1}^{\text{XRB}}, \lambda_i^{\text{XRB}}), \quad (4.50)$$

where the λ_i^{XRB} are analogous to the λ_i^{CMB} appearing in Eq. (4.38). Determining the net contribution to the differential photon flux from decays of the a_λ for any particular choice of model parameters is thus simply a matter of numerically evaluating Eq. (4.50).

We now turn to consider the observational limits on dn_γ/dE_γ . The diffuse extragalactic X-ray and gamma-ray background spectra have been probed by a number of experiments. In the keV – MeV region, the most current data are those from HEAO, COMPTEL, XMM, and Chandra; at energies above this, the most current data are those from EGRET and FERMI. Over this entire energy range, the diffuse photon spectrum is well-modeled by a set of power-law fits, and the non-observation of any discernible, sharp features in this spectrum imposes constraints on late relic-particle decays to photons. For the data from the COMPTEL instrument, the best power-law fit is found to be [52]

$$\frac{dn_\gamma}{dE_\gamma} = 10.5 \times 10^{-4} \left(\frac{E_\gamma}{5 \text{ MeV}} \right)^{-2.4} \text{ MeV}^{-1} \text{ cm}^{-1} \text{ s}^{-1} \text{ str}^{-1} \quad 800 \text{ keV} \lesssim E_\gamma \lesssim 30 \text{ MeV}, \quad (4.51)$$

while the best fit to the HEAO data is found to be [51]

$$\frac{dn_\gamma}{dE_\gamma} = \begin{cases} 7.88 \times 10^3 \left(\frac{E_\gamma}{\text{keV}} \right)^{-1.29} e^{-(E_\gamma/41.13 \text{ keV})} \text{ MeV}^{-1} \text{ cm}^{-1} \text{ s}^{-1} \text{ str}^{-1} & 0.1 \text{ keV} \lesssim E_\gamma \lesssim 60 \text{ keV} \\ 0.43 \left(\frac{E_\gamma}{60 \text{ keV}} \right)^{-6.5} + 8.4 \left(\frac{E_\gamma}{60 \text{ keV}} \right)^{-2.58} \\ \quad + 0.38 \left(\frac{E_\gamma}{60 \text{ keV}} \right)^{-2.05} \text{ MeV}^{-1} \text{ cm}^{-1} \text{ s}^{-1} \text{ str}^{-1} & 60 \text{ keV} \lesssim E_\gamma \lesssim 160 \text{ keV} \\ 3.8 \times 10^5 \times \left(\frac{E_\gamma}{\text{keV}} \right)^{-2.6} \text{ MeV}^{-1} \text{ cm}^{-1} \text{ s}^{-1} \text{ str}^{-1} & 160 \text{ keV} \lesssim E_\gamma \lesssim 350 \text{ keV} \\ 2.0 \times 10^3 \left(\frac{E_\gamma}{\text{keV}} \right)^{-1.7} \text{ MeV}^{-1} \text{ cm}^{-1} \text{ s}^{-1} \text{ str}^{-1} & 350 \text{ keV} \lesssim E_\gamma \lesssim 2 \text{ MeV} . \end{cases} \quad (4.52)$$

The Chandra satellite has improved upon these diffuse X-ray background constraints in the $1 \text{ keV} \lesssim E_\gamma \lesssim 8 \text{ keV}$ range by resolving a large fraction ($\sim 80\%$) of this background into point sources. The residual spectrum in this region is well represented by the power law [57]

$$\frac{dn_\gamma}{dE_\gamma} = 2.6 \times 10^3 \left(\frac{E_\gamma}{\text{keV}} \right)^{-1.5} \text{ MeV}^{-1} \text{ cm}^{-1} \text{ s}^{-1} \text{ str}^{-1} \quad 1 \text{ keV} \lesssim E_\gamma \lesssim 8 \text{ keV}. \quad (4.53)$$

In the gamma-ray region, the most stringent current limits are those from EGRET and FERMI. Data on the diffuse extragalactic gamma-ray background from the former instrument [55] are reliable for photon energies within the range $1.41 \text{ GeV} \lesssim E_\gamma \lesssim 30 \text{ MeV}$, for which we find the best fit

$$\frac{dn_\gamma}{dE_\gamma} = 7.35 \times 10^{-3} \left(\frac{E_\gamma}{\text{MeV}} \right)^{-2.35} \text{ MeV}^{-1} \text{ cm}^{-1} \text{ s}^{-1} \text{ str}^{-1} \quad 30 \text{ MeV} \lesssim E_\gamma \lesssim 1.41 \text{ GeV}. \quad (4.54)$$

Note that data exist for higher photon energies as well, but given that EGRET's energy resolution is not as good at such high energies, and given that these data have been superseded by data from FERMI, we do not use them in

computing this power-law fit. As for the FERMI data, they are well modeled by the power law [56]

$$\frac{dn_\gamma}{dE_\gamma} = 9.59 \times 10^{-3} \left(\frac{E_\gamma}{\text{MeV}} \right)^{-2.41} \text{MeV}^{-1} \text{cm}^{-1} \text{s}^{-1} \text{str}^{-1} \quad 274 \text{ MeV} \lesssim E_\gamma \lesssim 70.7 \text{ GeV} . \quad (4.55)$$

In Fig. 7, we show a set of curves (solid colored lines) depicting the total contribution to the diffuse gamma-ray background from the decaying a_λ fields, as given in Eq. (4.50), for several different values of \hat{f}_X within the range $10^6 - 10^{16}$ GeV. Results are shown for $\Lambda_G = 1$ GeV (upper left panel), $\Lambda_G = 1$ TeV (upper right panel), and $\Lambda_G = 100$ TeV (lower panel). In each case, we have taken $M_c = 10^{-11}$ GeV, $T_{\text{RH}} = 5$ MeV, and $\xi = g_G = \theta = 1$. In addition, we have chosen a value for H_I sufficiently large that none of the curves shown is significantly affected by the “inflating away” of heavy modes which begin oscillating before inflation ends. In addition to these curves,

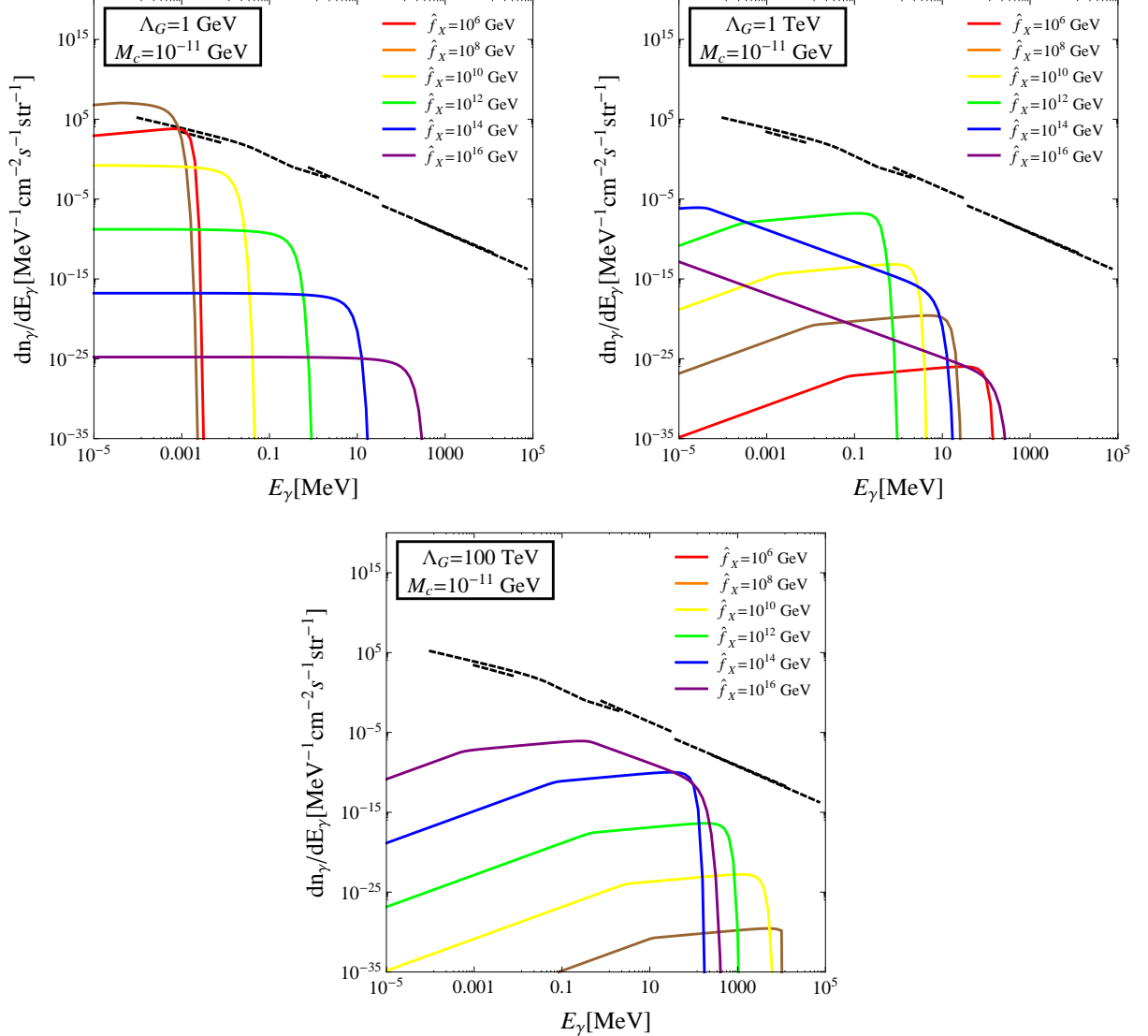


FIG. 7: The diffuse photon-flux spectrum dn_γ/dE_γ produced from axion decays in our bulk-axion DDM model with $\Lambda_G = 1$ GeV (upper left panel), $\Lambda_G = 1$ TeV (upper right panel), and $\Lambda_G = 100$ TeV (lower panel). Each solid colored curve corresponds to a different choice of \hat{f}_X , within the range $10^6 - 10^{16}$ GeV. In all panels, we have taken $M_c = 10^{-11}$ GeV, $H_I = 1$ GeV, $T_{\text{RH}} = 5$ MeV, and $\xi = g_G = \theta = 1$. By contrast, the dashed black contours represent the upper bounds on dn_γ/dE_γ derived from observational limits on the diffuse photon flux using a number of instruments sensitive in the X-ray and gamma-ray regions. As evident from these plots, the diffuse-photon-background contribution arising from axion decay in our bulk-axion DDM model is consistent with all observational limits when Λ_G is large.

we also display contours corresponding to the upper limits on the diffuse X-ray and gamma-ray fluxes (black dashed lines) given in Eqs. (4.51) through (4.55). Any choice of model parameters for which the differential photon flux dn_γ/dE_γ exceeds any one of these observational-limit contours for any value of E_γ is excluded. The results shown in Fig. 7 indicate that while it is not trivial to satisfy these observational limits in our bulk-axion DDM model, the contributions to the diffuse X-ray and gamma-ray fluxes from a_λ decay are indeed sufficiently small that these limits are satisfied when Λ_G is large.

We now consider the contribution to dn_γ/dE_γ from the population of axions generated by their interactions with SM fields in the thermal bath after inflation. The contribution to the diffuse photon flux spectrum dn_γ/dE_γ generated by such a population of axions is once again given by Eq. (4.48), but with $\rho_\lambda(t_{\text{LS}})$ in Eq. (3.8) now replaced by

$$\rho_\lambda(t_{\text{LS}}) \approx \lambda T_{\text{LS}}^3 t_{\text{LS}} \int_{T_{\text{MRE}}}^{T_{\text{RH}}} \frac{3}{\kappa(T)} \left(\frac{T_{\text{LS}}}{T} \right)^{3/\kappa(T)} \frac{g_{*s}(T_{\text{LS}})}{g_{*s}(T)} \left[C_\lambda^{\text{ID}}(T) + C_\lambda^{\text{Prim}}(T) e^{-(\lambda+m_e)/T} \right] dT, \quad (4.56)$$

as follows from Eq. (3.42). To derive an estimate for the expected contribution to dn_γ/dE_γ from the resulting equation, we proceed in essentially the same way as we did in calculating the contribution from axions produced via vacuum misalignment. The results of this calculation are shown in Fig. 8 for parameter values within or near the preferred region of parameter space for our bulk-axion DDM model. Specifically, we have taken $M_c = 10^{-11}$ GeV, $\Lambda_G = 1$ TeV, $T_{\text{RH}} = 5$ MeV, and $\xi = g_G = 1$. The solid colored curves shown correspond to several different choices of \hat{f}_X ranging from $\hat{f}_X = 10^{12}$ GeV to $\hat{f}_X = 10^{15}$ GeV. Once again, the dashed black lines indicate the observational limits on additional contributions to dn_γ/dE_γ . It is clear from Fig. 8 that while the contribution to the diffuse X-ray flux from thermal axions within our preferred region of parameter space is certainly not negligible, it is also consistent with current observational limits. We therefore conclude that even after the contribution from thermal axions is included, our bulk-axion DDM model is consistent with X-ray and gamma-ray data.

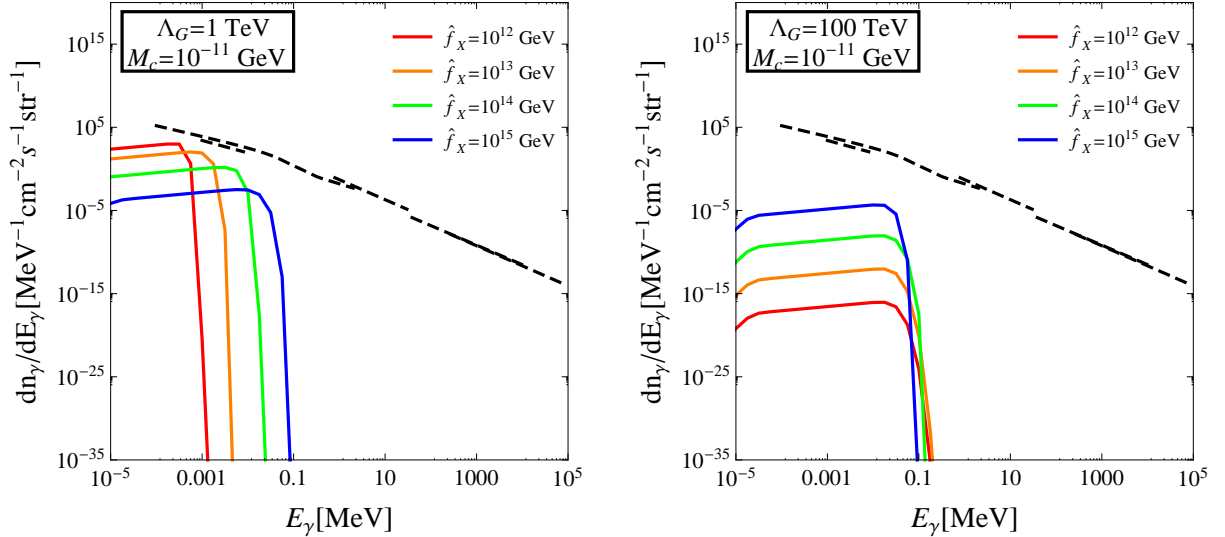


FIG. 8: The diffuse photon flux spectrum dn_γ/dE_γ produced from the decays of a population of a_λ produced by interactions among the SM particles in the thermal bath after inflation. The left panel shows the results for $\Lambda_G = 1$ TeV, while the right panel shows the results for $\Lambda_G = 100$ TeV. In each case, we have taken $M_c = 10^{-11}$ GeV, $T_{\text{RH}} = 5$ MeV, and $\xi = g_G = 1$. The solid colored curves indicate the diffuse-photon-flux contributions corresponding to different choices of \hat{f}_X . As in Fig. 7, the dashed black contours indicate the upper bounds on dn_γ/dE_γ derived from observational limits on the diffuse X-ray and gamma-ray fluxes, and we see that our model is consistent with these bounds.

H. Axion Decays and Big-Bang Nucleosynthesis

The accord between the primordial abundances of light nuclei inferred from observation and the predictions for those abundances within the framework of standard BBN has been one of the greatest triumphs of theoretical cosmology. However, these predictions depend sensitively on the cosmological parameters during the nucleosynthesis epoch. For

example, the presence of additional relativistic degrees of freedom in the thermal bath during BBN can substantially distort the abundances of the light elements away from their observed values. In addition, the decays of unstable particles during or after the BBN epoch can also alter these abundances via the injection of both entropy and energy into the thermal bath. We must therefore ensure that the collective effects of a_χ decays in our model are sufficiently small so as not to disrupt the successful generation of light-element abundances via standard BBN.

Limits on the abundance of a single unstable relic particle χ from BBN are typically phrased as bounds on the number density \hat{n}_χ^* that χ would have at present time if it were absolutely stable. In general, the BBN bound on \hat{n}_χ^* for any given relic particle depends on the lifetime τ_χ of that particle. The most stringent limits are obtained for lifetimes $\tau_\chi \sim \mathcal{O}(10^9 - 10^{10} \text{ s})$, for which the corresponding constraint is roughly [58, 59]

$$m_\chi \frac{\hat{n}_\chi^*}{n_\gamma^*} \lesssim 10^{-13} \text{ GeV}, \quad (4.57)$$

where $n_\gamma^* \approx 410.5 \text{ cm}^{-3}$ denotes the present-day number density of photons. This limit can also be written in the form

$$\hat{\Omega}_\chi^* \lesssim 1.7 \times 10^{-5}, \quad (4.58)$$

where $\hat{\Omega}_\chi^*$ is the relic abundance that χ would have at present time if it were absolutely stable.

Once again, however, as with other constraints on traditional models of decaying dark matter (such as those from the CMB and the diffuse X-ray and gamma-ray backgrounds), these constraints are not readily applicable to models within the DDM paradigm, since the dark-matter candidate in these models is an ensemble with no single, well-defined mass or lifetime. Thus, we must reexamine the derivation of the BBN constraints on decaying relic particles in order to determine what restrictions these considerations place on the parameter space of our bulk-axion DDM model. While a detailed calculation of the precise limits BBN considerations impose on DDM scenarios in general is beyond the scope of this paper, it is straightforward to demonstrate that BBN constraints do not significantly restrict the parameter space of the particular model which concerns us here.

We begin by noting that in traditional, single-particle dark-matter scenarios, an unstable dark-matter candidate χ with a relic abundance $\Omega_\chi \sim \Omega_{\text{CDM}}$ is generally consistent with all astrophysical and cosmological limits on dark-matter decays, provided that $\tau_\chi \gtrsim \tau_\chi^{\text{min}} \sim 10^{26} \text{ s}$ [54]. It therefore follows that any a_χ in the DDM ensemble with a lifetime $\tau_\chi \gtrsim \tau_\chi^{\text{min}}$ will have no impact on BBN within regions of parameter space in which the WMAP constraint $\Omega_{\text{tot}} \leq \Omega_{\text{CDM}}$ on the *total* dark-matter relic abundance is satisfied. Thus, we may safely conclude that our bulk-axion model of dynamical dark matter is consistent with BBN constraints within such regions of parameter space, provided that

$$\hat{\Omega}_{\text{tot}}^* \lesssim 1.7 \times 10^{-5}, \quad (4.59)$$

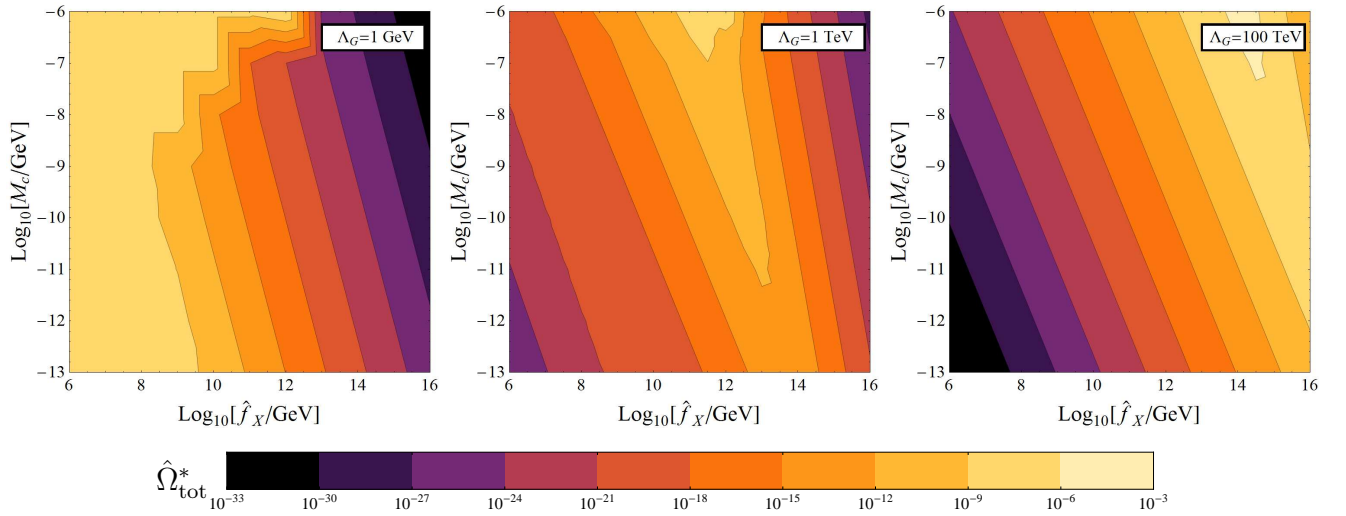


FIG. 9: Contours of the collective contribution to $\hat{\Omega}_{\text{tot}}^*$ from the set of a_χ with lifetimes $\tau_\chi < \tau_\chi^{\text{min}}$ for a DDM ensemble of photonic axions with $c_\gamma = 1$. The left, center, and right panels display the results for $\Lambda_G = 1 \text{ GeV}$, $\Lambda_G = 1 \text{ TeV}$, and $\Lambda_G = 100 \text{ TeV}$, respectively. In each case, we have taken $T_{\text{RH}} = 5 \text{ MeV}$, $H_I = 100 \text{ TeV}$, and $\xi = g_G = \theta = 1$. In each panel, we see that BBN constraints are amply satisfied throughout essentially the entire region of parameter space shown.

where $\hat{\Omega}_{\text{tot}}^*$ denotes the collective contribution which the set of a_λ with lifetimes $\tau_\lambda < \tau_\chi^{\min}$ would have made to the dark-matter relic abundance at present time if they were absolutely stable. In other words, the BBN constraint we are imposing in Eq. (4.59) effectively rests upon the extremely conservative approach of treating all states in the DDM ensemble whose lifetimes are less than τ_χ^{\min} as if they had lifetimes τ_λ which are in the range which is most dangerous for BBN, namely $\tau_\lambda \sim 10^9 - 10^{10}$ s. We emphasize that while this criterion is a sufficient condition for successful BBN, it does *not* represent the true BBN constraint, which is always far less stringent.

In Fig. 9, we display contours of $\hat{\Omega}_{\text{tot}}^*$ for a DDM ensemble of photonic axions with $c_\gamma = 1$, as a function of \hat{f}_X , M_c , and Λ_G . The left panel shows the results for $\Lambda_G = 1$ GeV, the center panel for $\Lambda_G = 1$ TeV, and the right panel for $\Lambda_G = 100$ TeV. In each case, we have taken $T_{\text{RH}} = 5$ MeV, $H_I = 100$ TeV, and $\xi = g_G = \theta = 1$. In each panel of Fig. 9, we see that the criterion in Eq. (4.59) is amply satisfied throughout essentially the entire region of parameter space shown. It therefore follows that our bulk axion model is consistent with successful BBN throughout this region of parameter space.

I. Axion Decays and Late Entropy Production

One additional physical consequence of the late decays of unstable relic particles is the generation of entropy as those particles “dump” their energy density into the radiation bath. Indeed, a number of considerations place constraints on late entropy production from decaying particles. For example, late entropy generation can upset the light-element predictions from standard BBN and produce observable features in the CMB. In this section, we examine the effect of the late decays of the a_λ on the entropy density of the universe in our bulk-axion DDM model as a function of time in order to verify that no perceptible effects can arise which might serve to exclude our model.

During any given epoch, the entropy density of the universe is dominated by the contribution from radiation and therefore well approximated by

$$s \approx \sum_i \frac{4\rho_i(T_i)}{3T_i} = \frac{\pi^2}{30} g_{*s}(T) T^3, \quad (4.60)$$

where the index i runs over all relativistic particle species, T_i is the temperature associated with any particular such species, and g_{*s} is the number of interacting degrees of freedom at temperature T . During the early stages of the history of the universe (prior to neutrino decoupling), all such species are characterized by a common temperature $T_i \approx T$. During such epochs, $g_{*s}(T) \approx g_*(T)$, and the entropy density is therefore directly proportional to the total energy density ρ_{rad} of radiation. Indeed, even during subsequent epochs, g_{*s} and g_* remain roughly similar, and ρ_{rad} remains a good indicator of the entropy density. Thus, by evaluating the contribution to ρ_{rad} from a_λ decays in our bulk axion DDM model, we can assess the effect of these decays on both the energy and entropy densities of the universe.

In the LTR cosmology, as in the standard cosmology, ρ_{rad} evolves according to an equation similar to Eq. (4.30):

$$\frac{d\rho_{\text{rad}}}{dt} = -4H\rho_{\text{rad}} + \Gamma_\phi \rho_\phi + \sum_\lambda \text{BR}_\lambda^{(\text{rad})} \Gamma_\lambda \rho_\lambda. \quad (4.61)$$

This equation assumes the presence of a tower of decaying a_λ , where $\text{BR}_\lambda^{(\text{rad})}$ is the total branching fraction of a_λ into relativistic particles. Note, however, that since we are working within the context of LTR cosmology, the effects of inflaton decays on the energy and entropy densities of the universe remain relevant until very late times $t \sim t_{\text{RH}}$. Thus we have explicitly included an additional source term $\Gamma_\phi \rho_\phi$ in Eq. (4.61) to account for the effect of such inflaton decays, where Γ_ϕ and ρ_ϕ respectively denote the decay rate and energy density of the inflaton field ϕ .

The contribution to ρ_{rad} from inflaton decays can readily be calculated from standard results pertaining to the LTR cosmology (for a review, see, *e.g.*, Ref. [16]). As the universe exits the inflationary epoch at a time $t_I \approx 2/(3H_I)$, the energy density stored in the inflaton field is initially $\rho_\phi = \rho_{\text{crit}} = 3H_I^2 M_P^2$. During subsequent epochs, the inflaton source term for radiation is approximately given by

$$\Gamma_\phi \rho_\phi \approx \frac{3H_I^2 M_P^2}{2t_{\text{RH}}} \left(\frac{t_I}{t} \right)^\kappa e^{-t/2t_{\text{RH}}}, \quad (4.62)$$

where κ is defined as in Eq. (3.3), and we have used the fact that the inflaton-decay rate is related to the reheating time by $\Gamma_\phi \approx 1/(2t_{\text{RH}})$. Note that this source term is negligible at times $t \gg t_{\text{RH}}$, when by definition $\rho_\phi \ll \rho_{\text{rad}}$, and hence can safely be neglected at such times. By contrast, at early times $t \lesssim t_{\text{RH}}$, the inflaton source term is expected

to dominate in Eq. (4.61), in the sense that

$$\Gamma_\phi \rho_\phi \gg \sum_\lambda \text{BR}_\lambda^{(\text{rad})} \Gamma_\lambda \rho_\lambda . \quad (4.63)$$

Whenever this condition is satisfied, the contribution to ρ_{rad} from a_λ decays is inconsequential compared to that from inflaton decays, and the axion source term can therefore safely be neglected.

In assessing the contribution from a_λ decay, we once again choose to focus on the case of a photonic axion with $c_\gamma = 1$; this implies that the decay mode $a_\lambda \rightarrow \gamma\gamma$ dominates the contribution to ρ_{rad} . In this case, the source term for radiation due to a_λ decay is just the source term for photons given in Eq. (4.37). In this case, solving Eq. (4.61) for ρ_{rad} , we find that

$$\rho_{\text{rad}}(t) = \bar{\rho}_{\text{rad}}(t) + \int_{t_G}^t \left(\frac{t'}{t}\right)^{4\kappa/3} \sum_\lambda \text{BR}_\lambda^{(2\gamma)} \Gamma_\lambda \rho_\lambda(t') dt' , \quad (4.64)$$

where $\bar{\rho}_{\text{rad}}(t)$ is the solution for $\rho_{\text{rad}}(t)$ in the absence of any additional contribution from a_λ decays. Once again making use of the integral functions $I_i(m, n, \alpha, \beta, \lambda_{\text{min}}, \lambda_{\text{max}})$ defined in Eq. (4.35) to approximate the sum over modes, we obtain

$$\rho_{\text{rad}}(t) = \bar{\rho}_{\text{rad}}(t) + \frac{2G_\gamma \theta^2}{M_c} \int_{t_G}^t dt' \frac{t'^{\kappa/3}}{t^{4\kappa/3}} \sum_{i=1}^4 I_i(m_i, n_i, \alpha_i, \beta_i, \lambda_{i-1}^{\text{CMB}}, \lambda_i^{\text{CMB}}) \times \begin{cases} t_{\text{RH}}^{1/2} & t \lesssim t_{\text{RH}} \\ 1 & t_{\text{RH}} \lesssim t \lesssim t_{\text{MRE}} \\ t_{\text{MRE}}^{1/2} & t \gtrsim t_{\text{MRE}} . \end{cases} \quad (4.65)$$

In Fig. 10, we show how the contribution to ρ_{rad} from a_λ decays in our bulk-axion DDM model evolves with time for a variety of different choices of model parameters. The left panel shows results for $\Lambda_G = 1$ GeV, the center panel for $\Lambda_G = 1$ TeV, and the right panel for $\Lambda_G = 100$ TeV. The solid colored curves in each panel correspond to different choices of \hat{f}_X within the range $10^{10} - 10^{16}$ GeV. For all curves shown, we have assumed a photonic axion with $c_\gamma = 1$, and we have taken $M_c = 10^{-11}$ GeV, $T_{\text{RH}} = 5$ MeV, $H_I = 100$ TeV, and $\xi = g_G = \theta = 1$. The black dashed curve represents the total value of ρ_{rad} , which includes the standard contribution from inflaton decays during the reheating epoch. Since such inflaton decays constitute the dominant source for radiation prior to the end of reheating, the range of times shown in each panel extends from t_{RH} to present time. The value of H_I has been chosen here to be

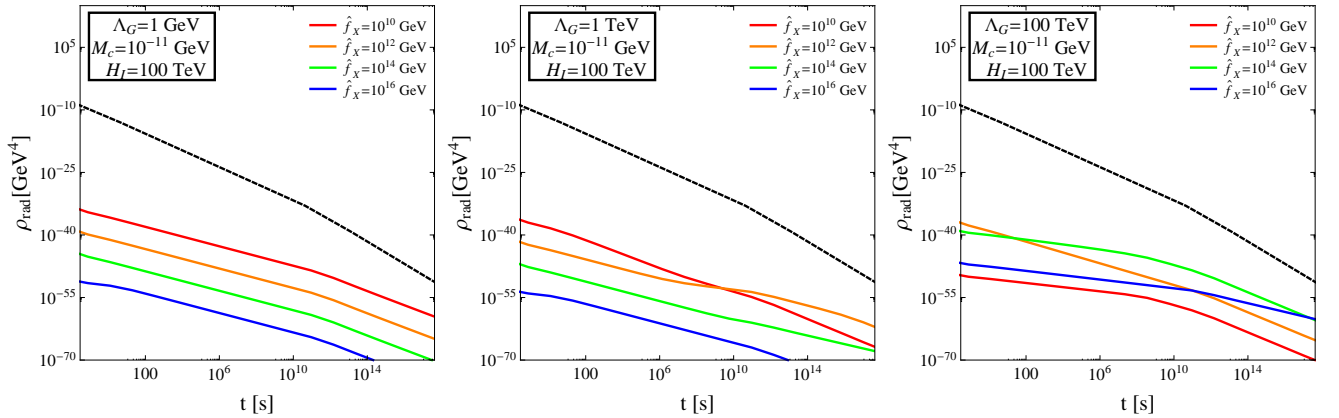


FIG. 10: The total contribution to the radiation energy density ρ_{rad} from photonic a_λ decays in our bulk-axion DDM model (solid lines), plotted as functions of time for a variety of different choices of f_X . The left panel shows the results for $\Lambda_G = 1$ GeV, the center panel for $\Lambda_G = 1$ TeV, and the right panel for $\Lambda_G = 100$ TeV. In each case, we have assumed a photonic axion with $\xi = g_G = \theta = 1$, and we have taken $M_c = 10^{-11}$ GeV, $T_{\text{RH}} = 5$ MeV, and $H_I = 100$ TeV. Also shown in each panel is the total value of ρ_{rad} as a function of time in the LTR cosmology (black dashed line), which includes the contribution from inflaton decay. In all cases, the collective contribution to ρ_{rad} from a_λ decays at all times $t < t_{\text{now}}$ remains negligible compared to the primordial contribution generated via inflaton decays during reheating. Thus our bulk-axion DDM model does not lead to overproduction of either radiation-energy density or entropy during any prior cosmological epoch.

sufficiently large that the effect of heavier a_λ with $\lambda \gtrsim 3H_I/2$ being inflated away is unimportant. Note, however, that for significantly smaller values of H_I , the contribution to ρ_{rad} from axion decays can be further suppressed by this effect.

The differences among the curves shown in Fig. 10 for different choices of \hat{f}_X and Λ_G ultimately stem from the effects of axion mixing on the abundances ρ_λ and decay widths Γ_λ of the individual axion modes. The results shown in the left panel correspond to the case in which Λ_G is sufficiently small that $y \gg 1$ for all choices of \hat{f}_X shown. In this small-mixing regime, $\lambda \gtrsim \lambda_{\text{trans}}$ for all but the lowest-lying mode in the axion KK tower, and Eqs. (2.12) and (3.8) imply that $\rho_\lambda \propto \hat{f}_X^{-2}$ and $\Gamma_\lambda \propto \hat{f}_X^{-2}$. It therefore follows that the photon source term $\text{BR}_\lambda^{(2\gamma)} \Gamma_\lambda \rho_\lambda$ associated with each a_λ within this regime decreases uniformly and substantially with increasing \hat{f}_X , as indicated. By contrast, as Λ_G is increased, several competing effects play an increasingly important role in determining the magnitude of $\text{BR}_\lambda^{(2\gamma)} \Gamma_\lambda \rho_\lambda$ for certain λ . This is because λ_{trans} increases with increasing Λ_G ; hence for large Λ_G a greater number of the a_λ are brought into the $\lambda \lesssim \lambda_{\text{trans}}$ regime, in which $\rho_\lambda \propto \hat{f}_X^2$ and $\Gamma_\lambda \propto \hat{f}_X^2$. Increasing \hat{f}_X therefore has the effect of increasing the initial magnitude of the photon source terms associated with the a_λ in this regime. However, the lifetimes of these modes also increase with increasing \hat{f}_X , and hence the transfer of their energy density to radiation is deferred until later times, when ρ_{rad} is smaller and the contribution from a_λ decays can have a proportionally greater impact. The interplay between these effects results in the behavior shown in the right two panels of Fig. 10.

Note that the curves for the total energy density shown in Fig. 10, which are dominated by the contribution from inflaton dynamics, drop more rapidly as a function of time than the contributions from axion dynamics. This reflects the continuing generation of new radiation energy density from the ongoing decays of the individual a_λ within our DDM ensemble. In all cases, however, the collective contribution to ρ_{rad} from a_λ decays at all times $t < t_{\text{now}}$ remains negligible compared to the primordial contribution generated via inflaton decays during reheating. Thus our bulk-axion DDM model does not lead to overproduction of either radiation-energy density or entropy during any prior cosmological epoch.

J. Vacuum Energy and Overclosure

In traditional dark-matter scenarios involving a single, stable dark-matter candidate χ , the dark-matter relic abundance Ω_χ increases monotonically up to and beyond the present time. As a result, verifying that Ω_χ satisfies WMAP constraints at the present time is sufficient to guarantee that χ does not overclose (or prematurely matter-dominate) the universe at all previous times as well. However, one of the hallmarks of the DDM scenario is that this is no longer true: although Ω_{tot} likewise experiences a Hubble-driven growth during the earliest phases of the evolution of the universe, this quantity can nevertheless drop during later epochs. This is possible within the DDM framework because the single, stable dark-matter candidate χ characteristic of most traditional dark-matter scenarios is replaced by a complex, multi-component dark-matter ensemble whose constituents can have a broad spectrum of lifetimes and abundances. As a result, the decays of certain dark-matter components within the ensemble can cause Ω_{tot} to decline — even prior to the present day. Indeed, such behavior for Ω_{tot} can be quite dramatic, and is illustrated in Fig. 6 of Ref. [1] for the special case in which the DDM ensemble consists of a KK tower of decaying dark fields. Thus, within the DDM framework, it is no longer sufficient to verify that Ω_{tot} satisfies overclosure constraints at the present time; we must also verify that it has satisfied such overclosure constraints (and constraints from premature matter- or vacuum-energy domination) at all prior moments during the history of the universe.

It turns out, however, that this is not a problem in our bulk-axion DDM model. Since our model already satisfies WMAP constraints at present time within our preferred region of parameter space [2], it can run afoul of overclosure constraints in the past only if the negative rate of change of Ω_{tot} is sufficiently great that Ω_{tot} might have exceeded unity within the past history of the universe. However, as discussed in Refs. [1, 2], this rate of change is described by an effective equation-of-state parameter w_{eff} , and two things are already known about the value of this parameter in our model: first, it is extremely small at the present day, *i.e.*, $10^{-23} \lesssim w_{\text{eff}} \lesssim 10^{-12}$ [2], and second, it was even smaller in the past. Indeed, this latter assertion follows from the generic behavior of w_{eff} shown in Fig. 8 of Ref. [1]: for a generic KK tower, w_{eff} reaches its maximum at the present day and is exponentially smaller prior to this time. Thus, working backwards from the present epoch, and given the finite age of the universe, we see that it is not possible for Ω_{tot} to have violated overclosure bounds at any point during the history of the universe.

One related concern which arises in our bulk-axion DDM model, due to our reliance on the misalignment mechanism for the generation of the primordial relic abundances of the a_λ is the risk of premature vacuum domination. Indeed, any a_λ for which $t_\lambda > t_G$ will contribute to the total dark-energy abundance Ω_{vac} during the period when $t_G \lesssim t \lesssim t_\lambda$, within which its energy density ρ_λ is non-vanishing but before which it begins oscillating. Since ρ_λ remains constant during this period, the contribution to Ω_{vac} scales like $\Omega_\lambda \propto t^2$ during any MD or RD epoch. Since this represents a rate of increase far faster than that associated with matter or radiation, the threat of premature vacuum domination

from fields which remain as vacuum energy for a long duration is of particular concern. Indeed, in extreme cases, such fields could potentially give rise to an additional period of inflation, leading to gross inconsistencies with the predictions of BBN, CMB data, and so forth.

In our bulk-axion model, however, it is straightforward to demonstrate that no such inconsistencies with observational data arise. The masses of all of the a_λ , with the sole exception of the zero mode a_0 , are bounded from below by the Newton's-law-modification constraint in Eq. (4.1), since $\lambda_i \geq M_c/2$ for $i > 0$. For all such modes with $t_\lambda > t_G$, this constraint on λ implies a bound $t_\lambda > 6.75 \times 10^{-14}$ s on the oscillation-onset time of the mode. (The remaining modes, for which $t_G = t_\lambda$, never contribute to Ω_{vac} .) This time scale is sufficiently early that the collective vacuum-energy contribution from these a_λ poses no threat of overclosure or premature vacuum-domination. The Ω_λ contributions from these fields simply do not have time to grow to a problematic size.

This leaves only the contribution from a_0 , whose oscillation time scale can be substantially longer than the upper limit quoted above for the higher modes in situations in which $y \gg 1$. Since $A_{\lambda_0} \approx 1$ in this limit, Eq. (3.8) implies that prior to the time t_{λ_0} at which it begins oscillating, the relic abundance of a_0 is given by

$$\Omega_{\lambda_0} \approx \frac{3}{2} \frac{m_X^2 \hat{f}_X^2}{M_P^2} \left(\frac{t}{\kappa} \right)^2. \quad (4.66)$$

Therefore, one finds that by the time of oscillation, which is given by $t_{\lambda_0} \approx \kappa_{\lambda_0}/2m_X$ in this limit, Ω_{λ_0} will have grown to

$$\Omega_{\lambda_0}(t_{\lambda_0}) \approx \frac{3}{8} \frac{\hat{f}_X^2}{M_P^2}. \quad (4.67)$$

This result is independent of m_X , and implies that the contribution of the a_0 to Ω_{vac} is not a cause for concern for sub-Planckian values of \hat{f}_X . Indeed, this is to be expected: in this regime, a_0 functions effectively like a four-dimensional axion. Early vacuum-energy domination is known not to be a problem for light axions and axion-like particles (see Ref. [35] and references therein) in purely four-dimensional theories.

K. Misalignment Production and Isocurvature Perturbations

In an inflationary cosmology, fluctuations in the energy density of any population of particles produced thermally, *i.e.*, via rapid interactions in the radiation bath during the reheating phase, stem from the primordial perturbations in the energy density of the inflaton field. Consequently, such fluctuations are of the so-called adiabatic type — that is, they represent spatial variations in the *total* energy density, but not in the relative contributions of individual particle species to that total density. Such variations, in turn, imply fluctuations in the local spacetime curvature and are therefore sometimes also referred to as curvature perturbations. By contrast, fluctuations in the energy density of any population of particles produced via means uncorrelated with the inflaton field (and therefore non-thermal) can also give rise to fluctuations of the isocurvature type — *i.e.*, perturbations in the relative contributions of different species to the total energy density, with that total energy density held fixed. Recent WMAP observations of the CMB power spectrum, taken in combination with baryon acoustic oscillation (BAO) measurements and supernova data, place a stringent bound [10] on any deviations from adiabaticity in primordial energy-density fluctuations. This bound is typically expressed in terms of the fractional contribution α_0 to the CMB power spectrum from axion isocurvature perturbations:

$$\alpha_0 \equiv \frac{\langle (\delta T/T)_{\text{iso}}^2 \rangle}{\langle (\delta T/T)_{\text{tot}}^2 \rangle} < 0.072, \quad (4.68)$$

where $\langle (\delta T/T)_{\text{tot}}^2 \rangle$ and $\langle (\delta T/T)_{\text{iso}}^2 \rangle$ respectively denote the total average root-mean-squared fluctuation in the CMB temperature, and the average root-mean-squared temperature fluctuation due to isocurvature perturbations alone. Since the a_λ fields which compose our dynamical dark-matter ensemble are presumed to be produced non-thermally, via the misalignment mechanism, it is necessary to investigate the implications of this bound for our model.

Our discussion of isocurvature perturbations in our bulk-axion DDM model in large part parallels the discussion of such perturbations in traditional QCD axion models presented in Ref. [60], to which we refer the reader for a more complete introduction and discussion of the formalism and methodologies used. It turns out to be convenient to express the fluctuations of any given a_λ in terms of the fractional change S_λ in the ratio of its number density n_λ to the entropy density s of the universe. This quantity can be written in the form

$$S_\lambda \equiv \frac{\delta(n_\lambda/s)}{(n_\lambda/s)} = \frac{\delta n_\lambda}{n_\lambda} - 3 \frac{\delta T}{T}. \quad (4.69)$$

We assume that the production of all other particle species ψ_i (*i.e.*, the SM fields) ultimately results from inflaton decay, and that the density fluctuations for these species are purely adiabatic, with $S_i = 0$. Since, by definition, the fluctuation $\delta\rho$ in the total energy density vanishes for isocurvature fluctuations, it therefore follows that the sum of the fluctuations in the energy densities of the various particle species obeys a constraint which may be written in the form

$$\sum_{\lambda} \rho_{\lambda} \left(S_{\lambda} + 3 \frac{\delta T}{T} \right) + 3 \sum_i \rho_i \frac{\delta T}{T} + 4 \rho_{\text{rad}} \frac{\delta T}{T} = 0, \quad (4.70)$$

where the ρ_i denote the energy densities associated with massive species other than the a_{λ} , and ρ_{rad} once again denotes the total energy density of radiation. In our bulk-axion DDM model, the abundances of all of the a_{λ} are determined by a single misalignment angle θ . As discussed in Ref. [1], this reflects the ultimate five-dimensional nature of the axion field. This in turn implies that the density fluctuations δn_{λ} for all of these fields are determined by the fluctuations $\delta\theta$ in this misalignment angle generated by quantum fluctuations during inflation. The fact that the fluctuations δn_{λ} are all determined by $\delta\theta$ implies that the $S_{\lambda} \equiv S$ are essentially equal for all a_{λ} ; hence Eq. (4.70) simplifies to

$$\Omega_{\text{tot}} S = -3 \left(\Omega_{\text{mat}} + \frac{4}{3} \Omega_{\text{rad}} \right) \frac{\delta T}{T}, \quad (4.71)$$

where Ω_{mat} denotes the total abundance of matter in the universe, including the contributions from baryonic matter, the ensemble of dark axions, and any other particles which might contribute to the dark-matter relic abundance, and Ω_{rad} is the relic-abundance contribution from radiation. This expression is identical to that which describes the isocurvature perturbations associated with a single, four-dimensional axion. Therefore, assuming that the fluctuations in θ are Gaussian, it follows that in our axion DDM model, α_0 is given by the standard expression [60]

$$\alpha_0 = \frac{8}{25} \left(\frac{\Omega_{\text{tot}}^*}{\Omega_{\text{mat}}^*} \right)^2 \frac{1}{\langle (\delta T/T)_{\text{tot}}^2 \rangle} \frac{\sigma_{\theta}^2 (2\theta^2 + \sigma_{\theta}^2)}{(\theta^2 + \sigma_{\theta}^2)^2}, \quad (4.72)$$

where Ω_{mat}^* denotes the present-day value of Ω_{mat} , and where $\sigma_{\theta}^2 \equiv \langle (\delta\theta)^2 \rangle$ denotes the variance associated with fluctuations in θ .

This result makes intuitive sense. Although our DDM model has essentially partitioned the total dark-matter abundance amongst a large number of different KK axion fields, the underlying five-dimensional nature of the KK tower has correlated the individual fluctuations of these fields so that they are governed by the fluctuation of a single misalignment angle θ . It is therefore not a surprise that the expected magnitude for isocurvature fluctuations in our model turns out to be no greater than it is standard, four-dimensional axion models.

All that remains, then, for us to do in order to determine the value of α_0 in our bulk-axion DDM model, is to assess the magnitude of σ_{θ}^2 . Assuming again that the fluctuations in θ are Gaussian, this quantity is given by

$$\sigma_{\theta}^2 = \frac{H_I^2}{4\pi^2 \hat{f}_X^2}. \quad (4.73)$$

Since we are operating within the context of an LTR cosmology with $T_{\text{RH}} \sim \mathcal{O}(\text{MeV})$, as discussed above, it is by no means problematic (and in fact quite natural) for $H_I \ll \hat{f}_X$. Therefore, as long as $\theta \sim \mathcal{O}(1)$, as might be expected from naturalness considerations, it can safely be assumed that $\theta \gg \sigma_{\theta}$. Substituting into Eq. (4.72) the experimentally observed [10] values $\langle (\delta T/T)_{\text{tot}}^2 \rangle \approx (1.1 \times 10^{-5})^2$ and $\Omega_{\text{mat}}^* \approx 0.262$ we find that α_0 is well approximated by

$$\alpha_0 \approx 1.95 \times 10^9 \left(\frac{H_I \Omega_{\text{tot}}^*}{\hat{f}_X \theta} \right)^2 \quad (4.74)$$

in our bulk-axion model. Combining this result with the upper bound on α_0 quoted in Eq. (4.68) yields the constraint

$$H_I \lesssim 6.07 \times 10^{-6} \left(\frac{\theta \hat{f}_X}{\Omega_{\text{tot}}^*} \right). \quad (4.75)$$

We consider the case in which $\Omega_{\text{tot}}^* \approx \Omega_{\text{CDM}}$ and in which the axion ensemble is responsible for essentially the entirety of the observed dark-matter relic abundance. This corresponds to $\hat{f}_X \approx 10^{14} - 10^{15}$ GeV. We then find that for $\theta \sim \mathcal{O}(1)$, the resulting constraint $H_I \lesssim 10^9 - 10^{10}$ GeV on the Hubble parameter during inflation is relatively mild.

Indeed, there is no difficulty in satisfying this constraint in either the standard or the LTR cosmology. We thus conclude that isocurvature perturbations do not present any problem for our bulk-axion model of dynamical dark matter. Moreover, a low scale for H_I can be regarded as natural in the context of an LTR cosmology.

It is worth remarking, however, that the above results have implications for the detection of primordial gravitational waves. Limits on primordial gravitational waves from observations of the CMB can be conveniently parametrized in terms of the scalar-to-tensor ratio r . For example, consider single-field models of inflation, in which $r = 16\epsilon$, where $\epsilon = M_P^2(V'/V)^2/(4\pi)$ is the inflaton slow-roll parameter, with V and V' denoting the inflaton potential and its first derivative with respect to the inflaton field, respectively [61]. In the context of our bulk-axion DDM model, the standard relation (see, *e.g.*, Ref. [10]) between r and α_0 takes the form

$$r = \frac{2\theta^2 \hat{f}_X^2}{M_P^2} \left(\frac{\Omega_{\text{CDM}}}{\Omega_{\text{tot}}^*} \right)^2 \frac{\alpha_0}{1 - \alpha_0}. \quad (4.76)$$

As discussed above, consistency with the bounds in Eqs. (4.68) and (4.75) requires that $H_I \ll 2\pi f_X \theta$ and $\alpha_0 \ll 1$. In this regime, one finds that the expected tensor-to-scalar ratio is essentially independent of Ω_{tot}^* and well approximated by

$$r \approx 2.7 \times 10^8 \left(\frac{H_I}{M_P} \right)^2. \quad (4.77)$$

Current WMAP observations, again in conjunction from BAO and supernova data, place an upper bound $r < 0.22$ on the tensor-to-scalar ratio [10]. Thus, Eq. (4.77) results in a constraint $H_I \lesssim 6.7 \times 10^{13}$ GeV on the Hubble scale during inflation — a constraint which Eq. (4.75) implies is already automatically satisfied, even for $\mathcal{O}(1)$ values of the misalignment angle θ . The upshot is therefore that while there is no conflict between current limits on isocurvature perturbations and the predictions of our bulk-axion DDM model, the requirement that H_I be relatively small in this model suggests that r should likewise be quite small — at least in the simplest of inflationary scenarios. Constraints on the spectral index n_s from WMAP [10] can simultaneously be satisfied for small r without difficulty, for example in negative-curvature models of inflation, which tend to predict small r [62].

In summary, we conclude that current constraints on isocurvature perturbations can be satisfied in our bulk-axion DDM model without too much difficulty. However, we note that any conclusive measurement of r within the sensitivity range of the Planck satellite would have severe ramifications for this model.

L. Axion Abundances and Quantum Fluctuations During Inflation

Thus far in this paper, we have disregarded the effects of the quantum fluctuations that naturally arise for any massless or nearly massless field during the inflationary epoch. In particular, the low-momentum modes of any a_λ in our model with a mass $\lambda \lesssim H_I$ have wavelengths which exceed the Hubble length during inflation; excitations of such low-momentum modes are therefore indistinguishable from a VEV and consequently do not inflate away. These excitations necessarily yield a primordial energy-density contribution in our bulk-axion DDM model which cannot be avoided in any inflationary cosmology. Consistency with the relic-abundance predictions discussed in Sect. III A therefore requires that this primordial energy density be small compared to that which results from misalignment production.

In particular, it is possible to formulate a condition that ensures that these quantum fluctuations not invalidate our previous analysis. Clearly, one criterion that any such condition must enforce is that such fluctuations not have a significant effect on the total relic abundance of the ensemble. We may formulate this constraint as a requirement that the difference between the full present-day relic abundance $\tilde{\Omega}_{\text{tot}}^*$, which incorporates the effect of these fluctuations, and the result Ω_{tot}^* obtained in the absence of such corrections be negligible — *i.e.*, that

$$|\tilde{\Omega}_{\text{tot}}^* - \Omega_{\text{tot}}^*| \ll \Omega_{\text{tot}}^*. \quad (4.78)$$

While the condition in Eq. (4.78) is certainly a necessary one, it is not by itself sufficient to ensure that vacuum fluctuations during inflation do not lead to phenomenological difficulties for our model. This is because within DDM framework, dark-matter stability is not a requirement, and consistency with observational constraints is arranged by balancing decay widths against abundances across the entire dark-matter ensemble. Indeed, as we have demonstrated, misalignment production provides precisely the right relationship between the Ω_λ and Γ_λ to mitigate the deleterious effects of the heavier, more unstable states in our ensemble and render our model phenomenologically viable. We must therefore ensure that this delicate balance is not disrupted by the effects of vacuum fluctuations during inflation.

Within the preferred region of parameter space of our bulk-axion DDM model, as discussed in Sect. III A, the oscillation-onset times for the lighter a_λ in the tower are staggered in time. As a result, these lighter modes collectively dominate in Ω_{tot} . It therefore follows that whether or not the total-relic-abundance constraint in Eq. (4.78) is satisfied depends primarily on how vacuum fluctuations affect the abundances of these most abundant modes alone. By contrast, the balancing of lifetimes against abundances depends on the properties of the full KK tower, and not merely on the attributes of the lighter modes which dominate Ω_{tot} . The corresponding condition we impose on our model therefore represents an even stronger constraint than the one appearing in Eq. (4.78) and indeed subsumes it. To wit, we require that the full relic abundance $\tilde{\Omega}_\lambda$ of *each axion mode* not differ significantly from the corresponding abundance Ω_λ obtained in the absence of corrections due to vacuum fluctuations during inflation — *i.e.*, that

$$|\tilde{\Omega}_\lambda - \Omega_\lambda| \ll \Omega_\lambda \quad \text{for all } \lambda. \quad (4.79)$$

We emphasize that this is an overly conservative constraint, and that consistency with observational data is certainly possible even if vacuum fluctuations do have a significant effect on the abundances of certain a_λ . However, as we shall demonstrate, the restriction that this overly conservative constraint imposes on our model (which primarily turns out to take the form of an upper bound on H_I for any allowed choice of \hat{f}_X , M_c , and Λ_G) is not terribly severe.

In order to determine how this condition restricts the parameter space of our model, we must first assess what effect vacuum fluctuations during inflation have on the individual energy densities ρ_λ and relic abundances Ω_λ of the constituent fields in our dark-matter ensemble. We begin by noting a generic result in inflationary cosmologies (for a review, see Ref. [63]), namely that the variance $\langle \phi^2 \rangle$ in the amplitude of any light scalar ϕ with a mass $m_\phi \lesssim H_I$ induced by vacuum fluctuations during inflation is given by

$$\langle \phi^2 \rangle \sim \frac{H_I^3 \delta t_I}{4\pi^2}, \quad (4.80)$$

where δt_I denotes the duration of inflation. A fluctuation of this order will therefore be induced in the amplitude of any axion in our dark-matter ensemble with a mass smaller than H_I . Moreover, we note that the relationship between δt_I and H_I is constrained by the fact that successful resolution of the smoothness and flatness problems requires $N_e \approx H_I \delta t_I \gtrsim 60$, where N_e denotes the number of e -foldings of inflation. In typical scenarios, N_e lies only slightly above this lower bound; hence δt_I is typically expected to be such that $H_I \delta t_I \sim \mathcal{O}(100)$. We will frequently express our results in terms of N_e in what follows.

We begin our discussion the effect of these fluctuations on the abundances of the constituent particles in our dark-matter ensemble by examining the simple case in which $t_G \lesssim t_I$. In this case, the axion mass-squared matrix attains its asymptotic, late-time form before inflation ends, and the a_λ are consequently already the axion mass eigenstates during the inflationary epoch. Thus, we find that the total energy density associated with each a_λ with $\lambda \lesssim H_I$ at the end of inflation is given by

$$\rho_\lambda(t_I) \approx \frac{1}{2} \lambda^2 \left(\theta A_\lambda \hat{f}_X + \eta_\lambda \frac{H_I \sqrt{N_e}}{2\pi} \right)^2, \quad (4.81)$$

where

$$\eta_\lambda \sim \begin{cases} \mathcal{O}(1) & \lambda \lesssim H_I \\ 0 & \lambda \gtrsim H_I \end{cases} \quad (4.82)$$

is a random coefficient of which parametrizes the fluctuation in the field a_λ .

Before proceeding further, we remark that the above results depend critically on the assumption that $t_G \lesssim t_I$. In other words, we have assumed that the instanton dynamics associated with the gauge group G has already occurred and made its contributions to the KK masses prior to the onset of the quantum fluctuations that arise due to inflation. By contrast, if $t_G \gtrsim t_I$, the quantum fluctuations will occur first, when the axion mass matrix is still diagonal and when the KK momentum modes and mass eigenstates coincide. In such cases, these are the modes which develop quantum fluctuations, and the mode-mixing induced by the instanton dynamics occurs only later.

This distinction is important, because the resulting energy density for each a_λ takes a somewhat different form when $t_G \gtrsim t_I$:

$$\rho_\lambda = \frac{1}{2} \lambda^2 \left[\sum_{n=0}^{\infty} U_{\lambda n} \left(\theta \hat{f}_X \delta_{n,0} + \eta_n \frac{H_I \sqrt{N_e}}{2\pi} \right) \right]^2. \quad (4.83)$$

In this expression, $U_{\lambda n}$ is the mixing matrix in Eq. (2.14) and η_n is the analogue of η_λ discussed above, with η_n taking non-zero values only when $n \lesssim H_I/M_c$.

A priori, this expression results in a different value for ρ_λ than that in Eq. (4.81). However, it turns out that the eventual constraints associated with Eq. (4.83) are no more stringent than those which we shall eventually calculate for Eq. (4.81). In order to understand why this is the case, let us consider an even more dramatic situation in which η_n actually takes a fixed, positive value $\bar{\eta}$ for all n — even values of n beyond the inflationary cutoff H_I/M_c . In this case, we can make use of the identity

$$\sum_{n=0}^{\infty} U_{\lambda n} = f(\tilde{\lambda}) A_\lambda, \quad (4.84)$$

where $f(\tilde{\lambda}) \equiv (\tilde{\lambda}^2 + \sqrt{2} - 1)/\sqrt{2}$, in order to rewrite Eq. (4.83) in the form

$$\rho_\lambda = \frac{1}{2} \lambda^2 \left[\theta A_\lambda \hat{f}_X + f(\tilde{\lambda}) \bar{\eta} \frac{H_I \sqrt{N_e}}{2\pi} \right]^2. \quad (4.85)$$

Remarkably, this is essentially the same expression as we would have obtained from Eq. (4.81) when $\eta_\lambda = \bar{\eta}$ for all λ , except that the fluctuation contribution now comes multiplied by an extra “scaling” factor $f(\tilde{\lambda})$. It is easy to verify that $f(\tilde{\lambda}) \rightarrow 1$ as $\tilde{\lambda} \rightarrow \infty$, whereas for small $\tilde{\lambda}$ we find that $f(\tilde{\lambda}) \ll 1$. This indicates that the effects of the inflation-related quantum fluctuations are actually *suppressed* for the lighter modes, relative to what occurs in the case with $t_G \lesssim t_I$. The magnitude of this suppression depends on y , and is more severe when $y \ll 1$ (*i.e.*, when the axion modes are more fully mixed). We thus conclude that the contributions from the quantum fluctuations that arise during inflation are greater when they occur *after* the instanton dynamics turns on (and after the KK mode-mixing), rather than before. We shall therefore concentrate on the $t_G \lesssim t_I$ case in what follows.

Given the result in Eq. (4.81), we see that the effect of vacuum fluctuations on the ρ_λ will be small for values of λ which satisfy the condition

$$\theta A_\lambda \hat{f}_X \gtrsim \frac{H_I \sqrt{N_e}}{2\pi}. \quad (4.86)$$

Since A_λ is a monotonically decreasing function of λ , it follows that within any given tower of a_λ , there exists a critical mass value

$$\lambda_{\text{fluc}} \equiv \frac{m_X}{\sqrt{2}} \left[\sqrt{\left(1 + \frac{\pi^2}{y^2}\right)^2 + \frac{32\pi^2 \theta^2 \hat{f}_X^2}{N_e H_I^2}} - \left(1 + \frac{\pi^2}{y^2}\right) \right]^{1/2} \quad (4.87)$$

below which the effect of vacuum fluctuations on the corresponding energy density ρ_λ is negligible. These ρ_λ are therefore well approximated by Eq. (3.8), and the corresponding abundances $\tilde{\Omega}_\lambda$ are given by Eq. (3.9) or Eq. (3.10), depending on the value of t_λ . By contrast, for $\lambda_{\text{fluc}} \lesssim \lambda \lesssim H_I$, the effect of vacuum fluctuations overwhelms the effect of vacuum misalignment. The initial energy density of each a_λ in this regime is therefore effectively set at t_I and is approximately given by

$$\rho_\lambda(t_I) \approx \frac{N_e}{8\pi^2} \lambda^2 H_I^2. \quad (4.88)$$

Since the Newton’s-law-modification bound on M_c in Eq. (4.1) implies that $t_\lambda \lesssim t_{\text{RH}}$ for each such field, it therefore follows that at all subsequent times, the corresponding relic abundance is given by

$$\tilde{\Omega}_\lambda \approx \frac{3N_e H_I^2}{4\pi^2 M_P^2} e^{-\Gamma_\lambda(t-t_I)} \times \begin{cases} \frac{1}{4} & 1/\lambda \lesssim t \lesssim t_{\text{RH}} \\ \frac{4}{9} \left(\frac{t}{t_{\text{RH}}}\right)^{1/2} & t_{\text{RH}} \lesssim t \lesssim t_{\text{MRE}} \\ \frac{1}{4} \left(\frac{t_{\text{MRE}}}{t_{\text{RH}}}\right)^{1/2} & t \gtrsim t_{\text{MRE}}. \end{cases} \quad (4.89)$$

To summarize, we see that the axion KK tower separates into three distinct regimes within each of which different physics plays a principal role in determining $\tilde{\Omega}_\lambda$. In the $\lambda \lesssim \lambda_{\text{fluc}}$ regime, the effect of vacuum fluctuations on $\tilde{\Omega}_\lambda$ is negligible and the results in Sect. III A continue to hold. In the $\lambda_{\text{fluc}} \lesssim \lambda \lesssim H_I$ regime, the opposite is true:

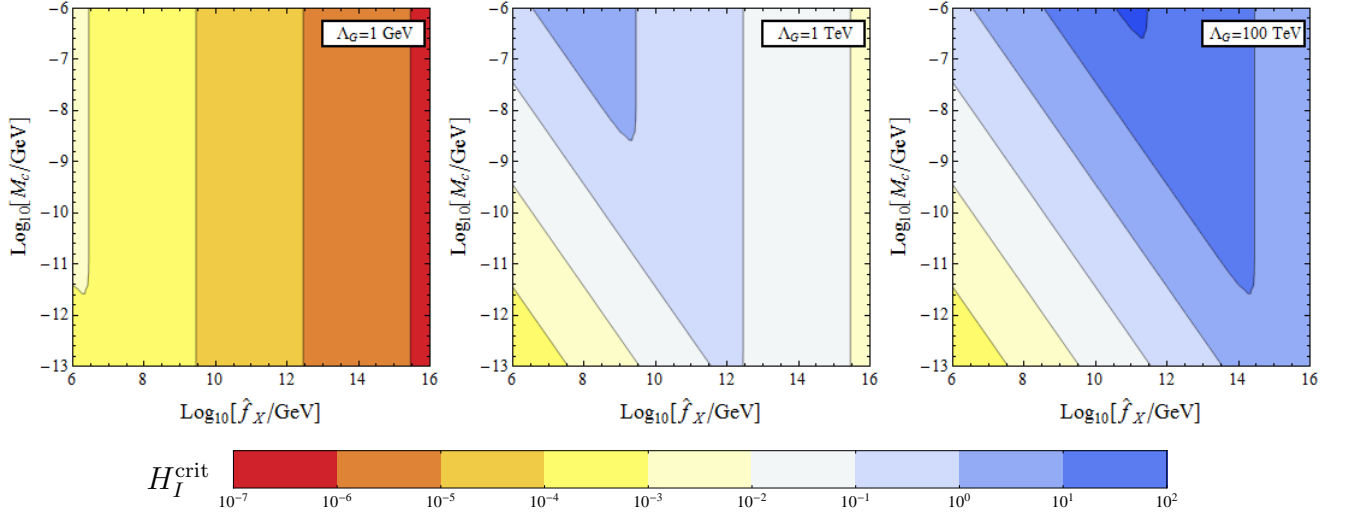


FIG. 11: Contours of the critical value H_I^{crit} in (\hat{f}_X, M_c) parameter space. As discussed in the text, choosing $H_I \ll H_I^{\text{crit}}$ guarantees that misalignment production dominates over vacuum fluctuations in determining the relic abundance $\tilde{\Omega}_\lambda$ of all a_λ in our DDM ensemble, as desired. Here, we have taken $T_{\text{RH}} = 5 \text{ MeV}$, $N_e = 100$, and $\xi = g_G = \theta = 1$ and assumed a photonic axion with $c_\gamma = 1$. The left, center, and right panels display the results for $\Lambda_G = 1 \text{ GeV}$, $\Lambda_G = 1 \text{ TeV}$, and $\Lambda_G = 100 \text{ TeV}$, respectively.

vacuum fluctuations dominate and the abundances of the a_λ are given by Eq. (4.89). Finally, in the $\lambda \gtrsim H_I$ regime, the wavelengths of even the lowest-lying momentum modes of each a_λ fall short of the Hubble length during the inflationary epoch. Such modes therefore behave unambiguously like particles, and are consequently inflated away.

We are now ready to address the constraint we have imposed on the individual abundances $\tilde{\Omega}_\lambda$ in Eq. (4.79). Since the effect of vacuum fluctuations is negligible both for $\lambda \gtrsim H_I$ and for $\lambda \lesssim \lambda_{\text{fluc}}$, it follows that this constraint will be satisfied whenever $H_I \ll \lambda_{\text{fluc}}$. Moreover, since λ_{fluc} itself decreases with increasing H_I , as indicated in Eq. (4.87), we find that our constraint may be expressed in the form $H_I \ll H_I^{\text{crit}}$, where H_I^{crit} is the value of the Hubble parameter during inflation for which $H_I = \lambda_{\text{fluc}}$. In Fig. 11, we display contours of H_I^{crit} as a function of the model parameters \hat{f}_X , M_c , and Λ_G . For the large values of Λ_G characteristic of our preferred region of parameter space, we observe that the constraint in Eq. (4.79) is satisfied for $H_I \ll H_I^{\text{crit}} \sim \mathcal{O}(10 - 100 \text{ GeV})$. For smaller values of Λ_G , although the constraint is certainly more severe, we nevertheless observe that the bound can be satisfied for $H_I \ll H_I^{\text{crit}} \sim \mathcal{O}(10 - 100 \text{ keV})$. This condition on H_I has non-trivial implications for the construction of explicit inflationary models, since values of H_I of this magnitude tend to be rather non-generic [65] among typical classes of inflationary potentials. However, as discussed in Ref. [2], such a scale for H_I is certainly not excluded (see, *e.g.*, Refs. [16, 64]). Moreover, a small value for H_I fits naturally within the context of the LTR cosmology.

M. Other Astrophysical Constraints on Light Axions

In addition to the constraints we have discussed above, there exist a number of additional astrophysical and cosmological bounds on theories involving light axions and axion-like particles. Indeed, particles of this sort can give rise to a number of potentially observable effects [9], such as a rotation of the CMB polarization, modifications of the matter power spectrum, and the enhanced spindown of rotating black holes. However, in order to give rise to observable effects of this sort, the particle in question must be exceedingly light, with a mass $m \lesssim 10^{-10} \text{ eV}$. In the extra-dimensional scenario we are discussing here, the Newton's-law-modification constraint on the compactification scale M_c stated in Eq. (4.1) implies that all a_λ in the tower have masses $\lambda \gtrsim 10^{-3} \text{ eV}$ in any scenario in which $y \lesssim 1$, *i.e.*, in which the full tower of a_λ contributes significantly to Ω_{tot} . Consequently, the additional constraints on ultra-light axions and axion-like fields discussed in Ref. [9] are not relevant for our bulk-axion DDM model.

V. SYNTHESIS: COMBINED PHENOMENOLOGICAL CONSTRAINTS ON AXION MODELS OF DYNAMICAL DARK MATTER

In the previous section, we enumerated the individual astrophysical, phenomenological, and cosmological considerations which potentially constrain our bulk-axion DDM model, and we evaluated the restrictions that each placed on the parameter space of this model. In this section, we summarize how these individual results, taken together, serve to constrain that parameter space. Our particular interest concerns the preferred region of parameter space outlined in Ref. [2], namely $\hat{f}_X \sim 10^{14} - 10^{15}$ GeV, $\Lambda_G \sim 10^2 - 10^5$ GeV, and M_c chosen sufficiently small that $y \lesssim 1$. Indeed, this is the region within which the full KK tower contributes non-trivially to the total dark-matter relic abundance.

In Fig. 12, we show the combined exclusion regions for a purely photonic axion with $c_\gamma = 1$ for $\Lambda_G = 1$ GeV (left panel), $\Lambda_G = 1$ TeV (center panel), and $\Lambda_G = 100$ TeV (right panel). The shaded regions displayed in each of the plots are excluded by the various considerations discussed in Sect. IV. Specifically, the exclusion regions appearing in these panels are those associated with helioscope limits on solar axion production (red), collider considerations (magenta),

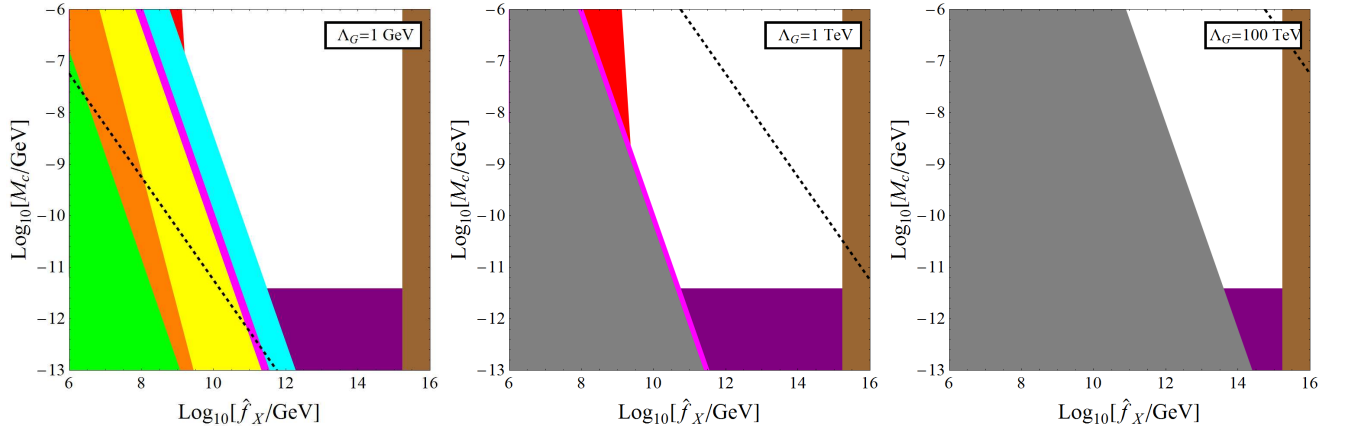


FIG. 12: Exclusion regions associated with all applicable phenomenological constraints discussed in this paper for our bulk-axion DDM model with $\Lambda_G = 1$ GeV (left panel), $\Lambda_G = 1$ TeV (center panel), and $\Lambda_G = 100$ TeV (right panel). In each case, we have taken $\xi = g_G = 1$, $T_{RH} = 5$ MeV, and $H_I = 10^{-3}$ GeV, and we have assumed that the axion only couples to the photon field with $c_\gamma = 1$. The shaded regions are respectively excluded by data from helioscope measurements (red), collider considerations (magenta), tests of Newton’s-law modifications via Eötvös-type experiments (purple), measurements of the diffuse extragalactic X-ray and gamma-ray spectra (orange), observations of the lifetimes of globular-cluster stars (yellow), energy-loss limits from supernova SN1987A (cyan), the model-consistency requirement $\Lambda_G < f_X$ (gray), overproduction of thermal axions (green), and the upper bound on the dark-matter relic abundance from WMAP (brown). The dashed black line corresponds to $y = \pi$; smaller values of y correspond to the region below and to the left of this line.

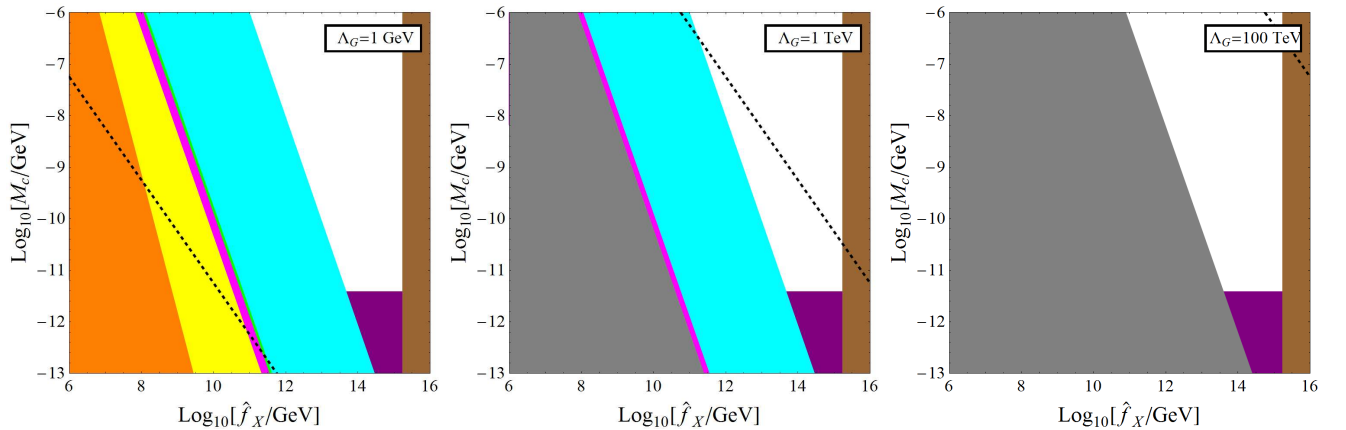


FIG. 13: Same as Fig. 12, but for a “hadronic” axion — *i.e.*, an axion which couples to both photons and gluons (and hence to pions, nucleons, and other hadrons), but not directly to SM quarks or leptons. For these panels, we have taken $c_g = c_\gamma = 1$.

tests of Newton’s-law modifications via Eötvös-type experiments (purple), measurements of the diffuse extragalactic X-ray and gamma-ray spectra (orange), observations of the lifetimes of globular-cluster stars (yellow), energy-loss limits from supernova SN1987A (cyan), the model-consistency requirement $\Lambda_G < f_X$ discussed in Ref. [2] (gray), and the 3σ upper bound on the dark-matter relic abundance from WMAP (brown). The additional requirement that the relic abundance be primarily determined by the misalignment mechanism (as envisioned in our DDM model) excludes the green-shaded region, within which a substantial population of a_λ is generated via interactions with SM particles in the thermal bath. The remaining unshaded regions of parameter space are the regions within which our DDM model is consistent with all of these constraints. The dashed black line indicates the contour $y = \pi$; smaller values of y correspond to the region below and to the left of this line. As discussed in Ref. [2], we are particularly interested in the unshaded region of parameter space which falls below and to the left of this line, since this is the region within which not only are all of the aforementioned constraints satisfied, but also the full tower of a_λ contributes non-trivially to Ω_{tot} .

As we see in Fig. 12, for small Λ_G the most stringent constraint on the parameter space of our model is the one derived from energy-loss limits from SN1987A. The constraint from globular-cluster stars is also reasonably stringent, and the constraint derived from missing-energy processes such as $pp \rightarrow \gamma + \cancel{E}_T$ at the LHC is estimated to be of roughly the same order. However, as the $y = \pi$ contour superimposed over each panel in Fig. 12 indicates, the full tower of a_λ contributes significantly to Ω_{tot} for all $\Lambda_G \gtrsim 100$ GeV. Indeed, this is precisely the Λ_G regime associated with the preferred region of parameter space for our model. We therefore conclude that within this region of parameter space, a photonic bulk-axion DDM ensemble constitutes a viable dark-matter candidate.

In Fig. 13, we consider all of the same constraints as in Fig. 12, but for the case of a hadronic axion with $c_g = c_\gamma = 1$. In this case, since the a_λ couple to hadrons, the constraints from SN1987A and from axion production via interactions among the SM particles in the radiation bath both become even more stringent. Again, as in the photonic-axion case, we find that the leading constraint for small Λ_G is that from SN1987A, and that as Λ_G increases, the model-consistency constraint becomes increasingly stringent. However, as in the photonic-axion case, we see that within the preferred region of parameter space for our model, a hadronic bulk axion is also consistent with experimental and observational limits. Thus a hadronic bulk-axion DDM ensemble is a viable dark-matter candidate as well.

We also observe that the exclusion contours in Figs. 12 and 13 associated with SN1987A energy-loss limits, globular-cluster-star evolution, collider constraints, and axion overproduction from SM particles in the radiation bath have the same slope. This is because all of these constraints involve the production of light axions which are never directly detected, and thus involve physical processes whose amplitudes include a single coupling factor between the a_λ and a pair of SM fields. By contrast, the slopes of the constraint contours associated with other classes of physical processes can be quite different. The helioscope-constraint contour, for example, is related to processes in which axions are both produced and subsequently detected via their interactions with SM fields. Likewise, the contour associated with limits on features in the diffuse X-ray and gamma-ray backgrounds is due to processes involving the decays of a preexisting cosmological population of axions, and therefore depends not only on the couplings of the a_λ to SM fields, but to their relative abundances as well. The slopes of these constraint contours consequently differ from those which characterize the contours associated with SN1987A energy-loss limits, globular-cluster-star evolution, and so forth.

VI. DISCUSSION AND CONCLUSIONS

In Ref. [1], we proposed a new framework for dark-matter physics which we call “dynamical dark matter” (DDM). The fundamental idea underpinning DDM is that the requirement of stability is replaced by a delicate balancing between lifetimes and cosmological abundances across a vast ensemble of individual dark-matter components. In Ref. [1], we developed the general theoretical features of this new framework. By contrast, in Ref. [2], we presented a “proof of concept,” namely an explicit realization of the DDM framework in which the DDM ensemble is realized as the infinite tower of KK excitations of an axion-like field propagating in the bulk of large extra spacetime dimensions.

In this paper, we have completed this study by systematically investigating all of the experimental, astrophysical, and cosmological constraints which apply to this DDM model. Some of these constraints pertain to theories with large extra dimensions in general, while others pertain specifically to our model. Among the bounds we have considered are constraints from limits on a_λ production by astrophysical sources such as stars and supernovae; constraints related to the effects of late relic-axion decays on BBN, the CMB, and the diffuse X-ray and gamma-ray backgrounds; collider constraints on missing-energy processes such as $pp \rightarrow j + \cancel{E}_T$ and $pp \rightarrow \gamma + \cancel{E}_T$; constraints on isocurvature perturbations generated as a consequence of misalignment production; constraints on the production of relativistic axions due to interactions in the thermal bath after inflation; and constraints on the direct detection of dark axions by microwave-cavity detectors and other, similar instruments. We have verified that all of these constraints are satisfied within the preferred region of parameter space for our model — namely, that in which the bulk-axion DDM ensemble accounts for the observed dark-matter relic abundance, while at the same time the full tower of

axion modes contributes meaningfully to that abundance. We therefore conclude that this bulk-axion DDM model is indeed phenomenologically viable, and that the overall DDM framework is a self-consistent alternative to traditional approaches to the dark-matter problem.

While the focus of this paper has been on the specific bulk-axion DDM model presented in Ref. [2], we note that many of our results, and in many places our entire methodology, have a far wider range of applicability. For example, much of the formalism developed in Sect. IV for evaluating the cosmological constraints on decaying dark matter in our bulk-axion DDM model is applicable to any model in which the dark sector comprises a large number of fields. This is true for issues as diverse as BBN, diffuse photon backgrounds, or stellar cooling. Likewise, irrespective of issues pertaining to dark-matter physics, many of our results and techniques may have applicability to theories with large numbers of axions, such as the recently discussed “axiverse” theories [9, 66]. Thus, we believe that the methods developed and employed in this paper can serve as a prototype for future phenomenological studies of not only the DDM framework, but also, more generally, any theories in which there exist large numbers of interacting and decaying particles.

Acknowledgments

We would like to thank K. Abazajian, Z. Chacko, M. Drees, J. Feng, J. Kumar, R. Mohapatra, M. Ramsey-Musolf, S. Su, T. Tait, S.-H. H. Tye, X. Tata, and N. Weiner for discussions. KRD is supported in part by the U.S. Department of Energy under Grant DE-FG02-04ER-41298 and by the National Science Foundation through its employee IR/D program. BT is supported in part by DOE grant DE-FG02-04ER41291. The opinions and conclusions expressed here are those of the authors, and do not represent either the Department of Energy or the National Science Foundation.

-
- [1] K. R. Dienes and B. Thomas, “Dynamical Dark Matter: I. Theoretical Overview,” arXiv:1106.4546 [hep-ph], to appear in Phys. Rev. D.
 - [2] K. R. Dienes and B. Thomas, “Dynamical Dark Matter: II. An Explicit Model,” arXiv:1107.0721 [hep-ph], to appear in Phys. Rev. D.
 - [3] K. R. Dienes, E. Dudas and T. Gherghetta, Phys. Rev. D **62**, 105023 (2000) [arXiv:hep-ph/9912455].
 - [4] R. D. Peccei and H. R. Quinn, Phys. Rev. Lett. **38**, 1440 (1977); Phys. Rev. D **16**, 1791 (1977).
 - [5] S. Weinberg, Phys. Rev. Lett. **40**, 223 (1978);
F. Wilczek, Phys. Rev. Lett. **40**, 279 (1978).
 - [6] N. Arkani-Hamed, S. Dimopoulos and G. R. Dvali, Phys. Lett. B **429**, 263 (1998) [arXiv:hep-ph/9803315].
 - [7] N. Arkani-Hamed, S. Dimopoulos and G. R. Dvali, Phys. Rev. D **59**, 086004 (1999) [arXiv:hep-ph/9807344].
 - [8] J. E. Kim, Phys. Rev. Lett. **43**, 103 (1979);
M. A. Shifman, A. I. Vainshtein and V. I. Zakharov, Nucl. Phys. B **166**, 493 (1980).
 - [9] A. Arvanitaki, S. Dimopoulos, S. Dubovsky, N. Kaloper and J. March-Russell, Phys. Rev. D **81**, 123530 (2010) [arXiv:0905.4720 [hep-th]].
 - [10] E. Komatsu *et al.* [WMAP Collaboration], Astrophys. J. Suppl. **180**, 330 (2009) [arXiv:0803.0547 [astro-ph]].
 - [11] G. F. Giudice, R. Rattazzi and J. D. Wells, Nucl. Phys. B **544**, 3 (1999) [arXiv:hep-ph/9811291].
 - [12] T. Han, J. D. Lykken and R. J. Zhang, Phys. Rev. D **59**, 105006 (1999) [arXiv:hep-ph/9811350].
 - [13] P. Graf and F. D. Steffen, arXiv:1008.4528 [hep-ph].
 - [14] S. Chang and K. Choi, Phys. Lett. B **316**, 51 (1993) [arXiv:hep-ph/9306216].
 - [15] S. Hannestad, A. Mirizzi and G. Raffelt, JCAP **0507**, 002 (2005) [arXiv:hep-ph/0504059].
 - [16] D. Grin, T. L. Smith and M. Kamionkowski, Phys. Rev. D **77**, 085020 (2008) [arXiv:0711.1352 [astro-ph]].
 - [17] M. Bolz, A. Brandenburg and W. Buchmuller, Nucl. Phys. B **606**, 518 (2001) [Erratum-ibid. B **790**, 336 (2008)] [arXiv:hep-ph/0012052].
 - [18] D. Cadamuro, S. Hannestad, G. Raffelt and J. Redondo, JCAP **1102**, 003 (2011) [arXiv:1011.3694 [hep-ph]].
 - [19] D. J. Kapner, T. S. Cook, E. G. Adelberger, J. H. Gundlach, B. R. Heckel, C. D. Hoyle and H. E. Swanson, Phys. Rev. Lett. **98**, 021101 (2007) [arXiv:hep-ph/0611184].
 - [20] S. Hannestad and G. G. Raffelt, Phys. Rev. Lett. **88**, 071301 (2002) [arXiv:hep-ph/0110067].
 - [21] C. Hanhart, J. A. Pons, D. R. Phillips and S. Reddy, Phys. Lett. B **509**, 1 (2001) [arXiv:astro-ph/0102063].
 - [22] S. Hannestad and G. Raffelt, Phys. Rev. Lett. **87**, 051301 (2001) [arXiv:hep-ph/0103201].
 - [23] J. M. Cline, C. Grojean and G. Servant, Phys. Rev. Lett. **83**, 4245 (1999) [arXiv:hep-ph/9906523].
 - [24] P. Binetruy, C. Deffayet, U. Ellwanger and D. Langlois, Phys. Lett. B **477**, 285 (2000) [arXiv:hep-th/9910219].
 - [25] T. Shiromizu, K. i. Maeda and M. Sasaki, Phys. Rev. D **62**, 024012 (2000) [arXiv:gr-qc/9910076].
 - [26] L. J. Hall and D. Tucker-Smith, Phys. Rev. D **60**, 085008 (1999) [arXiv:hep-ph/9904267].
 - [27] S. Hannestad, Phys. Rev. D **70**, 043506 (2004) [arXiv:astro-ph/0403291].
 - [28] M. Kawasaki, K. Kohri and N. Sugiyama, Phys. Rev. Lett. **82**, 4168 (1999) [arXiv:astro-ph/9811437].

- [29] G. Aad *et al.* [ATLAS Collaboration], Phys. Lett. B **705**, 294 (2011) [arXiv:1106.5327 [hep-ex]].
- [30] ATLAS Collaboration, ATLAS-CONF-2011-096.
- [31] CMS Collaboration, CMS-PAS-EXO-11-059.
- [32] S. Chatrchyan *et al.* [CMS Collaboration], JHEP **1105**, 085 (2011) [arXiv:1103.4279 [hep-ex]].
- [33] A. Ferapontov, arXiv:1109.1187 [hep-ex].
- [34] J. E. Kim and G. Carosi, Rev. Mod. Phys. **82**, 557 (2010) [arXiv:0807.3125 [hep-ph]].
- [35] J. Jaeckel and A. Ringwald, Ann. Rev. Nucl. Part. Sci. **60**, 405 (2010) [arXiv:1002.0329 [hep-ph]].
- [36] D. M. Lazarus, G. C. Smith, R. Cameron, A. C. Melissinos, G. Ruoso, Y. K. Semertzidis and F. A. Nezrick, Phys. Rev. Lett. **69**, 2333 (1992).
- [37] R. Bernabei, P. Belli, R. Cerulli, F. Montecchia, F. Nozzoli, A. Incicchitti, D. Prosperi, C. J. Dai *et al.*, Phys. Lett. B **515**, 6 (2001);
R. Bernabei, P. Belli, F. Cappella, R. Cerulli, F. Montecchia, F. Nozzoli, A. Incicchitti, D. Prosperi *et al.*, Riv. Nuovo Cim. **26N1**, 1 (2003). [astro-ph/0307403].
- [38] H. M. Chang *et al.* [TEXONO Collaboration], Phys. Rev. D **75**, 052004 (2007) [hep-ex/0609001].
- [39] F. T. Avignone, III *et al.* [SOLAX Collaboration], Phys. Rev. Lett. **81**, 5068 (1998) [astro-ph/9708008].
- [40] A. Morales *et al.* [COSME Collaboration], Astropart. Phys. **16**, 325 (2002) [hep-ex/0101037].
- [41] S. J. Asztalos *et al.* [The ADMX Collaboration], Phys. Rev. Lett. **104**, 041301 (2010) [arXiv:0910.5914 [astro-ph.CO]].
- [42] K. Yamamoto, M. Tada, Y. Kishimoto, M. Shibata, K. Kominato, T. Ooishi, S. Yamada and T. Saida *et al.*, hep-ph/0101200.
- [43] G. G. Raffelt, Lect. Notes Phys. **741**, 51 (2008) [arXiv:hep-ph/0611350].
- [44] E. Masso and R. Toldra, Phys. Rev. D **52**, 1755 (1995) [arXiv:hep-ph/9503293].
- [45] C. Amsler *et al.* [Particle Data Group], Phys. Lett. B **667**, 1 (2008).
- [46] P. Gondolo and G. Raffelt, Phys. Rev. D **79**, 107301 (2009) [arXiv:0807.2926 [astro-ph]].
- [47] G. F. Giudice, T. Plehn and A. Strumia, Nucl. Phys. B **706**, 455 (2005) [arXiv:hep-ph/0408320].
- [48] W. Hu and J. Silk, Phys. Rev. D **48**, 485 (1993).
- [49] W. Hu and J. Silk, Phys. Rev. Lett. **70**, 2661 (1993).
- [50] L. Danese and G. De Zotti, Riv. Nuovo Cimento Soc. Ital. Fis. **7**, 227 (1977).
- [51] R. L. Kinzer, G. V. Jung, D. E. Gruber, J. L. Matteson and L. E. Peterson, 1997, Astrophys. J. **475** 361 (1997);
D. E. Gruber, J. L. Matteson, L. E. Peterson and G. V. Jung, arXiv:astro-ph/9903492.
- [52] S. C. Kappadath *et al.*, BAAS **30** (2), 926 (1998);
S. C. Kappadath, Ph.D. Thesis, <http://www.gro.sr.unh.edu/users/ckappada/ckappada.html>.
- [53] W. N. Brandt *et al.*, Astron. J. **122**, 2810 (2001) [arXiv:astro-ph/0108404];
R. Giacconi *et al.*, Astrophys. J. Suppl. **139**, 369 (2002) [arXiv:astro-ph/0112184].
- [54] X. L. Chen and M. Kamionkowski, Phys. Rev. D **70**, 043502 (2004) [arXiv:astro-ph/0310473];
L. Zhang, X. Chen, M. Kamionkowski, Z. g. Si and Z. Zheng, Phys. Rev. D **76**, 061301 (2007) [arXiv:0704.2444 [astro-ph]].
- [55] A. W. Strong, I. V. Moskalenko and O. Reimer, Astrophys. J. **613**, 956 (2004) [arXiv:astro-ph/0405441].
- [56] A. A. Abdo *et al.* [The Fermi-LAT collaboration], Phys. Rev. Lett. **104**, 101101 (2010) [arXiv:1002.3603 [astro-ph.HE]].
- [57] R. C. Hickox and M. Markevitch, Astrophys. J. **645**, 95 (2006) [arXiv:astro-ph/0512542].
- [58] R. H. Cyburt, J. R. Ellis, B. D. Fields and K. A. Olive, Phys. Rev. D **67**, 103521 (2003) [arXiv:astro-ph/0211258].
- [59] M. Kawasaki, K. Kohri and T. Moroi, Phys. Lett. B **625**, 7 (2005) [arXiv:astro-ph/0402490]; Phys. Rev. D **71**, 083502 (2005) [arXiv:astro-ph/0408426].
- [60] M. P. Hertzberg, M. Tegmark and F. Wilczek, Phys. Rev. D **78**, 083507 (2008) [arXiv:0807.1726 [astro-ph]].
- [61] A. R. Liddle and D. H. Lyth, "Cosmological inflation and large scale structure," Cambridge, UK: Univ. Pr. (2000).
- [62] H. V. Peiris *et al.* [WMAP Collaboration], Astrophys. J. Suppl. **148**, 213 (2003) [astro-ph/0302225].
- [63] A. D. Linde, Chur, Switzerland: Harwood (1990) 362 p. (Contemporary concepts in physics, 5) [hep-th/0503203].
- [64] L. Randall and S. D. Thomas, Nucl. Phys. B **449**, 229 (1995) [arXiv:hep-ph/9407248];
G. German, G. G. Ross and S. Sarkar, Nucl. Phys. B **608**, 423 (2001) [arXiv:hep-ph/0103243];
M. Giovannini, Phys. Rev. D **67**, 123512 (2003) [arXiv:hep-ph/0301264];
K. Dimopoulos, D. H. Lyth and Y. Rodriguez, JHEP **0502**, 055 (2005) [arXiv:hep-ph/0411119];
P. Q. Hung, E. Masso and G. Zsembinszki, JCAP **0612**, 004 (2006) [arXiv:astro-ph/0609777];
R. Allahverdi, K. Enqvist, J. Garcia-Bellido, A. Jokinen and A. Mazumdar, JCAP **0706**, 019 (2007) [arXiv:hep-ph/0610134];
R. Allahverdi, B. Dutta and K. Sinha, Phys. Rev. D **81**, 083538 (2010) [arXiv:0912.2324 [hep-th]];
G. G. Ross and G. German, Phys. Lett. B **691**, 117 (2010) [arXiv:1002.0029 [hep-ph]].
- [65] L. A. Boyle, P. J. Steinhardt and N. Turok, Phys. Rev. Lett. **96**, 111301 (2006) [arXiv:astro-ph/0507455].
- [66] K. J. Mack and P. J. Steinhardt, JCAP **1105**, 001 (2011) [arXiv:0911.0418 [astro-ph.CO]];
A. Arvanitaki and S. Dubovsky, Phys. Rev. D **83**, 044026 (2011) [arXiv:1004.3558 [hep-th]];
B. S. Acharya, K. Bobkov and P. Kumar, JHEP **1011**, 105 (2010) [arXiv:1004.5138 [hep-th]];
B. S. Acharya, G. Kane and E. Kuflik, arXiv:1006.3272 [hep-ph];
D. J. E. Marsh and P. G. Ferreira, Phys. Rev. D **82**, 103528 (2010) [arXiv:1009.3501 [hep-ph]];
D. J. E. Marsh, Phys. Rev. D **83**, 123526 (2011) [arXiv:1102.4851 [astro-ph.CO]].